# Variable Speed Pumped Storage Hydropower for Balancing Variable Power Production in Continental Europe

## Andrea Linn Sætre

**Problem Description**

This master thesis will present aspects of control and operation of a variable speed pumped storage plant for operation in load levelling mode with respect to a given interconnected grid.

Three main objectives are to:
1) Review existing pumped storage technologies, and based on this propose an appropriate configuration for variable speed operation of a pumped storage hydropower plant in the given grid configuration.
2) Present a relevant case for investigation of the proposed configuration and perform simulations, using PSCAD, to investigate the control aspects of the variable speed system within the power system context.
3) Present and discuss basic methods for control of the variable speed pumped storage in the given configuration.

Assignment given: 18 January 2013
Main supervisor: Marta Molinas, ELKRAFT
Co-supervisor: Eivind Solvang, ELKRAFT

## Preface

This report was prepared during the spring semester of 2013 and is the final thesis towards the master's degree in Electrical Power Engineering at the Norwegian University of Science and Technology (NTNU). The thesis topic is in the field of electrical power systems.

The learning process has been extremely exponential during this master work. The master is not a continuation of my specialization project, although some aspects do correlate. In addition, the master work has crossed disciplines, which I have not had courses on. For this reason, much of this spring has been spent on theoretical background studies, and testing these theories through simulations has been a good way of understanding the nature of the electrical circuits and controller theory. The learning experience has been great and I have gained valuable insight into the control and stability discipline.

During my work with this master thesis there are a number of people I would like to address a great thanks to, and who have been of great importance towards the completion of my work. I would like to express my gratitude to my main supervisor Marta Molinas for providing guidance and assistance throughout this spring. She has always been quick in answering emails, and making time for meetings and discussions when necessary. Her enthusiasm and ideas have been great motivation towards the completion of this thesis.

Thanks should also be expressed to Jon Are Suul at SINTEF Energy, who also works part time as a post.doc at NTNU. He has always taken time to help me, even during busy weeks. Jon Are has been irreplaceable in solving my problems with the simulation program PSCAD, guiding me to helpful literature and sharing valuable insight and new ideas.

Last, but not least, I would like to thank my great classmates who have made this spring even more educational through interesting discussions and feedback, as well as being great sources of motivation. Also, thanks to my family for always offering encouragement.


Andrea Sætre
Trondheim, Juni 2013

**Abstract**

Europe is faced with a complex and challenging restructuring of its energy system. Increased penetration of variable renewable energy resources is a challenge for the stability of the transmission system. There is an obvious need for back up capacity, as well as energy storage. Pumped storage hydro power is one of the most economical storage alternatives, and Norway has the necessary reservoir capacity. However, in order to offer balancing services to Continental Europe, increased transmission capacity is required.

This master thesis has proposed and analyzed a system for balancing power in Europe. The test system consists of a pumped storage hydro power plant located in Southern Norway, directly connected by a High Voltage Direct Current (HVDC) transmission line to a varying load in Germany. The pumped storage plant is modeled by a synchronous machine and can run at variable speed in both generator and pump mode. The HVDC transmission is based on the Voltage Source Converter (VSC) technology and consists of a converter station at each end. The load profile in Germany is based on real measured wind data, and scaled to fit the power ratings of the test system.

A control strategy has been developed for the VSC-HVDC and is based on the vector control principle. The grid-side converter is chosen to control the active and reactive power flows, while the generator side converter controls the DC voltage. This control strategy does not require communication between the converter substations, which is a great advantage in an HVDC system that ranges over long distances. A current control strategy in the d-q rotating reference frame is used to decouple the non-linear and strongly coupled current equations to achieve independent control of the active and reactive power. The active power control is solved by dividing the reference active power by the d-axis voltage to give the d-axis current reference. Similarly, the q-axis current reference is achieved from the reactive power control.

The test system, with its control system, is implemented in the simulation software PSCAD/EMTDC, and fast response and stabile system operation is observed. The simulation results show that the pumped storage hydropower plant, and the whole test system, follow the active and reactive power references very well. Energy storage will play an inevitable role in achieving a clean European energy supply. The test system developed in this thesis, although quite simplified, has proven through simulations to be a promising alternative for offering balancing services to Germany (and Europe), and thereby support the integration of variable renewable resources. Many aspects, such as economics and the energy market, will, however, have a major say in how the energy challenges we stand before today are solved.

**Sammendrag**

Europa står ovenfor en kompleks og krevende omlegging av sitt energisystem. Økt utbredelse av varierende fornybare energiressurser er en utfordring for stabiliteten i nettet. Det finnes et klart behov for både reservekapasitet, så vel som energilagring. Pumpekraft er en av de mest økonomiske alternativene for lagring av energi og Norge har de nødvendige reservoarene. Men for å tilby balansetjenester til kontinentet, er økt overføringskapasitet en nødvendighet.

Denne masteroppgaven har foreslått og analysert et system for å balansere kraft i Europa. Testsystemet består av et pumpekraftverk i Sør-Norge, direkte koblet via en HVDC kabel til en varierende last i Tyskland. Pumpekraftverket er modellert med en synkronmaskin og kan kjøre på variabel hastighet, både i generator og pumpe modus. HVDC overføringen er basert på spenningsmatet omformer teknologi, og består av en omformer ved begge ender. Lastprofilen i Tyskland er basert på virkelige målte vinddata, og skalert til å passe totalytelsen til testsystemet.

En kontrollstrategi er utviklet for HVDC omformerne og er basert på vektor kontroll prinsippet. Omformeren på nettsiden er valgt til å styre den aktive og reaktive kraftflyten, mens omfomeren på generatorsiden kontrollerer DC spenningen. En slik kontrollstrategi krever ikke kommunikasjon mellom omformerstasjonene som er fordelaktig i et system med HVDC som strekker seg over lange avstander. Strømregulatorene er utført i d-q roterende referenseramme med foroverkopling for å dekoble de sterkt koblete strømlikningene og oppnå uavhengig styring av aktiv og reaktiv effekt. Den aktive effektstyringen er løst ved å dele referanse effekten på d-akse spenningen til å gi d-akse strømreferanse. Tilsvarende er q-akse strømreferanse oppnådd fra reaktiv effektkontroll.

Testsystemet, med kontrollsystem, er implementert i simuleringsprogrammet PSCAD/EMTDC, og rask respons og stabil systemdrift er observert. Resultatene viser hvordan pumpekraftverket kan kontrolleres for å balansere varierende kraft i Tyskland (og Europa), og derved støtte integrasjon av variable fornybare ressurser. Energilagring vil spille en uungåelig rolle i å oppnå en ren europeisk energiforsyning. Testsystemet utviklet i denne rapporten har vist gjennom simuleringer å være et lovende alternativ for å tilby balansetjenester til Europa. Mange aspekter, som for eksempel økonomi og energimarkedet, vil derimot ha stor påvirkning på hvordan energiutfordringene vi står ovenfor i dag vil bli løst.

# Contents

# List of Figures

# List of Tables

# 1 Introduction

## 1.1 Motivation

Europe is faced with a complex and challenging restructuring of its energy system. The European Union has agreed to undertake major cuts in its greenhouse gas emissions and to increase power generation from renewable resources, especially wind power. Several major projects are under construction on the Continent, in the North Sea and along the UK coastline. Norway, as well, is experiencing an increased power production from intermittent sources such as small hydropower and wind power.

Wind power is extremely variable and a large share of wind power is a challenge for the stability of the transmission system, as well as security of supply for the consumers. There is a need for back up capacity to generate power during no wind and high demand, as well as a need for storage capacity for surplus power. Norway can play an important role in developing storage technology in the form of pumped storage hydropower since half of Europe's reservoir capacity is found here. New pumped storage power plants in connection with existing reservoirs can be part of a solution in securing a reliable energy system.

In order for balancing capacity in Norway to be able to support Europe, more transmission capacity must be established to the major consumption areas. The development of semiconductors, especially IGBTs (Insulated-gate Bipolar Transistors), has led to High Voltage DC (HVDC) transmission based on Voltage Source Converters (VSCs). The VSC based transmission has several advantages compared to the conventional HVDC, such as independent and fast control of active and reactive power. For the long transmission distances between Norway and the continent, this technology is therefore very attractive.

By combining a pumped storage hydro power plant in Norway and VSC based HVDC transmission to Europe, balancing services can be delivered. This can ensure reliable and stabile system operation, also when the penetration from renewable intermittent resources increases. Whether or not Norway can profit on delivering a so called battery service to Europe has not been investigated. However, pumped storage hydro is one of the most economical methods to ensure a balance between production and consumption. In Norway pumped storage plants have a long history as long term storage, but they have not yet been built for short term energy storage.

## 1.2   Objectives

The main objectives of this master thesis are described through the following points:

1) Review existing pumped storage technologies, and based on this propose an appropriate configuration for variable speed operation of a pumped storage hydropower plant to deliver balancing services to Europe.

2) Present and discuss basic methods for control of the variable speed pumped storage in the given configuration.

3) Present a relevant case for investigation of the proposed configuration and perform simulations, using PSCAD, to investigate the control aspects of the variable speed system within the power system context.

## 1.3   Thesis Outline

To give a background for the thesis, background theory of the system components is reviewed in chapter 2. This includes a section on pumped storage hydro, covering the various possible electrical configurations, as well as other general information. A section on HVDC transmission introduces both the classical and voltage source based technology, and covers the main operation principles. Chapter 2 also discusses basic machine and control theory, and the per unit system.

Chapter 3 presents the simulation model and its control system design. The whole test system is discussed in detail by dividing it into smaller sections: the test case load, the grid-side converter, the HVDC transmission line, and the synchronous machine and converter. The electrical configuration, the main system parameters and the control system are reviewed for each section. When applicable, short simulation runs are included to illustrate the operation and behavior of the control system. The differences in the test model for generator and pump mode are discussed.

The system simulations and results are presented in chapter 4. A given load profile is applied to the test system, and the simulations will show how the variable speed pumped storage can balance this load. Two separate cases are simulated, one for generator operation and one for pump operation. The resulting graphs and discussion are thereafter divided into sections similar to the ones of chapter 3.

Chapter 5 presents a discussion on various topics relating to the test system model and the results achieved through simulations. Also, recommendations for further work are included. Lastly, the thesis is summarized through main conclusions in chapter 6.

Whether or not pumped storage hydro is a profitable solution has not been examined in this project, but is discussed in other reports such as [1] and [15].

## 1.4 Literature Review

The work behind this report involves an extensive literature search on variable speed pumped storage hydropower, VSC-HVDC (Voltage Source Converter High Voltage DC) transmission, control strategies and wind power data. The process started by collecting a few relevant reports to gain a good understanding and knowledge base in order to critically search for more material. Relevant material has been found through electronic sources, references of references, and through my main supervisor, Marta Molinas.

Electronic sources have been an important source, but as most know, such sources require a critical mind set. If not, hours and even days can be spent searching. Success through electronic searching was achieved by varying the search phrase from being general to very specific. The articles and reports used as references are found from legitimate and serious pages. To avoid collecting a lot of material that would ultimately not be relevant, the abstract was read to check the relevance of reports and articles. Using references of references has also been an important method in the literature search. After finding a few useful sources, my literature search continued by checking through their reference lists.

Relevant references on technical specific areas have often been quite difficult to acquire, and help has been sought amongst fellow students, as well as Jon Are Suul, from SINTEF. My process can be summed up by a suggestion by Wellington et al [2], "writing while you collect and collecting while you write". All references used are referred to throughout the text and collected in the reference list at the end of the report.

# 2 Background Theory of System Components

## 2.1 Pumped Storage Hydropower

### 2.1.1 Introduction

The demand for energy varies in several time scales; from hour to hour, day to day and also seasonal. Most renewable energy sources are intermittent and it is often a challenge to match the production with the demand. On a very windy day, the production of wind power may exceed the demand. Similarly, when the wind disappears the energy may be too little to meet demand. There is therefore a need to be able to store energy in systems that contain a large fraction of renewable energy, such as wind and solar. Demand can also vary in smaller time scales such as seconds and minutes, and in some cases even shorter variations occur. These shorter variations in demand must be compensated by automatic control, often called primary or frequency control.

Figure 1 shows the most commercial technologies of energy storage methods based on time perspectives, capacity and discharge time. Pumped storage is a good alternative for long term storage of large amounts of energy, while batteries and flywheels are better alternatives for short time intervals, as well as significantly lower capacities. Compressed air energy storage (CAES) can store large amounts of energy, but for shorter time intervals than pumped storage. The power-to-gas technologies, also have good potentials as storage technologies.

The main applications of pumped storage are load shifting, price arbitrage, primary and secondary reserves, peak power supply, grid congestion avoidance, load following, and for supporting variable electricity generation [4]. As a result of these applications pumped storage can have a central role in ensuring the grid stability. Grid stability involves maintaining all generators operating in the grid at synchronous frequency. In order to achieve this, balancing and reserve power are key issues.

According to JRC [5], pumped hydropower storage is currently the only widespread electricity storage technology able to offer the large-scale storage that is needed for accommodating renewable electricity under the 2020 EU energy targets [6]. Table 1 summarizes the advantages and drawbacks of pumped storage compared to other storage technologies [5].

From the first pumped storage plants in the 1890's until now, the technology has evolved and pumped storage plants have higher heads, capacities, efficiencies and generally improved operation. Today, pumped storage is a mature technology
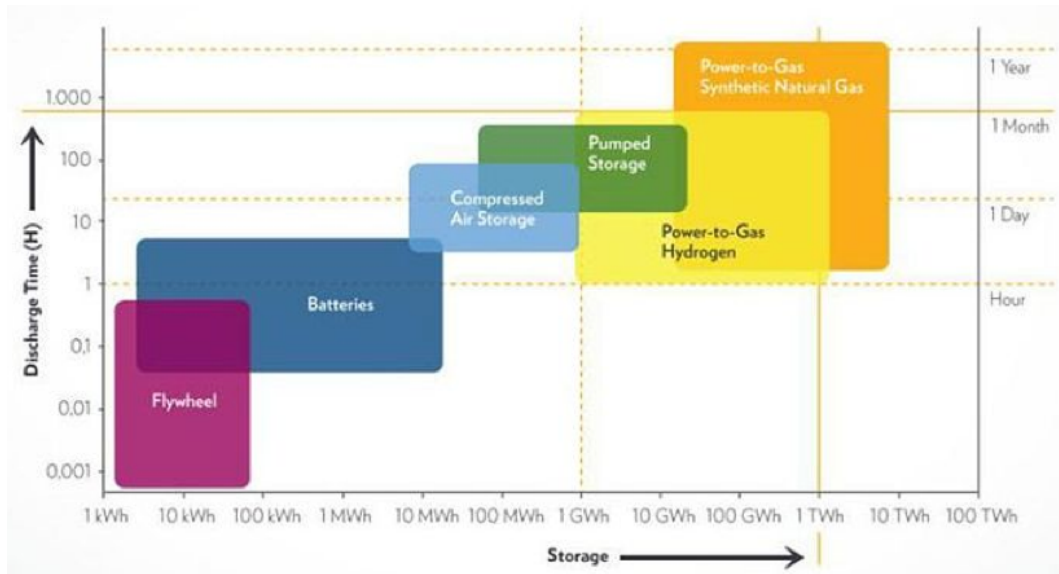
Figure 1: Various technologies for energy storage with corresponding areas of application

| Advantages | Drawbacks |
|---|---|
| + High storage capacity | - High initial investment costs |
| + Quick start capabilities (s-min) | - Long construction time |
| + Low self-discharge (%/day) | |
| + Long technical life-time (50-100yrs) | |
| + High number of cycles | |
| + Low energy losses | |

Table 1: Advantages & drawbacks of pumped storage

that accounts for more than 99% of bulk storage capacity worldwide, representing around 127,000 MW according to the Electric Power Research Institute (EPRI) [7]. As of early 2011, about 170 pumped-storage plants with a total capacity of almost 45 GW were operating in Europe [8]. An extensive, although not complete list of the large (>1500 MW) pumped storage plants in the world, as well as a list of the pumped storage plants in Europe with capacities larger than 1000 MW can be found in appendix B.

### 2.1.2 Operation Principle

Pumped storage is the method capable of storing the largest amount of energy, as well as having the largest production capacity. A pumped storage plant consists

of two water reservoirs at different heights. At the bottom reservoir, a reversible pump turbine is placed. Alternatively, both a turbine and a pump are mounted on the same generator.
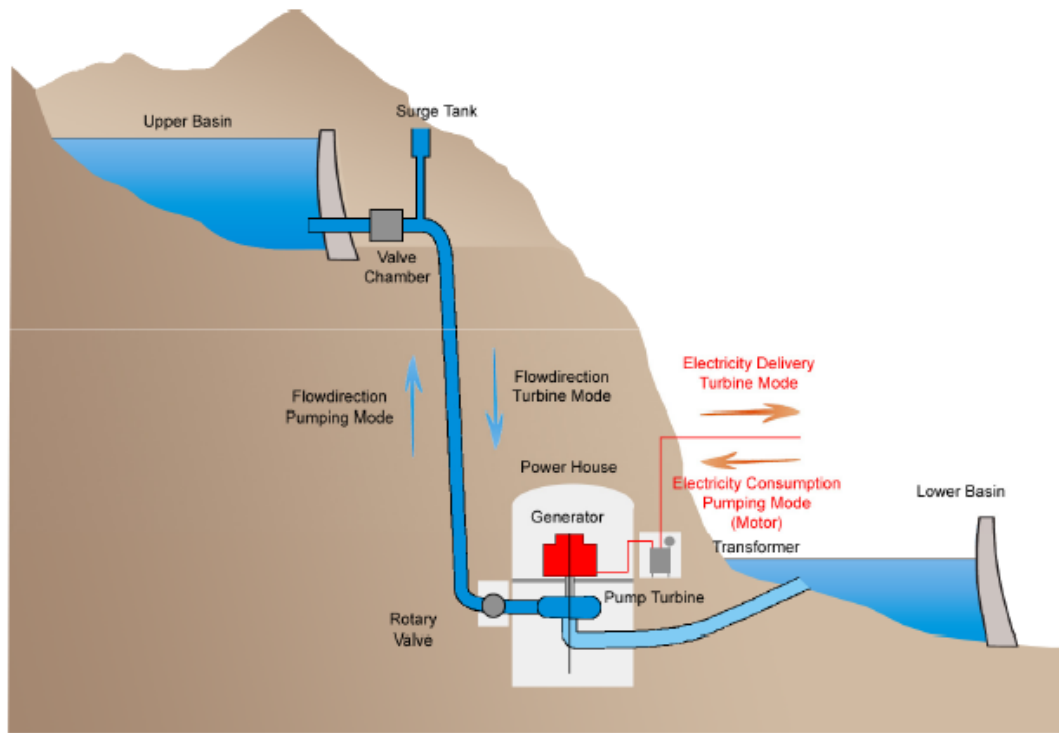


Figure 2: Pump Storage Main Operations [9]

In case of a surplus of power in the network, an electric motor drives a pump or pump turbine, pumping water from the lower reservoir up to a higher storage reservoir. On the other hand, if there is a demand for electricity, water is released back through the turbine or pump turbine. The turbine is used to drive the generator and within seconds electricity is generated and fed into the grid. Figure 2 shows a typical pumped storage layout.

The amount of energy that can be stored depends on the height difference between the reservoirs and the volume of the reservoir, while the power capacity depends on the size of the pump/turbine. Pumped storage is a mature technology with high efficiency. It is possible to recover more than 80% of the energy that is put into the system, which is very high in comparison to all other storage technologies [3].

Pumped storage power plants are able to react within short time to network fluctuations. Modern systems can start pump/turbine operation in just 30 seconds

from standstill. In the event of a power failure, pumped storage power plants can re-establish the power supply to the network without an external energy supply.

### 2.1.3   Norway Balancing Europe

Regarding electricity, Norway is very unique, since most of our electrical production comes from stored hydropower. Hydropower represents 99 % of the total electric power production in Norway and Norway's average annual hydro production of 124 TWh is the highest in Europe. In 2011 the total installed hydropower generation capacity was 29,6 GW, where 23,4 GW was in reservoir power stations. The total reservoir capacity is 84 TWh or 70 % of the annual generation. As mentioned earlier, Norway also has half of all hydropower storage in Europe [10]. The typical Norwegian hydropower system can be characterized by high head, and storage is often a combination of natural lakes with dams in order to increase the storage capacity above the natural level.

In Norway there are few existing pumped storage power plants in operation, with a total installed capacity of 1 GW. The largest one is Saurdal in the municipality of Rogaland. The power is 640 MW and the height difference between the lower and upper reservoir is 500 m. The upper reservoir, Blåsjø, is Norway's largest reservoir measured in energy. Most pumped hydropower plants in Norway are used for energy storage across seasons (from summer to winter), in order to take advantage of large rainfall during the fall and melted snow during spring. In most other areas, pumped hydropower plants are primarily used for daily regulation. Water is pumped up during the night when the price and demand is low, and hydropower is produced during the day when the price and demand is high.

Hydropower from reservoirs is simple to regulate and the response time is especially short. Due to capacity constraints in the grid, energy storage may also be needed in Norway. In this case, energy storage enables improved use of the grid capacity, and the grid operator avoids expensive expansions of the local grid. A storage solution can encourage local production, since transmission of electricity to the main grid is possible, and at the same time grid expansion is avoided. However, the main demand for energy storage comes from Continental Europe, and Norway's interest is mostly based on increased profits through energy trade with Europe.

Norway has a long history with hydropower and great experience with high heads and therefore high pressure systems. Through many years of experience, a technical competence within high pressure Francis- and Pelton turbines, and design of high pressure systems has been developed [11]. This competence gives Norway a great technological advantage regarding pumped storage and Norway has a central

role, among very few nations, to improve this technology.

The Norwegian hydro system has large development possibilities for being able to support the flexibility of the European energy system. It can greatly contribute to balancing and regulation, as well as peak and back-up production. Preliminary studies have identified that expansion possibilities are between 15 and 20 GW using only existing reservoirs, which is positive because it results in low environmental impacts.

Countries such as Germany and Denmark, among many others, are increasingly basing their energy production on renewable energy, such as wind and solar power, and are already experiencing the drawbacks of not having sufficient energy storage. Germany's power production is still dominated by coal and nuclear power plants with low flexibility, and therefore suitable as base load. As the German government has a goal to achieve a 100 % renewable electricity generation by 2050 [1], great amounts of energy storage possibilities will be necessary. Already, Germany is experiencing days where electricity generation from renewable sources is above 50 % of the total generation. Bloomberg sums this well up in the article by the name "In Germany and elsewhere, energy storage is the key to unlocking renewable energy" [12].

Denmark's power consumption is in average covered by 20 % wind power. At times with ideal wind conditions, the power production exceeds the national demand. When possible, this excess power is sold across borders, but there is not always a demand in the market. In these cases the electricity price becomes so low that the production companies have a net loss, due to transmission costs [3]. The cases mentioned are motivators of the strong focus on developing intelligent and economical storage technologies for electricity.

European power companies wish to sell power to Norway during low demand periods. Pumped storage has a possibility of adding value to the Norwegian community through profits from energy export, optimized utilization of the national power grid, and increased security of supply in Norway and in Europe. Connecting to offshore and onshore wind farms will take advantage of the flexible energy storage. Increased transmission capacity between Norway and the Continent will be necessary in order to import/export enough balancing power.

To sum up, Norway can provide a significant back-up to the Continental European electricity system. However, the following challenges need to be met in order to enable Norway to play this role [13]:

- Increased transmission capacity between Norway and Europe
- Incentivizing business models for pumped storage power plants due to market

uncertainty

- Technological issues relating to optimal system layout - minimizing losses and maximizing profits

- Environmental effects

### 2.1.4 Pump & Turbine Configurations

There are two main solutions to obtain both pumping and turbine operation in the same power plant. A pumped storage plant can either use a reversible pump turbine or be designed as a twin system that consists of separate generating and pumping equipment. The impeller on a reversible pump turbine is designed both for turbine and pump operation. For a twin system the impeller is designed only for turbine operation while the pump is designed exclusively for pump operation. A detailed description of these two solutions can be found in the specialization project [14]. To summarize, table 2 compares the two main technical solutions.

| *Concept* | *Twin System* | *Reversible Pump Turbine* |
|---|---|---|
| Investment | - | + |
| Size | - | + |
| Efficiency | + | - |
| Installation depth | + | - |
| Pressure head | + | - |
| Transition time P->T/T->P | + | - |
| Operation cost | - | + |
| Maintenance | - | + |
| Technical risk | - | + |

Table 2: Comparison of ternary systems and reversible pump turbines [16, 1]

A pump and a pump turbine in pump operation have similar efficiency, while a pump turbine in turbine operation has a lower efficiency than a turbine. This is a huge factor deciding which of the alternatives is the most economic. In Norway the most common choice has been a pump turbine [15].

### 2.1.5 Electrical System Overview

This chapter briefly presents the various power systems applicable for pumped storage plants. The power systems can be categorized into three different groups
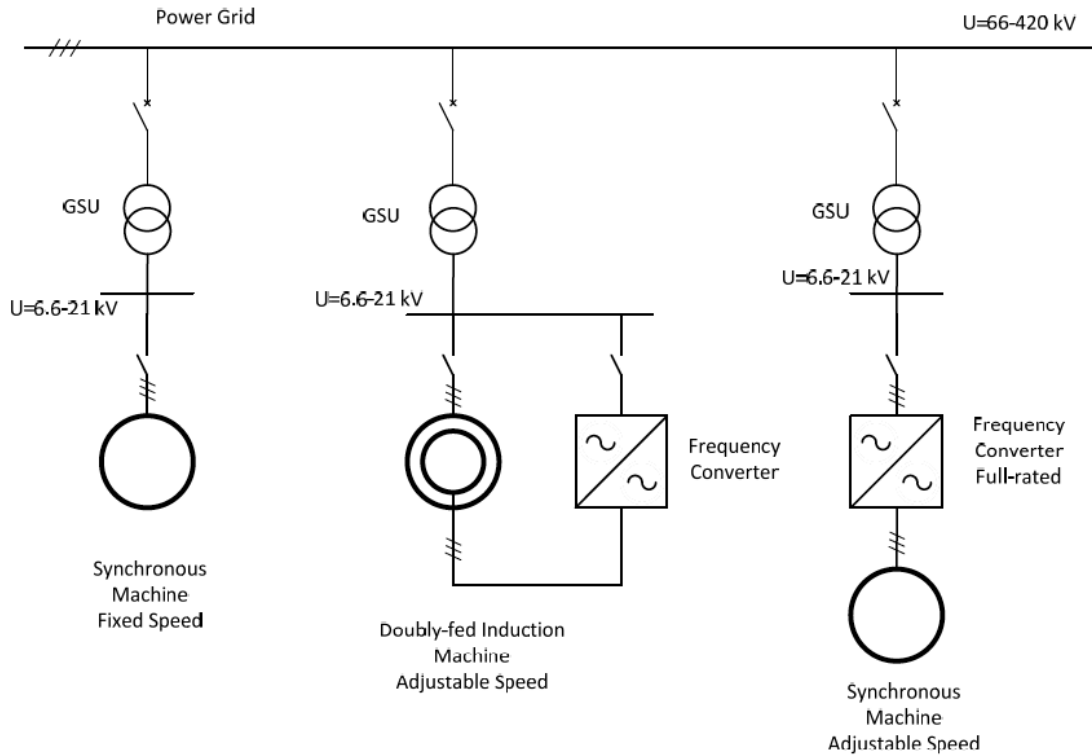
Figure 3: Three basic electric systems for pumped storage. Fixed speed (left), adjustable speed with a doubly-fed induction machine (middle) and adjustable speed with full rated frequency converter and synchronous machine (right) [18]

given by the generator and the converter technology. An overview of the three systems is shown in figure 3.

The three main electrical systems are covered in the following sections. A brief description of the two types of electrical machines applicable for pumped storage is given in the specialization project [14].

### 2.1.5.1   Fixed Speed Systems

The fixed speed system consists of a synchronous machine connected directly to the power system. This is the simplest solution and also the most dominating in use today. These systems run at constant speed and are therefore used for bulk energy storage. Pumping can be done during the night utilizing cheap electricity and the energy can be regenerated during peak hours with high electricity prices.

If it is used with a reversible turbine, a soft-starter or start-up motor is used. When the machine reaches synchronous speed, it is connected directly to the power grid by a circuit breaker. State-of-the-art within starting methods is to use static frequency converters (soft-starters) [17]. Soft-starters reduce the load both on the machine and the power grid due to excellent controllability [18].

Advantages and drawbacks of the fixed speed system based on a synchronous machine are summarised in table 3.

| Advantages | Drawbacks |
|---|---|
| + Conventional & reliable technology | - Limited operating area |
| + Low cost | - Constant load in pump mode |
| + Energy recovery during braking | (no power control) |
| (with start-up converter) | |

Table 3: Advantages and drawbacks of the fixed speed synchronous machine [1]

### 2.1.5.2 Adjustable Speed Systems

One of the most important advances during the last decades has been the development of adjustable speed systems to allow for controllable power in the pumping mode [18]. Such systems use a reversible Francis-turbine and a power electronically controlled machine. They have been constructed commercially in Japan since the early 1990's and have recently also been introduced in Europe [18]. Pumped storage plants with high degree of controllability both in generating mode and in pumping mode are needed to improve the daily balance between production and load, as well as to improve the frequency control of systems with large share of nuclear, thermal, wind or photovoltaic [18].

Regarding the development of electrical solutions for pumped storage systems, the main issue during the last two decades has been the introduction to power electronic equipment. Power electronics have experienced huge developments in the latter years, and the main achievement for pumped storage has been the development of electronically controlled adjustable speed systems. Adjustable speed operation has several advantages [18, 1]:

- Improving the efficiency

- Optimal speed during turbine and pump operation

- Load/frequency control in pumping mode, as well as turbine mode

- Less vibrations and noise (especially at partial load)

- Lower minimum generation limits for the turbines

- Additional support to dynamic stability problems in weak grids

Adjustable speed improves the turbine efficiency, since the speed corresponding to maximum efficiency is different for turbine and pump operation. The efficiency also varies for different heads, and adjustable speed may be necessary for plants with large variations in water head.

Traditional pump-turbines with synchronous machines operate at constant speed and therefore constant power for pumping operation. Adjustable speed systems allow power control in pumping mode, as well as extending the allowable operation range in generator mode [18]. This means that for a given pressure head, the power delivered to the pump can be varied, and therefore also the water flow. If the speed can be varied to +/- 10% of synchronous speed, the power can be varied to +/- 30% with today's technology [1]. This allows the power station to adjust to various needs in the power grid.

Adjustable speed systems can be operated with both synchronous and induction machines. Both solutions require frequency converters. The two main configurations to achieve adjustable speed operation are covered below.

**Full Rated Frequency Converter Systems**

This configuration consists of a full rated frequency converter connected to the stator of the synchronous generator. With increased rating of semi-conductor switches and available high-power motor drives based on the voltage source converter topology, this configuration is an attractive solution [20]. The layout is shown in figure 4 and, as shown, it will be possible to bypass the converter and operate the machine directly connected to the grid. This can provide redundancy for the converter in the case of operational problems [18].

Advantages and drawbacks of the full rated frequency converter system based on a synchronous machine are summarised in table 4.

Due to design constraints, frequency converters only exist for power ratings up to about 100 MW. For medium and large systems, a design based on an induction machine will be economically preferable [1].

13
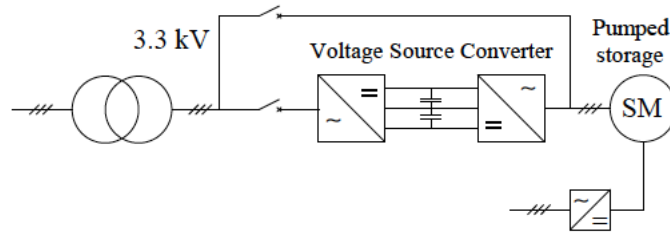
Figure 4: Schematic configuration of a full rated converter system with a synchronous machine [18]

| Advantages | Drawbacks |
|---|---|
| + Flexible operating area in turbine & pump operation | - Expensive frequency converter |
| + No need for start-up converter | - Generation limit at about 100MW for frequency converter |
| + Energy recovery during braking | |
| + Synchronous generator has low cost | |
| + Low maintenance requirements for synchronous generator | |
| + Operation direction can change with filled water way | |

Table 4: Advantages and drawbacks of the full rated converter with synchronous machine [1]

**Doubly-Fed Induction Machine Systems**

This configuration consists of a partially rated frequency converter connected to the rotor of the induction machine. With this configuration, variable speed can be obtained with a partially rated frequency converter (less than the generator rating). This is the preferred system in large scale implementations of pumped storage, since the converters rating does not limit the total system rating. Another advantage is that the reactive power to and from the grid can be controlled. This can be utilized for voltage control in the grid and contribute to improve the stability and the operating conditions in the rest of the power system [18]. Figure 5 shows two basic configurations. Solutions with cycloconverters are suitable solutions and can be made with rugged design for high capacity and low losses [18]. However, today the most preferred topology is the back-to-back voltage source converter, and it has been used in some of the most recent pumped storage implementations [18].

14

The back-to-back converter system is able to generate power both above and below synchronous speed. The configuration is often called doubly-fed induction generator (DFIG), which emphasizes the ability to transfer power into or out of the rotor, as well as out of the stator. The back-to-back converter is connected between the rotor of the DFIG and the three winding transformer (to the grid), while the stator is connected directly to the transformer and then to grid. In this topology, the power converter is partially scaled requiring a rated power of about 30% of the overall generated power.
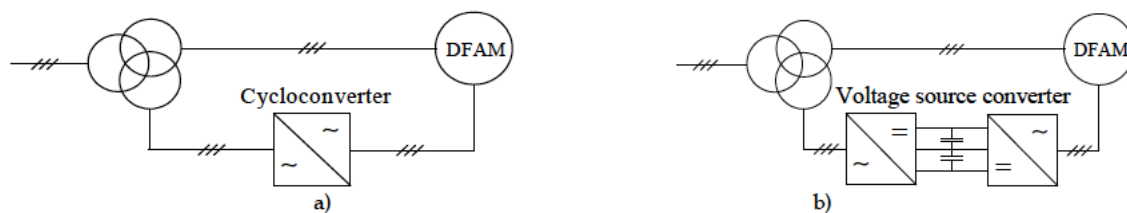


Figure 5: Basic configurations of doubly-fed induction machines: a) system with a cycloconverter, b) system with a back-to-back voltage source converter [18]

Advantages and drawbacks of the doubly-fed induction machine system are summarised in table 5.

| Advantages | Drawbacks |
|---|---|
| + Flexible operating area in turbine & pump mode | - More complicated maintenance for asynchronous machines |
| + Possible for generator ratings > 100MW | - Needs separate rotor transformer and converter |
| + Energy recovery during braking | - Doubly-fed induction machines are more expensive |
| + Reactive power control to/from grid | |

Table 5: Advantages and drawbacks of the doubly-fed induction machine system [1]

Toshiba [21] has delivered pumped storage variable speed systems since 1990.

## 2.2 High Voltage DC Transmission

### 2.2.1 Introduction

In order for Norway to be able to support the European system with balancing power, there must exist sufficient transmission capacity between the separate interconnected networks. The optimal way of achieving this is through HVDC (High Voltage Direct Current) technology, which will be covered in this chapter.

In a HVDC system the electric power is taken from one point in a three-phase AC network, converted to DC in a converter station, transmitted to the receiving point by an overhead line or cable and then converted back to AC in another converter station and injected into the receiving AC network. The HVDC technology is used to transmit electricity over long distances by overhead transmission lines or underground/underwater cables, because it then becomes economically attractive over conventional AC lines due to reduced losses. This breakeven distance for HVDC overhead transmission lines is about 600 km or more, and for submarine cables longer than approximately 80 km is only possible with HVDC transmission [22].

It is also possible to interconnect two AC systems that are at different frequencies or that are not synchronized, by means of an HVDC transmission line. Other advantageous properties such as the improved transient stability and the dynamic damping of the electrical system oscillations, may influence the selection of DC transmission over AC transmission [23]. With an HVDC system, the power flow can be controlled rapidly and accurately. It is a key enabler in the future energy system based on intermittent renewables and will truly be an inevitable part of the future grid.

ABB pioneered the HVDC technology and is the world leader in this field [24]. Other main suppliers are Alstom [25] and Siemens [26].

The HVDC technologies can be divided into the classical HVDC and the state of the art VSC (Voltage Source Converter) based HVDC.

### 2.2.2 Classic HVDC System

A classical HVDC transmission system for interconnecting two AC systems is shown in figure 6. If we assume the power flow to be from system A to B, the system A voltage is transformed up to the transmission level and then rectified at the sending end converter station. The DC power flows through the HVDC transmission line and is inverted at the receiving end converter station. The AC

voltage is then transformed down to match the voltage of system B. The system also consists of AC filters, reactive compensation equipment, DC smoothing reactors and DC filters. The power flow over the transmission line can be reversed by reversing the polarity of the voltages at both ends.
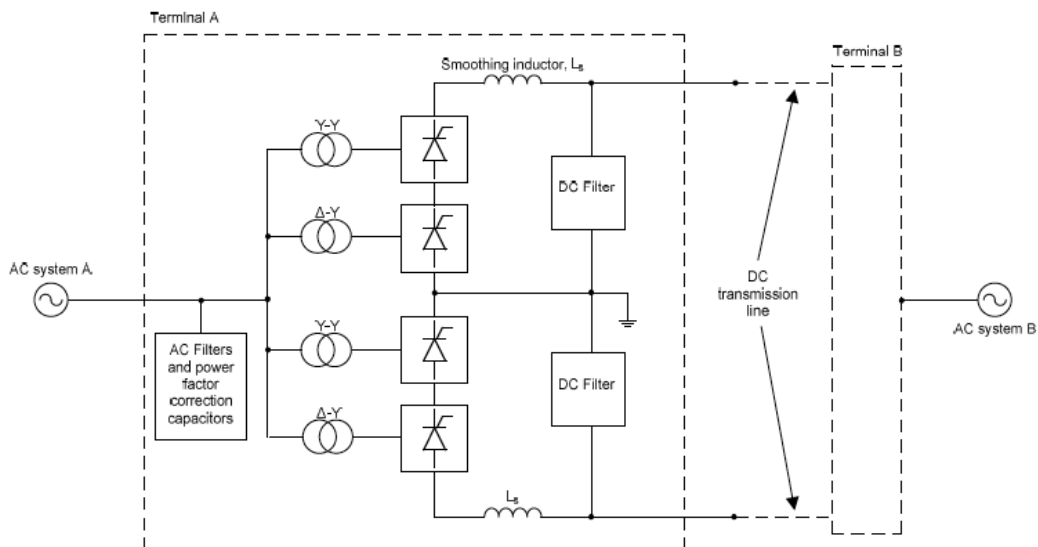


Figure 6: Basic configuration for a classic HVDC transmission [27]

Conventional HVDC transmission consists of line-commutated current source converters (CSCs) with thyristor valves. Each thyristor valve is built up with series-connected thyristors in order to achieve the desired DC voltage rating. Such converters require a synchronous voltage source in order to operate [28]. The basic building block is the three-phase, full-wave bridge referred to as a six-pulse bridge. The term six pulse is due to six switching operations per period resulting in a characteristic harmonic ripple of six times the fundamental frequency in the DC output voltage.

Each converter terminal in figure 6 consists of a positive and a negative pole. Each pole consists of two 6-pulse bridges with AC voltage sources phase displaced by 30 degrees and series connected on the DC side. This arrangement results in 12-pulse operation, which increases the DC voltage. It also reduces both the current harmonics generated on the AC side and the voltage ripple produced on the DC side. The 30 degrees phase displacement is achieved by feeding one bridge through a transformer with a Y-connected secondary and the other bridge through a transformer with a △-connected secondary.

The AC filters are required to reduce the current harmonics generated by the converters and the power factor correction capacitors are included to supply reactive

17

power. On the DC side, the smoothing inductors and DC filters prevent ripple in the DC transmission line current [23].

The power transmitted over the HVDC link is controlled by one of the converters controlling the DC voltage and the other converter regulating the DC current by controlling its output voltage relative to that maintained by the votlage-setting terminal. Since the DC line resistance is low, large changes in current and hence power can be made with relatively small changes in firing angle (alpha). Control of the DC voltage is achieved by varying the delay angle or by adjusting the tap changers of the converter transformers [23]. The control systems of the two converter stations usually communicate through a telecommunication link.

Typically the power rating of a classical HVDC system is in the range 100 MW - 3000 MW.

An HVDC system has a lot of technical advantages compared to AC transmission. Some of these are [24, 25]:

- More economical and efficient over long transmission distances than AC transmission: undersea cable links ( >(50-80) km) and overhead lines ( >600 km).

- Enables interconnection of different grids or networks.

- Fast and accurate control of power flow and voltage. The operator or automatic controller determine how much power flows via the DC link.

- Does not increase the systems short circuit level.

- HVDC enables the integration of remote renewable energy.

- Bidirectional power flow.

- Less environmental impact.

- HVDC prevents the transmission of faults between to connected AC grids, and hence blackouts.

### 2.2.3   VSC-HVDC System

The HVDC transmission based on voltage source converters (VSC), shown in figure 7, is a newer technology where the switching is done by self-commutated IGBT (Insulated Gate Bipolar Transistor) valves. Typically, each IGBT valve consists of several series-connected IGBTs in order to increase the DC bus voltage level (by delivering a higher blocking voltage capability for the converter). The antiparallel

diodes are necessary in order to allow for the bidirectional current flow [23]. The DC bus capacitor provides the required energy storage so that the power flow can be controlled and offers filtering of the DC harmonics. VSC technology can rapidly control both active and reactive power independently of one another. This control gives total flexibility to place converters anywhere in the AC network since there is no restriction on minimum short-circuit capacity [28]. VSC-HVDC technology permits black-start, which means that the converter can be used to synthesize a balanced set of three phased voltages. Unlike conventional HVDC converters, the converters themselves have no reactive power demand and can control their reactive power to regulate the AC system (just like a generator) [28].
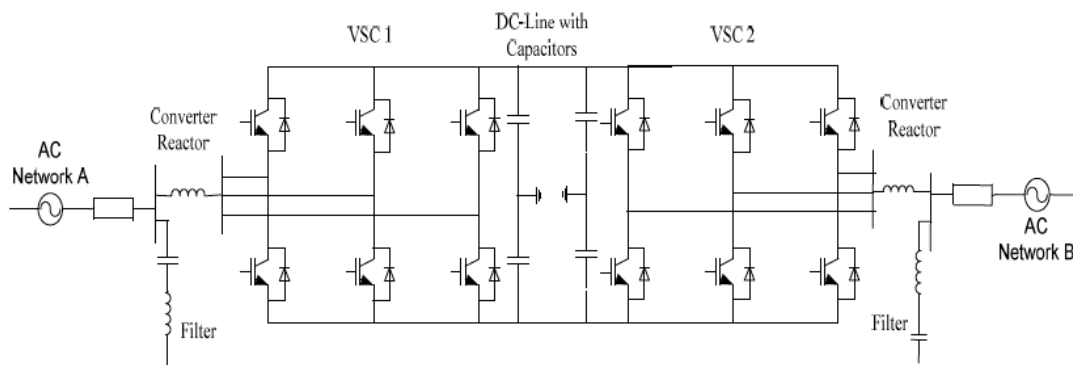


Figure 7: Basic configuration for VSC-HVDC transmission [27]
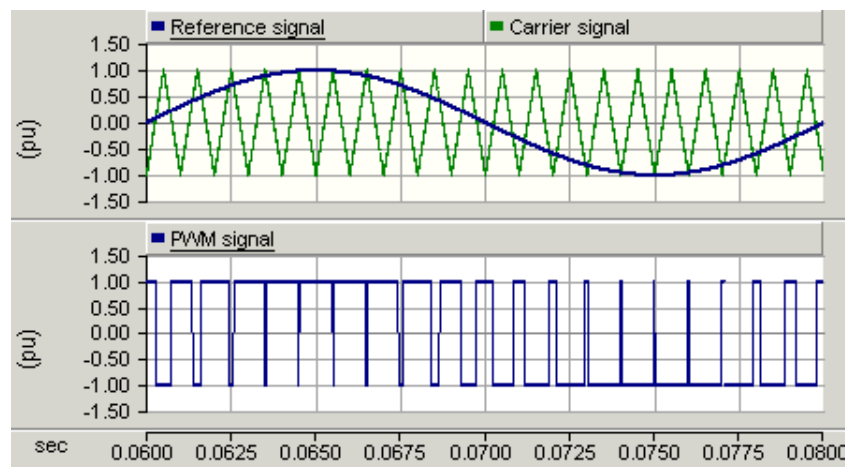


Figure 8: Two-level sinusoidal PWM method: reference (sinusoidal) waveform, carrier (triangular) signal and PWM output voltage waveform

The switches are turned on and off by a control trigger signal generated by different control strategies. A typical switching strategy, sinusoidal PWM (Pulse Width

Modulation), is used to create the desired voltage waveform. This is done by comparing sinusoidal control signals with a triangular waveform, often called the carrier signal, as shown in figure 8. The sinusoidal control signal has a frequency equal to the desired fundamental frequency of the inverter voltage output, in this case equal to 50 Hz, while the frequency of the triangular waveform establishes the switching frequency, $f_s$, in this case 1 kHz. The PWM outputs a signal, which appears to be a sinusoidal wave, even though it is switching between two voltage levels. This is done for each of the three phases (120 degrees phase shifted). Filters are also included on the AC side to reduce the harmonic content flowing into the AC system [29].
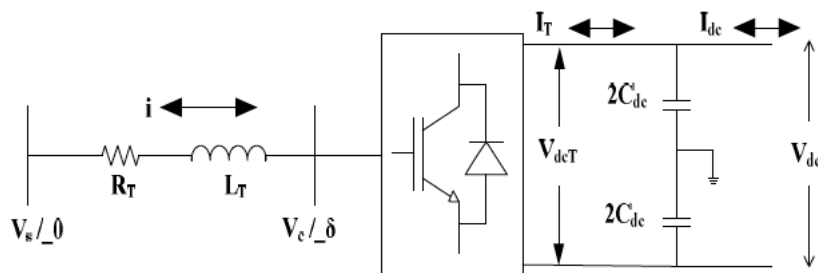


Figure 9: Interconnection of two AC voltage sources through a lossless reactor [29]

The fundamental operation of the VSC-HVDC can be explained by considering the terminal of the voltage source converter connected to the AC transmission system via a series reactor as shown in figure 9. $V_c$ is generated by the VSC and $V_s$ is the AC system voltage. The converter AC voltage fundamental component and DC voltage relationship can be expressed by :

$$V_c(t) = \frac{1}{2} V_{dc} M \sin{(\omega t + \delta)} \tag{1}$$

where M is the modulation index, $\omega$ is the fundamental frequency and $\delta$ is the phase shift between the converter voltage and the system voltage [30].

At the fundamental frequency, the active and reactive powers are defined by the following relationships, assuming an ideal reactor [29]:

$$P = \frac{V_c \sin{\delta}}{X_T} V_s \tag{2}$$

$$Q = \frac{V_s - V_c \cos{\delta}}{X_T} V_s \tag{3}$$

where $\delta$ is the phase angle between the two AC voltages and $X_T$ is the transformer reactance. P and Q can be controlled by controlling $V_s$, $V_c$ and the angle $\delta$ between them. The transformer resistance is small compared to its reactance so it can be neglected. The AC system voltage can be considered as constant in the case of a strong AC system. The only input to the converter is firing pulses to open/close the converter switches. By controlling the phase shift and duration of PWM pulses, the active and reactive powers can be controlled. The pulse width of PWM pulses depends on the modulation index M and the phase shift of the pulses depends on the angle $\delta$ [30].

The independent control of AC voltage magnitude and phase relative to the system voltage allows use of separate active and reactive power control loops for the HVDC system regulation. The active power loop can be set to control either the active power or the DC-side voltage. The reactive power control loop can be set to control either the reactive power or the AC-side voltage. Either of these two modes can be selected independently at either end of the DC link [28].

The VSC-technology extends the economical power range of HVDC transmission down to just a few tens of MW and ranging up to 1200MW and +/-500kV [24]. This technology is available by various names such as HVDC light [24] and HVDC plus [26].

The same applications as for classical HVDC are also valid for VSC-HVDC, but due to the improved performance of VSC-HVDC, there are many more potential applications. In DC transmission, an independent control of active and reactive power, the capability to supply weak networks, black start capability and lower space requirements are some of the advantages. Also bidirectional power flow is possible without changing the polarity of the DC voltage. VSC converters do not require any "driving" system voltage and can build up a 3-phase AC voltage using the DC voltage. Low switching frequencies lead to reduced losses.

VSC-HVDC has many key drivers and applications as follows:

- small, isolated remote loads/generation
- power supply to islands
- infeed to city centers
- offshore generation and deep-sea crossings
- multiterminal systems

### 2.2.4  Comparison

The higher controllability of the VSC-HVDC compared to the classic HVDC is a major difference between the two technologies. Table 6 summarizes the main differences [31].

| *HVDC Classic* | *VSC-HVDC* |
|---|---|
| - Current source converters | - Voltage source converters |
| - Line-commutated thyristor valves | - Self-commutated IGBT valves |
| - Requires 50% reactive power compensation | - Requires no reactive power compensation |
| - Converter transformers | - Standard transformers |
| - Minimum short circuit capacity | - No minimum short circuit capacity, |
| > 2x converter rating | black start |
| - 100 - 3000 MW | - 10's - 1200 MW |

Table 6: Comparison of HVDC classic and VSC-HVDC

### 2.2.5  Existing Installations

In order for Norway to offer balancing services to Continental Europe, sufficient transmission capacity is a must. Table 7 lists the existing HVDC transmission lines connecting Norway and the Continent [32]. The 580 km long NorNed link is the longest submarine high-voltage cable in the world [33]. All connections extend from Southern Norway.

| *Name* | *To* | *P [MW]* | *DC Volt. [kV]* | *Length [km]* | *Year* |
|---|---|---|---|---|---|
| Skagerrak 1&2 | Tjele (DK) | 500 | 250 | 240 | 1977 |
| Skagerrak 3 | Tjele (DK) | 440 | 350 | 240 | 1993 |
| NorNed | Eemshaven (NL) | 700 | 450 | 580 | 2008 |
| Skagerrak 4 | Tjele (DK) | 700 | 500 | 244 | 2014 |

Table 7: Existing HVDC connections between Norway and Europe

There exist two HVDC cables from Norway to offshore plattforms Troll A and Valhall. The use of HVDC for green electrification of oil platforms in the North Sea is yet another use of the technology. Other HVDC transmission systems are under discussion, such as a connection to the UK with a power rating of 1.2 GW and a 600 MW connection to Germany.

## 2.3 Basic Machine & Control Theory

### 2.3.1 Introduction

This section covers basic machine and control theory, which is a basis for the control developed in the next chapter. A brief description of the synchronous machine is followed by some basic control theory, including the transformation to the d-q rotating reference frame, and the last section introduces the per unit system.

### 2.3.2 Synchronous Machine

The motivation of this section is to give a basic understanding of the synchronous machine in order to better understand the control required and its function in the total electrical system for the pumped storage plant.

Electrical machines can be used both as a motor or a generator. The operation is defined by the direction of the power flow. The rotational speed of the machine depends on the number of poles and the input voltage frequency. Varying the frequency of the input voltage can control the speed, since the number of poles cannot be changed for a specific construction.

#### 2.3.2.1 Structure and Equivalent Circuit

A synchronous machine is an AC machine whose speed under steady-state conditions is proportional to the frequency of the current in its armature. The machine consists of a stator and a rotor, both made of magnetic steel. The armature winding, which carries the load current and supplies power to the system, is placed in slots on the inner surface of the stator and consists of three identical phase windings. The field winding is wound on the rotor. The rotor has additional short-circuited damper windings to help damp mechanical oscillations of the rotor. The damper windings are mounted in axial slots in the pole face. The field winding is excited by direct current to produce a rotating magnetic flux, the strength of which is proportional to the excitation current. The power rating of the exciter is usually in the range 0.2-0.8 % of the generator's MW rating.

During generator operation the rotor is turned at a constant speed by a source of mechanical power connected to its shaft. The rotating magnetic flux induces an electromotive force (emf) in each phase of the three-phase stator armature winding, which forces alternating currents to flow out to the power system. The

induced sinusoidal voltage has the same frequency (Hz) as the speed of the rotor: the electrical frequency is synchronized with the mechanical speed [34].
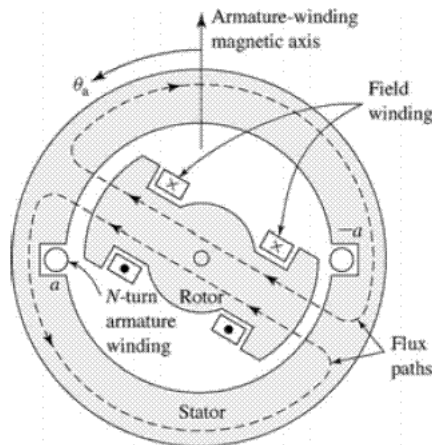


Figure 10: Single phase synchronous machine

A salient pole construction (rather than cylindrical rotor) as shown in figure 10 is characteristic of hydroelectric generators because hydraulic turbines operate at relatively low speeds, typically 500 rpm, and hence a relatively large number of poles is required to produce the desired frequency (often 50 or 60 Hz). High speed generators are typically driven by steam or gas turbines and have few pole pairs, a small diameter and run at, for example, 3000 rpm or 1500 rpm. The number of poles depends on the required speed and nominal frequency of the power system, according to equation 4. Where n is the mechanical speed in revolutions per minute and f is the electrical frequency. Although the figure 10 shows a single-phase machine, most power systems are three phase systems, and a minimum of three coils phase-displaced by 120 electrical degrees in space are used.

$$poles = \frac{60}{n} * \frac{2}{f} \tag{4}$$

Today, most synchronous machines are found with a power electronic interface and generate large amounts of electricity. The power electronics control the reactive power and also allow the machine to operate at a different speed than the system frequency.

Figure 11 shows the equivalent circuit, on a per-phase basis, of a synchronous machine. $E_f$ is the internally-induced back-emf, while $V_t$ is the terminal (or grid) voltage. $V_t$ is chosen as the reference phasor and the torque angle $\delta$ associated with $E_f$ is positive in the generator mode. Following the generator convention,
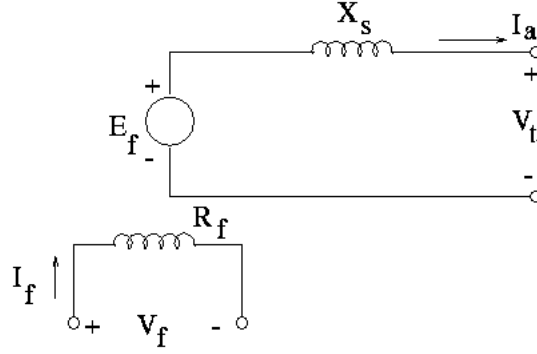
Figure 11: Simplified equivalent circuit for a synchronous machine [34]

the current is defined as being supplied by the synchronous generator and is defined as:

$$I_a = \frac{E_f - V_t}{jX_s} = \frac{\hat{E}_f \sin \delta}{X_s} - \frac{\hat{E}_f \cos \delta - \hat{V}_t}{X_s} \qquad (5)$$

### 2.3.2.2   Active & Reactive Power Control

The total (three-phase) power supplied by the generator, in terms of rms quantities, is:

$$P_{em} = \frac{3E_f V_t \sin \delta}{X_s} \qquad (6)$$

If the field current is constant, $E_f$ at synchronous speed is also constant, and thus the power output of the generator is proportional to the sine of the torque angle $\delta$. The maximum power supplied by the synchronous generator reaches its peak at $\delta = 90°$, as shown in figure 12. Loss of synchronism happens when $\delta > 90°$ and to avoid this generators are often operated with $\delta$ in a range of 30 to 45 degrees. The torque in the third quadrant is negative because this represents motor operation where the armature current direction is reversed. Figure 13 shows the synchronous machine phasor diagrams for motor and generator operation.

The reactive power associated with synchronous machines can be controlled in magnitude as well as in sign. This is achieved by changes in field current, and hence the rotor-produced field. In the case of a lagging power factor, the rotor field current is so small that some reactive power is required from the power supply,
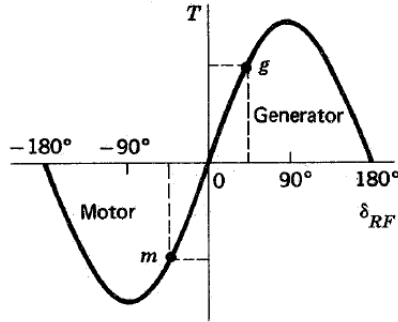
Figure 12: Electromagnetic torque vs. load angle [34]
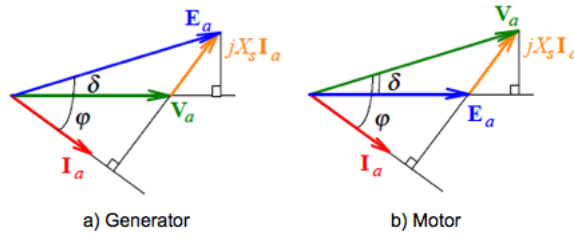


Figure 13: Synchronous machine phasor diagrams

and hence the current lags the terminal voltage. This state is known as under excitation. Similarly, if the rotor field current is more than required, reactive power is produced and this state is known as over excitation [36]. The reactive power is calculated from the reactive component of the armature current given in equation 7.

$$Q = \frac{3}{2} \hat{V} I_{a,q} \tag{7}$$

Let us assume that the prime mover is a hydro turbine. If the active power demand increases, the power reference $P_{ref}$ to the turbine governor will be increased. The governor will control the gate opening to let more water through, which will increase the electrical power generation of the turbine. This happens while keeping the field voltage constant. The change in active power will decrease the reactive power as seen in figure 14.

Another example of control is to increase the field current, which will in turn increase the field voltage. Since the terminal voltage and active power is constant, this causes an increase in the reactive power.
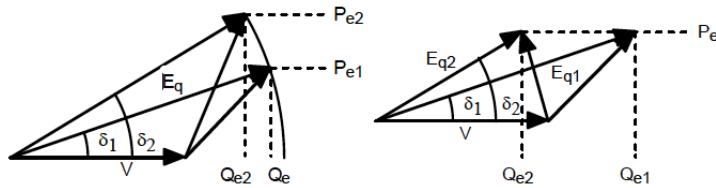
Figure 14: Control examples [55]

### 2.3.2.3 Torque

In motor operation, the torque produced by the stator windings in a synchronous machine with two poles is [35]:

$$T_{em} = k_T \hat{I}_s, \qquad where \qquad k_T = \pi \frac{N_s}{2} r l \hat{B}_r \qquad (8)$$

$k_T$ is the machine torque constant, which has the units of Nm/A and is usually listed in the motor specification sheet. The equation shows that by controlling the stator phase currents so that the corresponding stator current space vector is ahead of the rotor-produced flux density space vector by 90 degrees, the torque developed is only proportional to $\hat{I}_s$ [36]. The electromagnetic torque produced by the rotor is equal to that in equation 8 in the opposite direction.

### 2.3.2.4 Turbine & Governing System

A turbine is equipped with a governing system to provide a means by which the turbine can be started, run up to the operating speed and operate on load with the required power output. Hydraulic turbines derive power from the force exerted by water as it falls from an upper to a lower reservoir. Hydro-electric power plants are classified as high-, medium- or low-head plants. Hydro turbines typically use a large volume of water, require large water passages and operate at low speed. The low rotational speed requires a large generator diameter. In operation, the water enters the turbine from the intake passage or penstock, passes through wicket gates and onto the runner of the turbine. The moveable wicket gates, with their axes parallel to the main shaft, control the power output of the turbine.

Governing systems used to be of a mechanical-hydraulic type and used the Watt centrifugal mechanism as the speed governor [37]. New machines use an electro-

hydraulic governor. In these systems the turbine rotor speed is measured electronically with high accuracy. The resulting electrical signal is amplified and acts on the pilot valve via an electro-hydraulic converter. High forces are required to move the control gates in hydro turbines and as a result hydro turbine governing systems usually employ two cascaded servomotors.

For stable operation the turbine must have a power-speed characteristic such that as the speed increases the mechanical input power reduces. Similarly, a decrease in speed should result in an increase of power. This will restore the balance between the electrical output power and mechanical input power.

The turbine and the governing system are responsible for controlling the torque, speed, and position of the mechanical system. They will be covered in more detail, and the model used for the test system will be developed in the next chapter.

### 2.3.3 Swing Equation

Important equations in power system stability analysis are the rotational inertia equations describing the effect of unbalance between the electromagnetic torque and the mechanical torque of the machine. The swing equation will now be developed in per unit form [37].

An unbalance between the torques acting on the rotor, the net torque, causes acceleration (or deceleration) according to equation 9.

$$T_a = T_m - T_e \tag{9}$$

Where $T_a$ is the accelerating torque, $T_m$ is the mechanical torque, and $T_e$ is the electromagnetic torque, all in Nm. The mechanical and electromagnetic torque are positive for a generator and negative for a motor. The combined inertia of the generator and prime mover is accelerated by the unbalance in the applied torques, hence the swing equation (or equation of motion) is given in equation 10. Under steady state $T_m = T_e$, and there is no acceleration.

$$J_{eq}\frac{d\omega}{dt} = T_a = T_m - T_e \tag{10}$$

where $J_{eq}[kgm^2]$ is the equivalent combined (generator and turbine) moment of inertia and $\omega$ is the angular velocity of the rotor in rad/s. The equation can also be expressed in terms of power, based on $P = \omega T$ as in equation 11.

$$P_e - P_m = J_{eq}\omega\frac{d\omega}{dt} \tag{11}$$

where $P_e$ and $P_m$ are, respectively, the electrical and mechanical power. The control of the mechanical power involves controlling the opening of the "water gate" and, in turn, the amount of water which runs through the turbine, and therefore also the amount of electrical power produced. From the swing equation we can see that under balanced conditions $P_e = P_m$ and the change in mechanical speed is therefore zero. If $P_e > P_m$, the derivative of the angular velocity is positive, which shows that the shaft rotation increases until a new balanced condition is achieved. If $P_e < P_m$ the opposite will occur.

Figure 15 shows the torques acting on the shaft between the turbine and the machine.
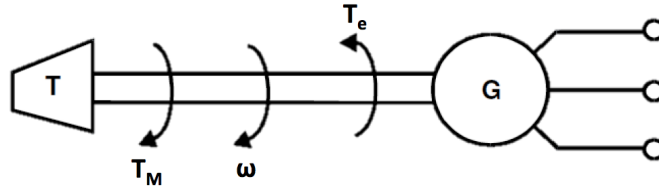


Figure 15: Mechanical and electrical torque applied to the shaft

The inertia constant, H, is defined as the kinetic energy in watt-seconds at rated speed divided by the VA base, as given in equation 12.

$$H = \frac{1}{2}\frac{J\omega_{base}^2}{S_{base}} \tag{12}$$

Rearranging to get the moment of inertia, J, in terms of H and substituting in equation 10 gives:

$$\frac{2H}{\omega_{base}^2}S_{base}\frac{d\omega}{dt} = T_m - T_e \tag{13}$$

Rearranging yields:

$$2H\frac{d}{dt}\left(\frac{\omega}{\omega_{base}}\right) = \frac{T_m - T_e}{S_{base}/\omega_{base}} \tag{14}$$

Noting that $T_{base} = S_{base}/\omega_{base}$, the swing equation in per unit form is achieved.

$$2H\frac{d\omega}{dt} = T_m - T_e \tag{15}$$

The mechanical starting time, $T_M$, is the time required for rated torque to accelerate the rotor from standstill to rated speed and is given by equation 16.

$$T_M = 2H \tag{16}$$

Typical values of H, representing the combined inertia of the generator and turbine, for a hydraulic unit are 2-4 s [37].

### 2.3.4 Basic Control Theory

#### 2.3.4.1 The PI controller

The PI (proportional + integral) controller is widely used in industrial control systems. The proportional function multiplies the current error by a set value P and subtracts the resultant value from the process's input. The main problem is that it often will overreact to small errors, causing the system to oscillate. It is also almost impossible to avoid a constant error at steady state. The integral part integrates the error over a period of time (average error). This is then multiplied by a constant and subtracted from the process's input. The integral term subtracts part of the average error, hence the steady state error is reduced to zero, as well as reducing the oscillations. The transfer function of an ideal PI controller is:

$$H_r(s) = K_p + \frac{K_i}{s} = K_p(1 + \frac{1}{T_i s}) = K_p(\frac{1 + T_i s}{T_i s}) \tag{17}$$

where $K_p$ is the proportional gain and $T_i = \frac{K_p}{K_i}$ is the integration time [38].

The reference signal must be constant in order to obtain zero steady-state deviation by use of a PI controller.

#### 2.3.4.2 Feed-Forward

Feed-forward is a main principle in control theory, which is used when a process is exposed to a disturbance that causes the output signal to differ from what is wanted. In this case, a feed-forward is used to generate a change in the control

30

signal so that the control signal will suppress the effect of the disturbance on the process [38]. The ideal feed-forward is achieved by completely offsetting the disturbance on the process.

### 2.3.4.3 Poles and Zeros

If we consider a linear system with the transfer function:

$G(s) = \frac{b(s)}{a(s)}$

Zeros are the roots of the numerator, b(s), obtained by setting it equal to zero and solving for s. The poles are the roots of the denominator, a(s), obtained by setting it equal to zero and solving for s. A restriction is that a transfer function must not have more zeros than poles.

Poles and zeros of a transfer function are the frequencies for which the value of the transfer function becomes infinity or zero respectively. The values of the poles and the zeros of a system determine whether the system is stable and therefore its performance.

### 2.3.5 DQ Transformation

DQ transformation is the transformation of coordinates from the three-phase stationary abc system to the rotating d-q system. The transformation is done in the two steps given below, and the transformation matrices are given in appendix C1.

1. Clark transformation: a transformation from the three-phase stationary coordinate system to the two-phase $\alpha - \beta$ stationary coordinate system.

2. Park transformation: a transformation from the two-phase $\alpha - \beta$ stationary coordinate system to the two-phase d-q rotating coordinate system.

The reference frames and transformations are shown in figure 16. The stationary $\alpha$-axis is chosen to be aligned with the stationary three-phase a-axis to simplify analysis. The d-q reference frame rotates at synchronous speed $\omega$ with respect to the abc and $\alpha - \beta$ reference frame. At any instant the position of the d-axis with respect to the $\alpha$-axis is given by $\Theta = \omega t$.

By transforming the three-phase AC variables to the d-q reference frame, they become constant signals. This makes it possible to use simple PI controllers and is one of the reasons why the d-q transformation is used in the control system.
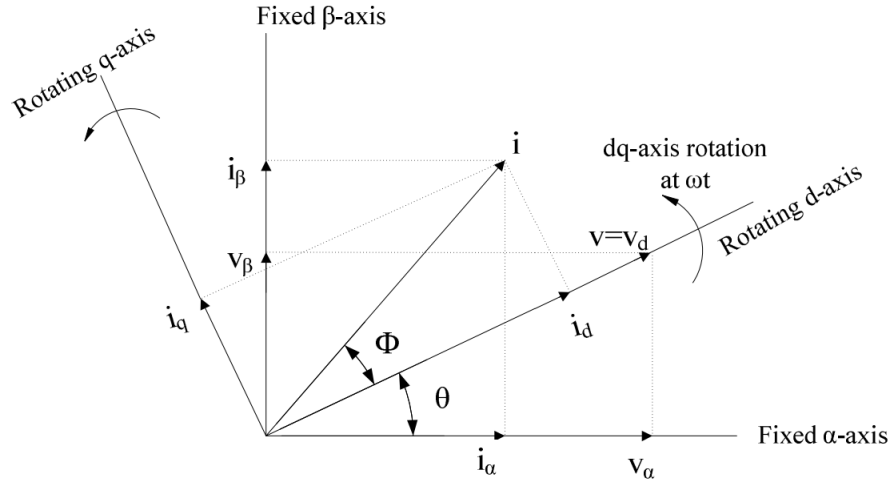
Figure 16: Transformation of axes for vector control [27]

## 2.4 The Per-Unit System

Computations relating to machines, transformers and systems of machines are often carried out in per-unit form. In per-unit all quantities are expressed as decimal fractions of appropriately chosen base values. All the usual computations are then carried out in these per unit values instead of the familiar volts, amperes, ohms, and so on [34].

There are many advantages to the system. One is that the parameter values often fall in a reasonably narrow numerical range when expressed in a per unit system based on machine ratings. This allows quick and easy analysis of results, as well as comparison between different designs and ratings. The general transformation into per-unit form is as follows:

$$Quantity\ in\ per\ unit = \frac{Actual\ quantity}{Base\ value\ of\ quantity} \tag{18}$$

Base values can be chosen arbitrarily as long as the normal electrical laws hold. Important relations between base values in this report are given in equation 19.

$$S_{base}, P_{base}, Q_{base} = \sqrt{3} * V_{L-L,rms} * I_{rms} = 3V_{rms}I_{rms} = \frac{3}{2}V_{peak,ph}I_{peak,ph} \quad \text{(19a)}$$

$$V_{base} = V_{peak,ph} \quad \text{(19b)}$$

$$I_{base} = I_{peak,ph} = \frac{2}{3}\frac{S_{base}}{V_{base}} \quad \text{(19c)}$$

$$Z_{base}, R_{base} = \frac{V_{rms}}{I_{rms}} = \frac{V_{peak,ph}}{I_{peak,ph}} = \frac{V_{base}}{I_{base}} \quad \text{(19d)}$$

$$L_{base} = \frac{Z_{base}}{\omega_{base}} = \frac{Z_{base}}{2\pi * f_{base}} \quad \text{(19e)}$$

$$C_{base} = \frac{1}{Z_{base} * \omega_{base}} = \frac{1}{Z_{base} * 2\pi * f_{base}} \quad \text{(19f)}$$

$$V_{DC,base} = 2 * V_{base} \quad \text{(19g)}$$

$$I_{DC,base} = \frac{S_{base}}{V_{DC,base}} = \frac{3}{4}I_{base} \quad \text{(19h)}$$

$$Z_{DC,base} = \frac{V_{DC,base}}{I_{DC,base}} = \frac{8}{3}Z_{base} \quad \text{(19i)}$$

$$f_{base} = nominal\ system\ frequency \quad \text{(19j)}$$

$$\omega_{base} = 2 * \pi * f_{base} \quad \text{(19k)}$$

Equation 20 shows a necessary relationship between the DC link voltage, $V_{dc}$, and the line to line rms voltage, $V_{LL}$, in order to achieve satisfactory control. This relationship prevents the PWM from going into over modulation, keeping the output current distortion low and therefore to maintain a stabile system [23].

$$V_{dc} \geq 2\frac{\sqrt{2}}{\sqrt{3}}V_{LL,rms} = 2 * V_{peak,ph} \quad \text{(20)}$$

Hence, the base value for the DC voltage is chosen as:

$$V_{DC,base} = 2 * V_{peak,ph} = 2 * V_{base} \quad \text{(21)}$$

The inductor and capacitance bases are derived from their relationship to Z in equation 22, where X and Z both have the unit ohm.

$$Z = R + jX \tag{22a}$$

$$X_L = \omega L \tag{22b}$$

$$X_C = \frac{1}{\omega C} \tag{22c}$$

As seen in equation 19, the voltage and current base values are chosen as the peak phase values. This choice of pu base values has advantages when transformation to the d-q rotating reference frame is used. When the peak values are chosen as base values, the d-axis parameter will equal unity at rated conditions. This allows quick analysis of the results when presented in pu values.

# 3 Simulation Model & Control System Design

## 3.1 Introduction

This chapter starts by introducing the test system. Thereafter the test system is thoroughly described by dividing it into subsections as shown in figure 17, and covering each section on its own. Modeling and control aspects will be the focus of the discussion, and graphs from the simulation model will be used to show important characteristics. The four subsections are (from left to right):

1. Test case load

2. Grid-side converter

3. HVDC transmission line

4. Synchronous machine and converter
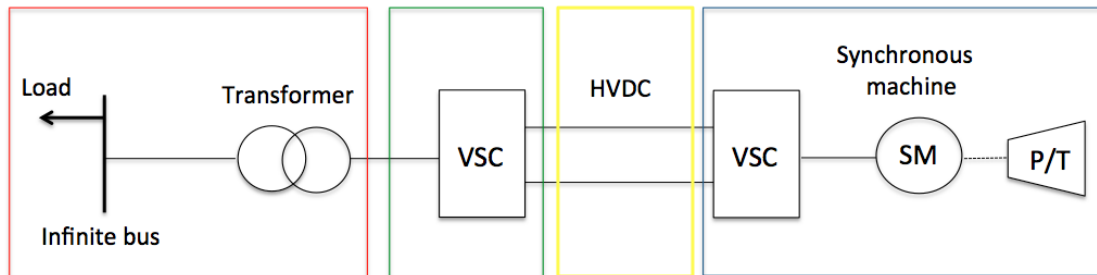


Figure 17: Test system divided into sections

Tuning techniques and optimizing controller parameters has not been a focus of this thesis work and will not be covered. Controller parameters have instead been adapted from a similar model, been given typical values, and when necessary manually tuned to achieve satisfactory operation. Reference [27] discusses tuning techniques in detail.

## 3.2 Test System

The test system consists of a pumped storage hydro plant driven by a synchronous machine, which can run either as a generator or a machine. This is shown in figure 17 where the machine is driving a pump or being driven by a turbine, depending on the operation mode. The power plant is connected by an HVDC cable and via a transformer to an infinite bus, which for our test system is chosen to be Germany.

The pumped storage plant is situated in Southern Norway and will be able to balance both excess and lack of power through pumping or power generation, respectively. At each end of the HVDC line is a converter based on the voltage source technology. These converters allow bidirectional power flow, and convert the voltages between AC and DC. More detailed discussion of the system, regarding both its electrical and control system will be covered in the next sections. Firstly, the main system parameters, the choice of control strategy for the power electronic converters and the choice of topology for the test system will be discussed.

### 3.2.1 Parameters

#### 3.2.1.1 System Parameters

The parameters chosen for the test system are based on the discussion in this section, and the selection is only one of many possibilities.

The pumped storage hydro station is chosen to have a power rating of 100 MW, in both generation and pumping mode.

In Germany, the interconnected system consists of 380 kV and 220 kV systems, which are electrically connected with each other through transformers. The grid voltage on the European side of the test system is chosen to be at 380 kV. International tie-lines from Germany to neighboring countries, as well as tie-lines between foreign partners, link the subsystems to form a synchronous European high voltage system. An HVDC to Germany can therefore balance the European interconnected system.

Based on table 7, the Skagerrak 1&2 HVDC to Denmark has a DC voltage of 250 kV. The test system will transfer less power than the Skagerrak cable, and the DC voltage has been given a lower voltage level of 140 kV. This same DC voltage level is used in the Chatequguay back-to-back station in Quebec, Canada, where the HVDC is used to connect to asynchronous networks.

Equation 20 presented the necessary relationship between the DC link voltage, $V_{dc}$, and the line to line rms voltage, $V_{LL}$, in order to achieve satisfactory control:

$$V_{dc} \geq 2\frac{\sqrt{2}}{\sqrt{3}}V_{LL,rms}$$

Hence, when $V_{dc} = 140kV$, then $V_{LL} \leq 85.7kV$. We choose $V_{LL} = 70kV$. The converter transformer on the European side of the HVDC link has therefore a power rating of 100MVA and a transformation ratio 380 kV : 70 kV.

Table 8 summarizes the main system parameters that have been chosen for the test system.

| Generator | Rated power | 100 MVA |
|---|---|---|
| | Rated terminal line-line voltage | 70 kV |
| | Rated rms line current | 0.82477 kA |
| | Inertia time constant | 5 s |
| **HVDC line** | Rated DC voltage | 140 kV |
| **Transformer** | Rated voltage | 380 kV : 70kV |
| | Reactance | 0.07 pu |
| **Infinite bus** | System frequency | 50 Hz |
| | Rated Voltage | 380 kV |

Table 8: System parameters

The resistance, inductance and capacitance values that are included in the test system are covered in the more detailed sections, and are included to model a more realistic system.

### 3.2.1.2 Synchronous Machine Parameters

Basis for the simulation and controller design has been a synchronous machine in the 100 MVA class, at line voltage 70 kV. It should be noted, that having a synchronous machine operating at such a high line voltage is quite unusual, but for the sake of not complicating the simulations, this has been an assumption. Reducing the line voltage would require a transformer between the machine and the converter station, which would require several changes in the control system.

As mentioned earlier, the test system is a development of the model produced in the thesis work by Suul [19], and therefore the same synchronous machine will be used. The data sheet for this machine, which has a lower voltage and power rating, is given in appendix F3. The reactances and time constants from this machine are also considered representative for a 70 kV, 100 MVA machine. An overview over the basic parameter set of the synchronous machine is given in table 9.

Choosing a different machine with a different parameter set, would involve extensive changes to the control system. This is because these values are used to calculate equivalent circuit parameters to be used in the simulation model. These values are calculated in [19] and are given in table 10. The base values are new for this test system as the power and voltage ratings have changed. All values are given in per-unit, except for the time constants which are in seconds. All values

| $S_n = 100MVA$ | $V_n = 70kV$ | $I_n = 1166A$ |
|---|---|---|
| $x_d = 1.1715$ | $x_0 = 0.0545$ | $T'_d0 = 5.120s$ |
| $x'_d = 0.2563$ | $T'_d = 1.120s$ | $T''_d0 = 0.038s$ |
| $x''_d = 0.1731$ | $T''_d = 0.026s$ | $T''_q0 = 0.133s$ |
| $x_q = 0.5317$ | $T''_q = 0.060s$ | $T_a = 0.163s$ |
| $x'_q = 0.5317$ | $x''_q = 0.2411$ | |

Table 9: Synchronous machine parameter set

given in table 9 are within the standard parameter ranges for hydraulic units as given in [37], except $T''_q0$ which is slightly higher.

| $r_s = 0.0040443$ | $x_{ad} = 1.117$ | $x_{aq} = 0.4772$ |
|---|---|---|
| $r_f = 0.00084756$ | $x_{f\sigma} = 0.2463$ | $x_f = 1.3633$ |
| $r_D = 0.041$ | $x_{D\sigma} = 0.28766$ | $x_D = 1.4047$ |
| $r_Q = 0.028587$ | $x_{Q\sigma} = 0.71725$ | $x_Q = 1.1944$ |
| $\sigma_d = 0.048791$ | $\sigma_f = 0.2205$ | $\sigma_D = 0.25753$ |
| $\sigma_{dD} = 0.24179$ | $\sigma_{Df} = 0.34846$ | |
| $\sigma_q = 0.11421$ | $\sigma_{qQ} = 0.64144$ | |

Table 10: Base values, calculated equivalent circuit parameters and leakage factors

Theory on synchronous machine parameters can be found in [37].

### 3.2.1.3  Per-Unit Base Values

The control system of the simulated test system operates in per unit values. Table 11 summarizes the base values that are used in the simulations based on equation 19, derived in section 2.4. These values are for the system on the converter side of the transformer, where the grid voltage is 70 kV.

| | |
|---|---|
| $S_{base}$ | 100 MW |
| $V_{base}$ | 57,155 kV |
| $I_{base}$ | 1,166 kA |
| $Z_{base}$ | 49 $\Omega$ |
| $L_{base}$ | 0,156 H |
| $C_{base}$ | 64,9612 $\mu$F |
| $V_{DC,base}$ | 114,30952 kV |
| $I_{DC,base}$ | 0,87482 kA |
| $f_{base}$ | 50 Hz |
| $\omega_{base}$ | 314,1593 rad/s |

Table 11: Test system base values

### 3.2.2 Control Strategy

The VSC usually has four different control modes:

1. Constant DC voltage control

2. Constant active power control

3. Constant DC current control

4. Constant AC voltage control

There exist several combinations of possible control schemes, but for the test system the main aim is active power balance. In the test system, the German end voltage source converter is designed as the power controller to control the flow of both active and reactive power. The other converter station is assigned the duty as the DC voltage controller to secure the stability of the DC link voltage. When the DC line power is zero, the two converters can function as independent STATCOMs [40].

This choice of control is quite strategic for the control of the test system, which is a balancing service. The pumped storage hydro has an aim to balance power for Germany. By having the German end control the power flow according to the power balance in the system, the Norwegian end converter station will simply follow this control by keeping a constant DC link voltage, and therefore receive or send the necessary power. This control does not require communication between the converter stations, which is advantageous due to long transmission distances.

### 3.2.3   Topology Decisions

#### 3.2.3.1   Connection Point

The test system has been chosen to connect to Germany, which is an important country when it comes to pumped storage hydropower. Both a lot of the technology and the existing pumped storage plants exist in Germany, and in addition Germany represents a lot of the potential demand for balancing power, being the largest economy in Europe.

Germany's experience with pumped storage, and also knowledge of the market aspects, makes it a possible partner when it comes to implementing a balancing service with connection to Norway. Reference [1] covers the development of pumped storage power in Germany, both when it comes to the market and the technology. It points out how the thermal power has made pumped storage hydropower profitable, but also how the focus on renewables is making pumped storage more attractive.

#### 3.2.3.2   Machine and Converter

As discussed in section 2.1.5, there are two main topologies to achieve variable speed operation of a pumped storage hydro power plant. These are either an induction machine with a partially rated converter system or a synchronous machine with a full rated converter system. From literature it is understood that for high power ratings, the doubly fed induction machine with a partially scaled electronic converter is preferred. This is due to the advantage of having a converter rating of only about 30 % of the total machine rating, and thus economical savings. However, our choice fell on the synchronous machine topology since it is more uncommon. The report named "Electric Systems for Pumped Storage Plants" concludes that little attention has until now been directed towards systems with a full scale voltage source converter and a synchronous machine for driving a variable speed pump-turbine [18]. Recent advances in semiconductor components and voltage source converter drive systems has made this an interesting topology for small and medium sized pumped storage systems and it is therefore chosen for the test system.

To reduce the amount of power electronics and modeling, the synchronous machine is connected directly to an HVDC link in the test system. In this way the HVDC system will play the part of the full-rated frequency converter. An HVDC topology can be compared to a back-to-back converter, but with a higher DC-link voltage

40

level and impedance in the line to model the transmission distance. As will be discussed in the next section, a more realistic topology would be to have a back-to-back voltage source converter, and from there connect to the HVDC line.

### 3.2.3.3 Integration with the System

A pumped storage hydro plant in Norway has various connection possibilities to connect to the rest of the system. Since variable speed has been the subject of discussion, power electronics are required as an interface to the pumped storage plant. This section will shortly introduce a few of the interconnection alternatives.

One alternative is to have the pumped storage plant with a back-to-back voltage source converter connected to the Norwegian grid, and thereafter have the possibility to balance Europe through an HVDC connection. An advantage of this system is that the PSH plant offers increased flexibility to the Norwegian power system as well as to the European.
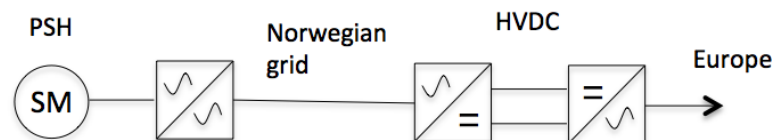


Figure 18: Pumped storage power plant with a back-to-back converter and a HVDC link

Another connection possibility, which is the choice for the test system in this report, is a unit connected pumped storage plant to an HVDC to Europe. This connection is evaluated in [41], and the same connection but with fixed speed generators attracted attention of researchers and system designers as early as 1973 [41]. This configuration allows the pumped storage plant to operate solely as a balancing service to Europe. This topology is chosen for the test system mostly because of its simplified modeling, while the system shown in figure 18 is a more realistic implementation.

Either of the topologies just mentioned can be extended to include several pumped storage plants connected in parallel to increase both the power rating of the system and the DC link voltage. Each of the plants can then be connected or disconnected by switches as shown in figure 19. Alternatively, the generators could be paralleled to a common bus and thereafter connected to converter transformers and converters.

41
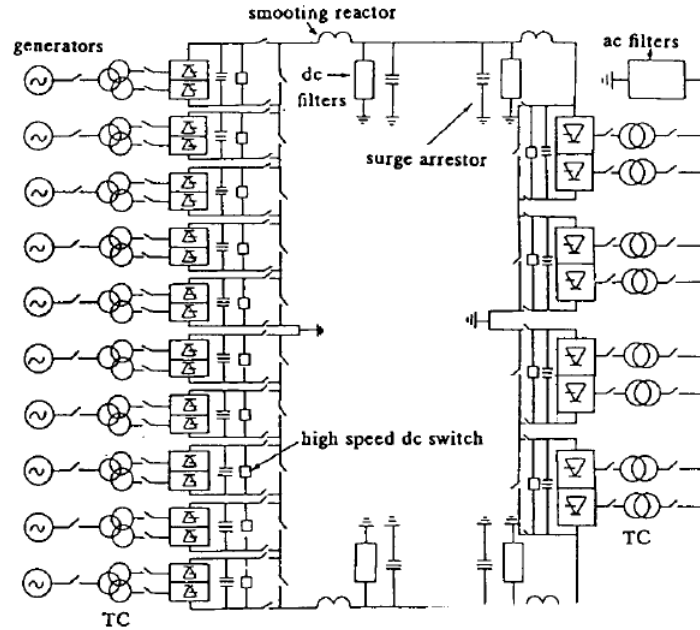
Figure 19: Several power plants in parallel to increase the DC-link voltage and power rating [41]

Alternatively, a topology, which is still facing technical challenges, is the multi-terminal HVDC connection. This configuration could include a separate converter terminal interfacing both the Norwegian grid and the European grid. This could be thought of as a combination of a back-to-back converter and an HVDC, but reducing the number of converter terminals from four to three.

In reality, the economics will play an important part in deciding which interconnection is the most cost effective for a given application. Reference [41] concludes that the unit connection grossly simplifies the station layout, as well as resulting in big capital savings due to elimination of transformers, AC filters and breakers. The disadvantage, as mentioned earlier, is that this topology will not be able to support the Norwegian network.

## 3.3 Test Case Load

### 3.3.1 Electrical Representation

Germany has been chosen to be the load in the test system and the German end of the test system is shown in figure 20. A voltage source decides the voltage

level and models a stiff grid voltage, which can be expected when connecting to a large system, such as Germany. The voltage level is 380 kV and this is assumed to be part of Germany's main high voltage grid. No line impedance is included, but would be necessary if the system was expanded to include end customers and other production, and therefore transmission distances must be included by adding impedances in the line. A transformer steps the voltage down to 70 kV prior to connection with the converter station, which is covered in the next section.
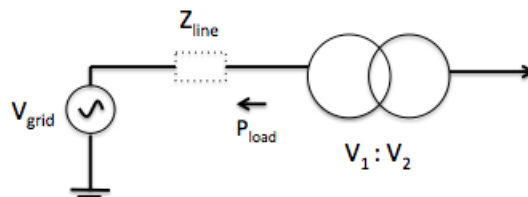


Figure 20: German end of test system

### 3.3.2 Load

The aim of the test system is to balance varying power generation in Germany. To achieve this, the system is developed with the grid side converter controlling the active power flow. The converter detects the lack or excess of power and in turn either feeds the German grid with power or consumes power. In the test system this is achieved by giving the active power reference, $P_{ref}$, values through an input data file.

For the sake of achieving a simulation which is as realistic as possible, real measured data from Amprion is used. Amprion is the transmission system operator with the largest extra-high-voltage grid in Germany and lines stretching from the North of Germany to the Alps in the South. Germany's central geographic position in Europe makes it the number one electricity transit country with interconnection lines to the five neighboring countries. Amprion coordinates the power output and frequency for Germany. The data and graphs presented further in this section are generated in Excel and are from Amprion [42].

Balancing services are becoming increasingly important as renewable energy production, such as wind power, is representing larger shares of the total production. On this basis, the wind power production throughout a day in Germany is used to create the load profile for the test system. Figure 21 shows the wind power production in Germany on May 6 from midnight to midnight, and in steps of 15 minutes.
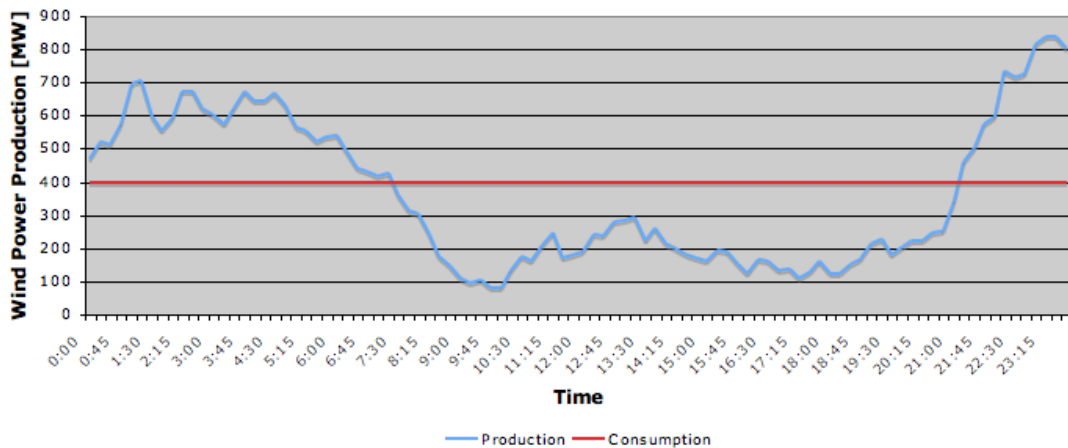
Figure 21: Wind Power Production in Germany May 6

Figure 22 shows the consumption in Germany on May 6. The graph shows the general characteristic that the consumption during the daytime hours is higher than during the night. The consumption during May 6 hits its peak of 26084 MW at 13:15 and its bottom of 15757 MW at 02:30. Comparing the wind power generation and the consumption shows opposite characteristics, which strengthens the need for balancing power. The maximum wind power production is 839 MW, only 3.2 % of the maximum consumption, which makes it hard to actually combine the two graphs.
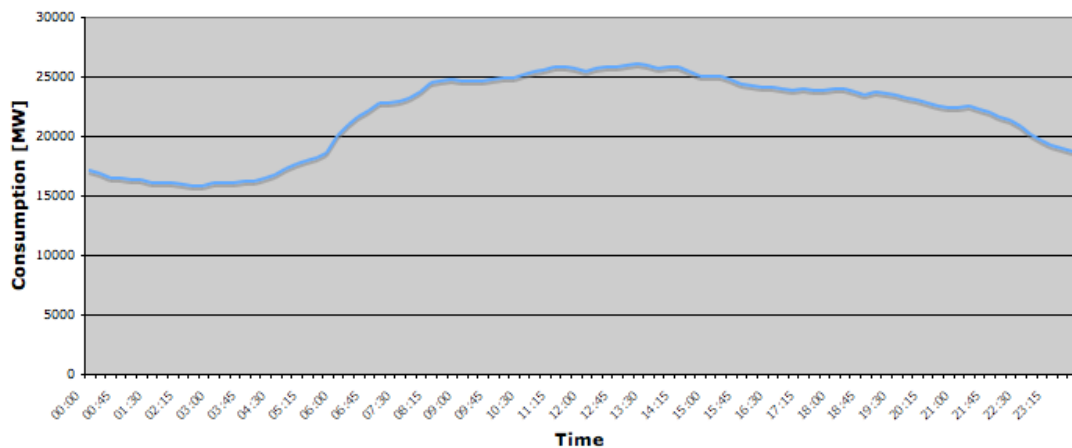


Figure 22: Consumption in Germany May 6

Many assumptions and simplifications are made to create input data for the test

44

system. A main simplification is done by assuming a constant consumption at about half of the maximum wind power production, and thereby showing the need for power consumption during nighttime and power production during daytime, as shown in figure 21. The test system is rated at 100 MW, and it is clear that the test system alone cannot nearly deliver the required balancing power. A simplification to account for this is achieved by assuming that the test system will balance a share of the total system, which is chosen to 40 %.
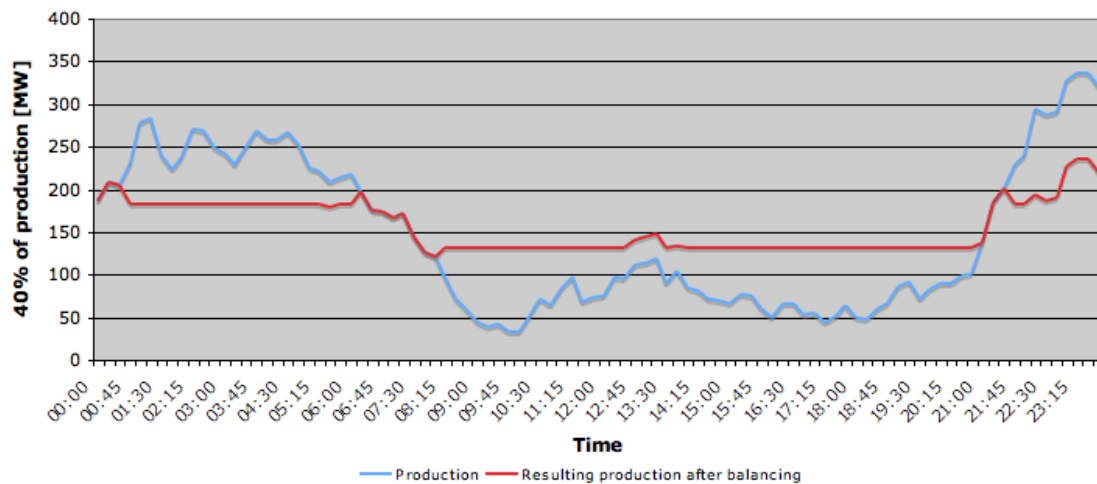


Figure 23: 40% of wind power production in Germany May 6

Another assumption is that the test system can operate between 30 and 100 MW. This is related to the technical characteristics of the synchronous machine and is discussed in section 3.6.3.1. Figure 23 shows 40 % of the wind power production and also the resulting production after balancing. It is obvious that the pumped storage power plant causes the resulting power profile to become more constant and thereby easier to predict. With high renewable penetration from sources such as wind power, such balancing will be necessary to ensure grid stability. Grid stability is ensured through active power balance and thereby stabile frequency, as well as reactive power balance and by this voltage stability.

Figure 24 shows the pump and generation profile, which is used as input to the test system. Pumping operation will in reality be negative. For obvious reasons, the pumping operation, which in graph 24 is separated due to the time axis, has been collected to one continuous section in the input file. Running the simulation is quite time consuming, and therefore each 15 minute interval is instead converted to a 15 second interval in the simulation. In other words, 1 minute from the real time data equals 1 second in the simulation results. The results are expected to
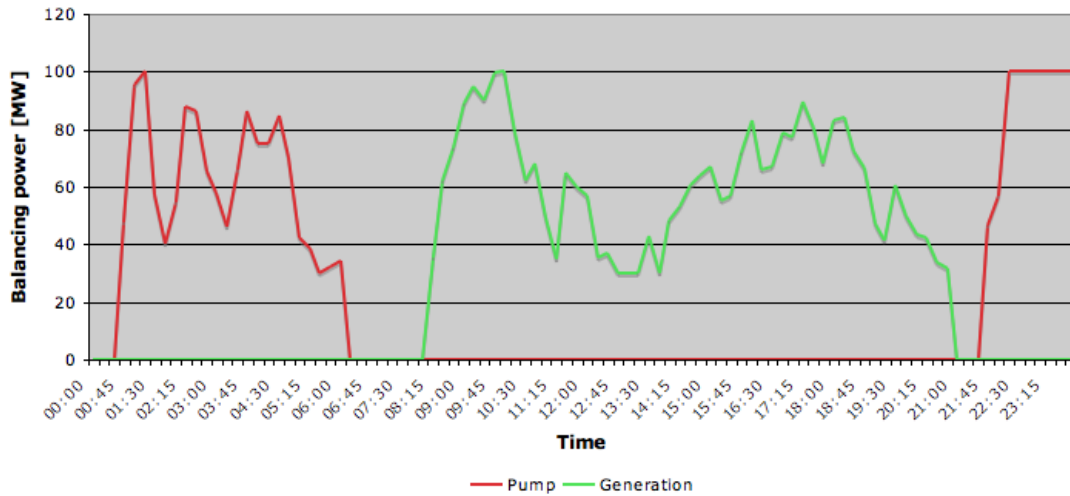
Figure 24: Balancing operation in Germany May 6

be quite similar to the real time simulation and in this way a daily profile can be simulated more effectively.

The overall balancing strategy of a system is something that has not been analyzed in detail here and should be further investigated. The chosen strategy will depend on expected variations in power production and consumption, the rating of the system, maximum and minimum limits, among others.

## 3.4 Grid-side Converter

### 3.4.1 Electrical Representation

The grid-side converter is shown in figure 25. It converts the current between AC and DC, depending on the operation. During pumping operation, the converter acts as a rectifier and converts the AC currents to DC. During generator operation the power flow has changed direction and the converter acts as an inverter, converting the DC currents to AC. An inductor is included on the AC side to reduce the current harmonics and the transformer leakage reactance performs as a second inductance in the filter. A shunt capacitor could be included (shown dashed in the figure), but since the converter is modeled by an average value model (described in section 3.4.2), the filter capacitor does not play an important role, except delivering some reactive power. If a more detailed converter model was used, the filter capacitors would be necessary to absorb the ripple currents generated by the

46

switching.

The series reactor $(L_1)$, between the converter and the grid, is important for control of active and reactive powers, as well as low-pass filtering of the PWM pattern. It also limits the short-circuit currents [43]. The parameter values are explained in appendix F1 and equal: $L = 15.597mH$ and $R = 0.245\Omega$. The AC voltage measurement, which is input to the PLL and voltage control, is done after the filter as shown in the figure.
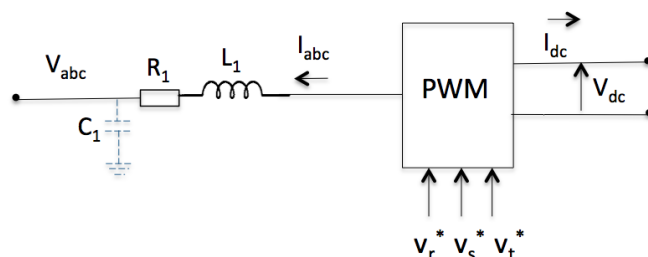


Figure 25: Grid-side converter

The control of a VSC-HVDC system is basically accurate control of energy transfer with an aim to independently control active and reactive power. Different control strategies are found in literature, but the focus of this section will be on the widely used vector control method. Another technique is the Direct Power Control (DPC) method [45].

Before the control strategy is covered some discussion on the converter model will be given.

### 3.4.2 Converter Model

A voltage source converter topology is assumed for the controlled three phase power electronic converters used on both sides of the HVDC link. An overview of the VSC and also the classical HVDC topologies has been covered in section 2.2. The power circuit schematic of a two level three phase voltage source converter, as well as its equivalent block model, is given in figure 26. As seen from the figure there is an anti-parallel diode for every switch, which will conduct the reverse current. The losses in both the transistors and diodes can be divided into conduction losses and switching losses. These losses will not be further considered, except for a small resistance on the AC side to account for some conduction losses.

As seen in figure 25, the converter is modelled by a PWM block, which receives reference voltages for each of the three phases. These reference voltages are calculated
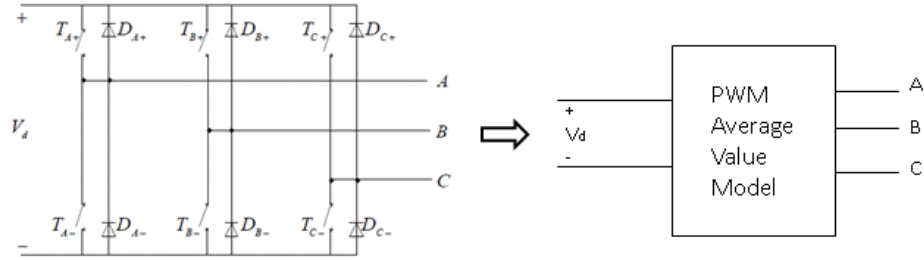
Figure 26: Two level three phase voltage source converter and equivalent block model

by the vector control technique, which is covered in the next section. The PWM block is an "average value model", which is relevant for representing a traditional two-level voltage source converter, neglecting nonlinearities and harmonics [46]. The valves of the voltage source converter are built up of semiconductors, usually IGBTs. There are various schemes to pulse width modulate converter switches in order to shape the output voltages to be as close to a sine wave as possible. Sinusoidal pulse width modulation is used here, which was described in section 2.2.3.

Detailed modeling of VSC-HVDC systems, such as including the representation of semiconductor switches, requires small integration time-steps to accurately represent the fast switching events. This causes significant deterioration in computational speed, which highlights the need for more efficient models that provide similar dynamic response. Reference [43] presents the concept of average-value modeling applied to two- and three-level VSC-HVDC systems. Dynamic performance simulation results using average-value models are compared against detailed model results.

An average-value model replicates the average response of switching devices, converters and controls by using controlled sources and switching or averaged functions. More information on the average-value method can be found in references [43] and [44].

The PWM block, the average-value model, used in the test system is developed by SINTEF and the model is based on traditional simplifications [46]. Using this model is an alternative to adding the actual switches and generating firing pulses to control these.

48

### 3.4.3 Vector Control Principle

The vector control technique offers decoupled control of active and reactive power. Its fast dynamic response allows for a system control in the form of a cascade structure, with an inner and an outer control loop. Cascade control requires that the bandwidth (speed of response) increases towards the inner loop. The outer voltage loop controller receives signals from the system side and supplies the current references to the fast inner current controller. In turn, the inner controller supplies signals for the PWM generator to control the VSC [47]. Vector control involves simplified representation of the three phase systems known as d-q transformations, as explained in section 2.3.5. This is advantageous because the vectors of AC currents and voltages occur as constant vectors in steady state, and hence static errors in the control system can be avoided by using PI controllers. The overall scheme of the vector base control used in the test system is shown in figure 27.
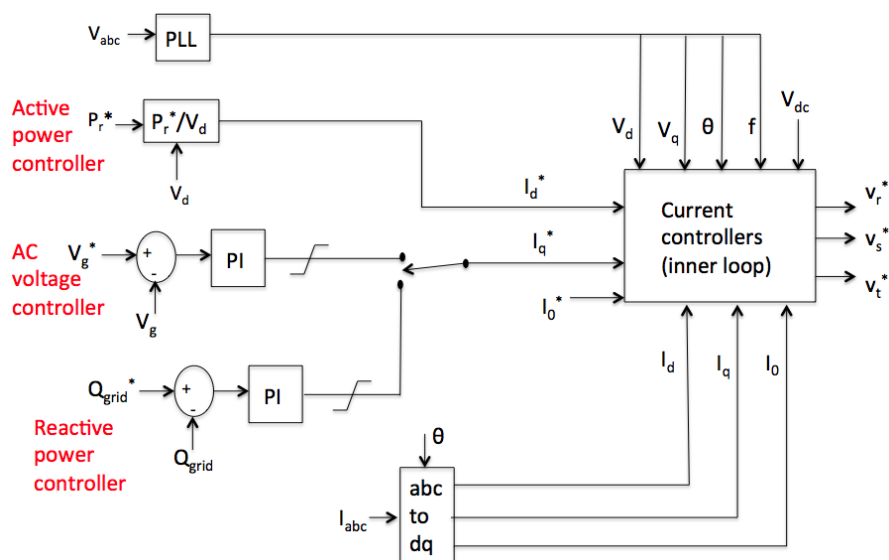


Figure 27: Vector based control used in test system

The outer controllers include the active power controller, the reactive power controller and the AC voltage controller. In a more general configuration, a DC voltage controller could also be included. The reference value for active current is provided by the active power controller, while the reference value for the reactive current is either provided by the AC voltage controller or the reactive power controller, depending on the input signal to the switch.

Vector control is used to analyze the VSC of the HVDC system. The three phase

currents and voltages are described in a rotating reference frame. Since the d-q frame is synchronized with the AC grid, the voltages and currents occur as constant vectors in this reference frame in steady state.

### 3.4.3.1 System Model

Basic equations are developed for the system in figure 28 based on analysis from [48]. The converter system is connected to the grid with voltages $v_{abc}$, currents $i_{abc}$, and converter input voltages $v_{abc,conv}$. The resistance and inductance between the converter and the grid are also shown.
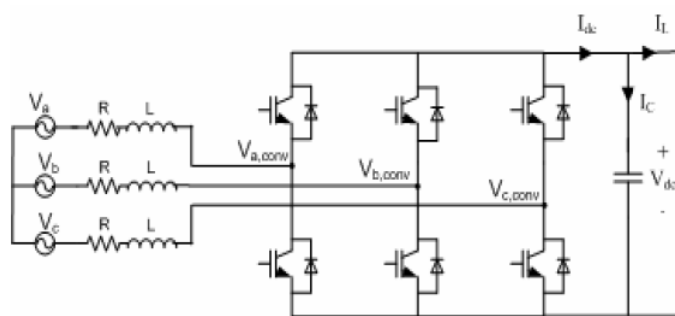


Figure 28: Schematic of the system [27]

The voltage at the grid side can be expressed as:

$$v_{abc} = Ri_{abc} + L\frac{d}{dt}i_{abc} + v_{abc,conv} \tag{23}$$

Using the abc to d-q transformations, the converter 3-phase currents and voltages are expressed in the d-q reference frame, synchronously rotating at the AC frequency, $\omega$. The extra $\omega L$ term, which appears, is the speed voltage [48]. The complete derivation is found in appendix D. This transformation is necessary to decouple the active and reactive power controls.

$$v_d = Ri_d + L\frac{d}{dt}i_d - \omega Li_q + v_{d,conv} \tag{24a}$$

$$v_q = Ri_q + L\frac{d}{dt}i_q + \omega Li_d + v_{q,conv} \tag{24b}$$

Similarly, on the DC side:

$$I_{dc} = C\frac{dV_{dc}}{dt} + I_L \tag{25}$$

Equation 24 defines the mathematical model of the VSC in the synchronous d-q reference frame. The controllers will be developed with reference to the d-q quantities and finally the output will be transformed back to the abc stationary frame before it is sent to the pulse width modulator (PWM) of the converter.

The angle between the $\alpha$-axis of the $\alpha - \beta$ reference frame and the d-axis of the d-q reference frame is used for transformation between the $\alpha - \beta$ frame and the d-q frame. The angular position of the voltage vector in the stationary two-axis $\alpha - \beta$ reference frame is given by:

$$\Theta = \arctan\frac{v_\beta}{v_\alpha} \tag{26}$$

The value of the angle $\Theta$ is necessary for independent control of active and reactive power, and it is computed by using a synchronization technique called phase locked loop (PLL).

### 3.4.3.2  Phase Locked Loop (PLL)

The phase locked loop (PLL) is a device which causes one signal to track another. It keeps an output signal synchronizing with a reference sinusoidal input in both frequency and phase. In the test system the PLL detects the phase of the grid voltage by transforming the measured AC voltages to a rotating d-q-frame. The d and q components are smoothed by a filter to reduce harmonics before they are fed into an arctan function that calculates the phase of the voltage. The reference angle $\theta_{ref}$ is set to zero, and the deviation from this value is fed into a PI controller that outputs a deviation from the base frequency. The proportional-integral (PI) loop filter can be given as:

$$K_f(s) = K_p(\frac{1 + sT_{PLL}}{sT_{PLL}}) \tag{27}$$

where $K_p$ and $T_{PLL}$ denote respectively the gain and the integral time. The grid voltage is achieved by adding the base frequency and this is input to a voltage controlled oscillator (VCO). The VCO produces an output ramp, $\theta$, whose rate of change is proportional to the magnitude of the input at any instant. The output angle, $\theta$, is a triangular waveform between 0 and $2\pi$ with a period corresponding

to the grid frequency. In the VSC the PLL is phase locked with the voltage phasor of phase a. The output is used to synchronize and phase lock the d-q plane with the AC source voltage, and is therefore an input to the d-q transformation. The block diagram implemented in the test system is shown in figure 29.
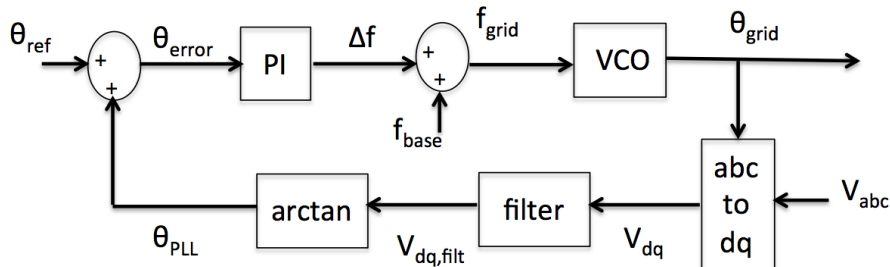


Figure 29: Block diagram of test system phase lock loop (PLL)

Figure 30 shows some of the main variables, which are used in the PLL loop and discussed above. The graphs show the initialization of the simulation. The system stabilizes after about 0.2 seconds and we see that the grid frequency equals 50 Hz, $V_d = 1$ pu, $V_q = 0$, and the phase angle, $\theta$, varies between 0 and $2\pi$ with a period equal to the grid frequency and in phase with the voltage in phase a.

In other words, the phase locked loop block measures the system frequency and provides the phase synchronous angle $\Theta$ for the d-q transformations. The information from phase lock loop is used to synchronize the turning on/off of the power devices, and to calculate and control the flow of active/reactive power. The synchronous d-q reference frame is chosen in order to align the d-axis with the voltage phasor of phase a. This results in Vq = 0 and Vd = V.

More details on PLL for grid connected three phase power conversion systems can be found in reference [49] by the same name.
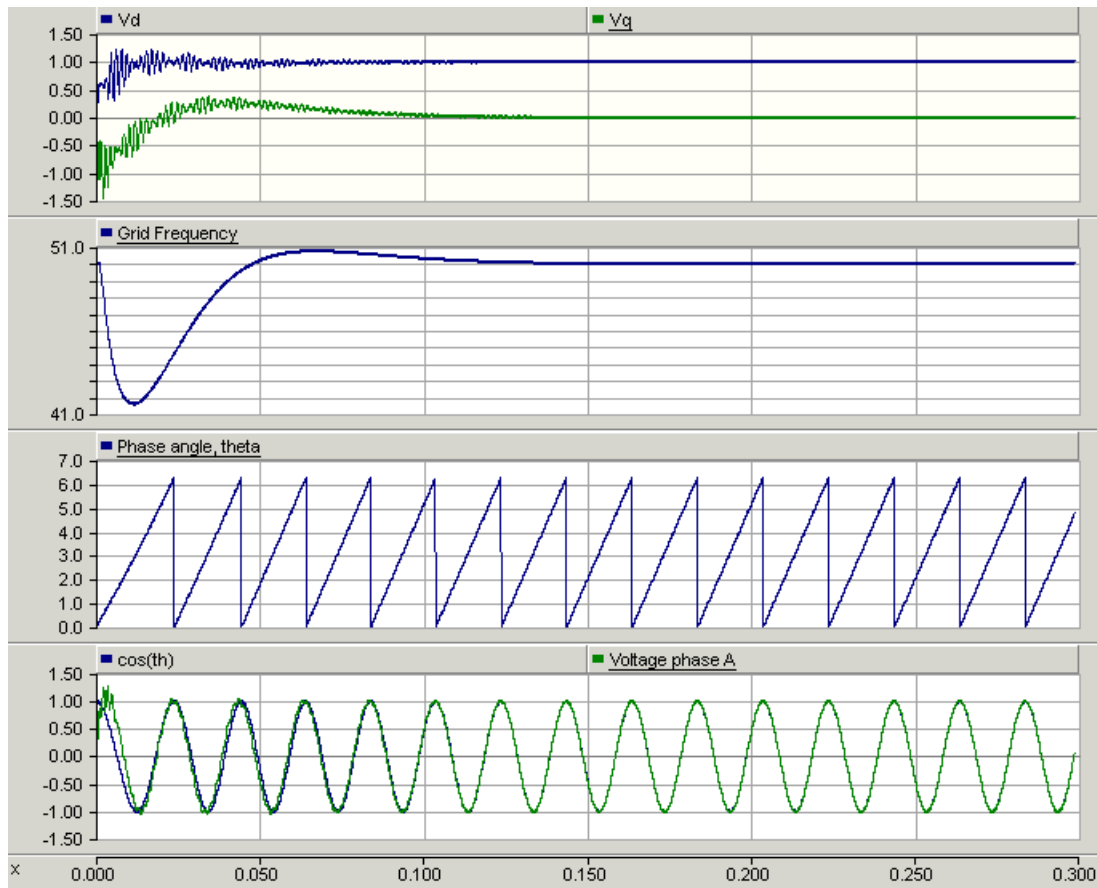
Figure 30: Graphs of some of the main variables in the PLL loop

### 3.4.3.3 Inner Current Controller

The inner controller, which is presented in figure 31, permits controlling of the d- and q-axis components of the converter's reference voltage, $V_{conv}$ (from figure 28), that will be used to generate the required PWM switching pattern.

The inner loop current controllers are developed based on equation 24. As seen from these equations, the VSC-HVDC is a nonlinear coupled control system due to the coupling between the d- and q-axis components. In order to decouple the d- and q-axis, a feed-forward technique is used to compensate for the cross-coupling terms. Thus, AC currents through the equivalent inductance, L (transformer reactance plus series reactor), in the d-q frame can be independently controlled via a PI controller.

53
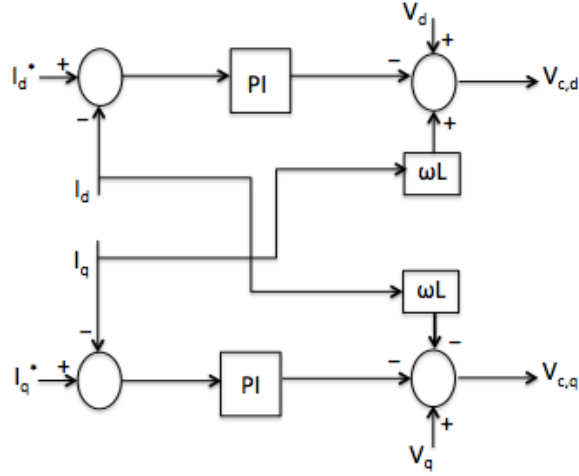
Figure 31: Inner current controller

Assume that the VSC output voltage is determined by the following PI controller [39]:

$$v_{q,conv} = -(K_p + \frac{K_i}{s})(i_q^* - i_q) - \omega L i_d + v_q \tag{28a}$$

$$v_{d,conv} = -(K_p + \frac{K_i}{s})(i_d^* - i_d) + \omega L i_q + v_d \tag{28b}$$

where $K_p$ and $K_i$ are the proportional and integral gains. Substituting equation 28 into equation 24 yields:

$$L\frac{di_q}{dt} = -Ri_q + (K_p - \frac{K_i}{s})(i_q^* - i_q) \tag{29a}$$

$$L\frac{di_d}{dt} = -Ri_d + (K_p - \frac{K_i}{s})(i_d^* - i_d) \tag{29b}$$

From equation 29 it is obvious that decoupling is achieved. The cross coupling currents in equation 24 are compensated for by feed forward terms in the controllers. The current references are inputs from the outer controllers and are compared to the measured current, $i_{dq}$. A more general block diagram of the inner current controller, connecting it to the rest of the control system is given in figure 32.

Figure 32 includes blocks representing the physical system. From a control point of view, the converter is considered an ideal power transformer with a time delay

54
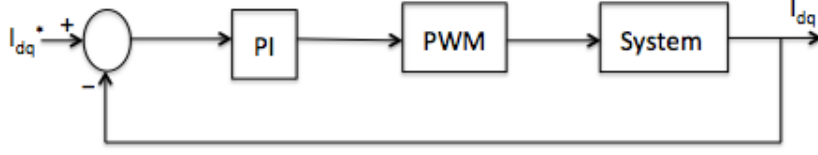
Figure 32: General block diagram of inner control loop

due to the converter switching. The output voltage of the converter is assumed to follow an input voltage reference with an average time delay equal to half of a switching cycle. The time delay is expressed by the general transfer function:

$$e^{-T_w s} = \frac{1}{1 + T_w s} \qquad\qquad T_w = \frac{1}{2} f_s \tag{30}$$

where $f_s$ is the switching frequency of the converter.

The proportional integral controllers are used to eliminate the steady state error. The zeroes of the PI controllers are selected to cancel the dominant pole in the external circuit. A typical VSC has a time constant $\tau$ which is much higher than $T_w$ and hence is the dominant pole [50].

The system transfer function is given as [50]:

$$G(s) = \frac{1}{R} \frac{1}{1 + \tau s} \tag{31}$$

where the time constant of the line is defined as $\tau = \frac{L}{R}$.

### 3.4.3.4    Reference Converter Voltages

The switch-on and -off commands of the switches of the converters are generated by the technique of Sinusoidal Pulse Width Modulation (SPWM). The modulation signal is sinusoidal while the carrier signal takes a triangular form. The ratio between the peak values of the two is defined as the modulation index M. The converter AC voltage fundamental component and DC voltage relationship can be expressed by equation 1, repeated below:

$$V_c(t) = \frac{1}{2} V_{dc} M \sin(\omega t + \delta) \tag{32}$$

55

M is the modulation index and $\delta$ is the phase shift between the fundamental component of converter AC voltage and AC system voltage and $V_{dc}$ is the DC link voltage. Equation 32 can be transformed into the d-q reference frame, as described in [51], and the modulation index and angle $\delta$ can be expressed as in equation 33.

$$M = \frac{2\sqrt{V_{c,d}^2 + V_{c,q}^2}}{V_{dc}}, \quad \delta = \arctan\frac{V_{c,q}}{V_{c,d}} \tag{33}$$

$V_{c,d}$ and $V_{c,q}$ represent the d- and q-axis components of converter AC voltage and $V_{dc}$ is the DC voltage. As seen in figure 33, the modulation index and the angle are transformed into three phase sinusoidal pulse width modulated voltages. These reference voltages are used as input to the converter model. As described in section 3.4.2, the converter is modeled by an average-value model, which replicates the average response of switching devices, converters and controls by using averaged functions.
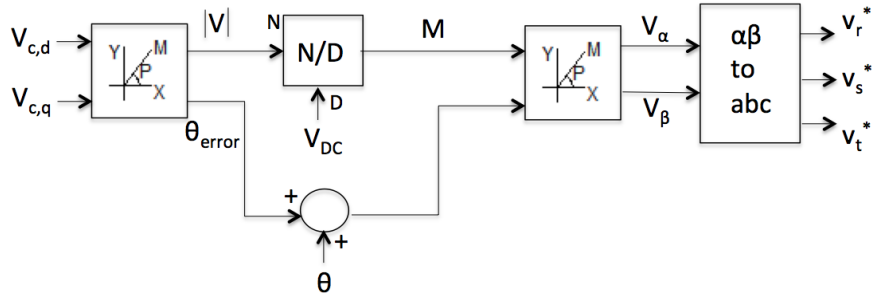


Figure 33: From d-q voltages to PWM voltages

### 3.4.3.5   Outer Voltage Controller

The expressions for active and reactive power in the d-q system are given in equation 34. The reference direction is from the converter into the AC network.

$$P = \frac{3}{2}(v_d i_d + v_q i_q) \tag{34a}$$

$$Q = \frac{3}{2}(v_q i_d - v_d i_q) \tag{34b}$$

The grid voltage vector is assumed to be aligned with the d-axis, which means that the q-axis voltage must be zero. The equations for active and reactive power are simplified to:

$$P = \frac{3}{2}v_d i_d \tag{35a}$$

$$Q = -\frac{3}{2}v_d i_q \tag{35b}$$

The above equations show that the active and reactive power can be controlled independently, by controlling the q- and d-axis current.

The outer control loop includes the DC voltage controller, the AC voltage controller, the active power controller and the reactive power controller. From equation 35 it can be seen that active power is related to $i_d$, while reactive power is related to $i_q$. Appendix E derivates the correlation between the DC voltage, $V_{DC}$, and $i_d$. Hence controller structures are given as in figure 34.
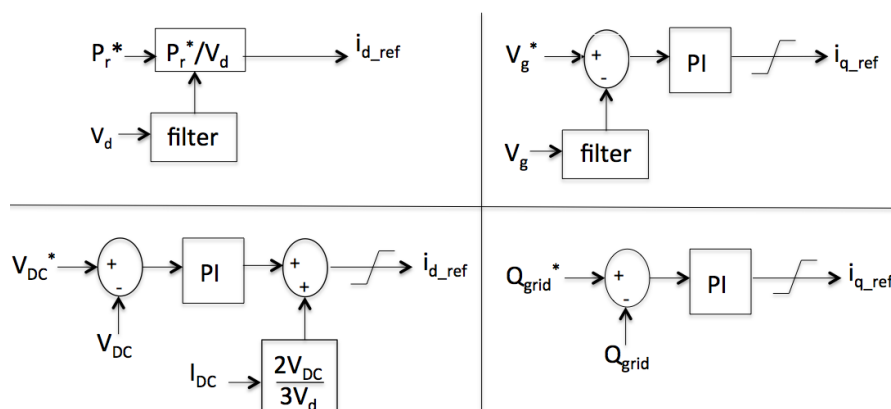


Figure 34: Outer controllers: Active power controller, AC voltage controller, DC voltage controller and reactive power controller

A relation between $I_{DC}$ and $i_d$ is used in the DC voltage controller. This relation comes from the active power balance on the AC and DC side (assuming an ideal system) given in equation 36 and 37.

$$P = \frac{3}{2}v_d i_d = I_{DC}V_{DC} \tag{36}$$

$$I_{DC} = \frac{3}{2}\frac{v_d}{V_{DC}}i_d \tag{37}$$

The grid side converter in the test system utilizes an active power controller and a reactive power controller. The active power controller receives its reference value from an input data file as described in section 3.3.2. This input load file replaces information which would have been available from on-line measurements in a real system. The reactive power reference in the test system is set to zero (unity power factor), but it may be changed depending on the operational requirements of the system. The DC current is feed forward compensated in the DC voltage controller [50].

Figure 35 summarizes the test system control circuit of the grid side converter.
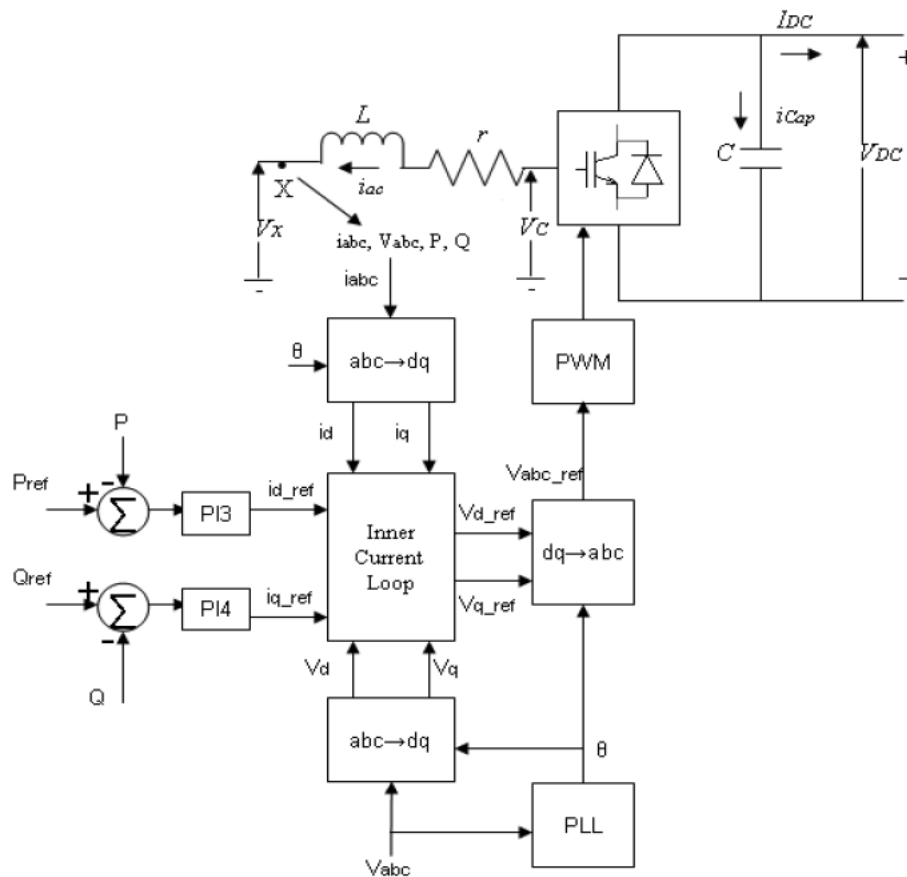


Figure 35: Block diagram of the inner and outer controllers [50]

## 3.5 HVDC Transmission Line

The DC transmission lines in the VSC-HVDC can be either overhead lines or submarine cables. In this system, a combination of overhead transmission lines and DC cables are applied. The DC cables are necessary to traverse the ocean. The physical length of the DC line has been set to 100 km, although this is not a realistic distance for a cable between Norway and Germany. The DC cable is modeled with a lumped series resistance, while the inductance has been omitted in the test system. The DC line resistance is included to take into account the conductor losses caused by the conductor current. The value of the resistance has been derived from the first CIGRE HVDC benchmark model [52] as described in appendix F1. There are two shunt capacitances, one at each end of the HVDC cable whose primary objective is to provide a low impedance path for the turned-off current and also to serve as an energy storage device [43]. The capacitor also reduces the ripple on the DC voltage. The DC-link capacitance value is taken from the simulation model by Suul [19], and has been proportioned to the new pu base values. The resulting HVDC transmission line parameters are given in table 12.

| *Parameter* | *Value* |
|---|---|
| Length | 100 km |
| Resistance | 2.6133 ohm/100 km |
| Capacitance | 222.2 $\mu F$ |

Table 12: DC-link parameters

## 3.6 Synchronous Machine & Converter

### 3.6.1 Electrical Representation

The pumped storage hydro plant is driven by a synchronous machine, which can operate in both pump and generation mode. The synchronous machine is connected to a hydro turbine and turbine governor, which control the power output, by controlling the water which runs through the turbine (usually according to a preset power-frequency characteristic). The synchronous machine is directly connected to a voltage source converter which handles the current transformations between AC and DC depending on the power direction. The power plant is assumed to be located in Southern Norway, and the converter is connected to a HVDC cable crossing southwards towards the other converter substation in Germany. Figure 36 shows the electrical configuration of the system.

59
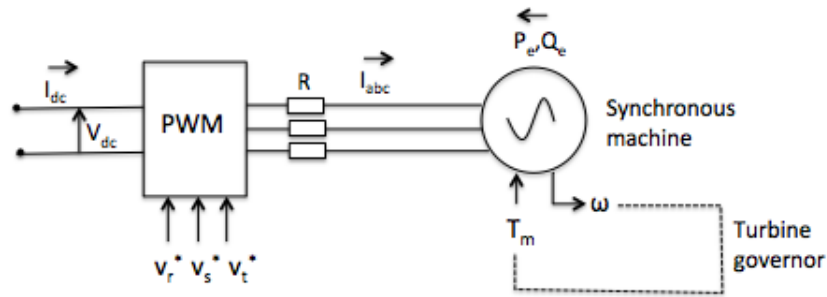
Figure 36: Pump-side converter

The converter, shown as the PWM block, is modeled in the same way as the grid side converter by the average value method discussed in section 3.4.2. The resistance in the line represents the on-state conduction losses of the converter and has to be considered for the design of the synchronous machine control system [19].

The synchronous machine model of the PSCAD main library is used for the simulations. This model is programmed in state variable form in a two-axis reference frame with the q-axis lagging the d-axis by 90 degrees. The model operates in the generator mode so a positive real power indicates electrical power leaving the machine, and a positive mechanical torque indicates mechanical power entering the machine. A positive reactive power indicates the machine is supplying reactive power [53].

This system varies depending on pump or generator operation and will be covered in detail below.

### 3.6.2  Synchronous Machine Control

The synchronous machine control system has been adapted from the master thesis work by Suul. An overview will be given here, but more details can be found in [19].

Torque and power control of a synchronous machine can be done in several different ways. The test system is a variable speed system, and therefore the control of machine power is independent of the speed. The control system developed for the simulation purpose is based on vector control principles. The basic control structure, with current control in the d-q reference frame, is given in figure 37.

A synchronous machine has three controllable input variables: the two components of the stator voltage and the field voltage. These can be used to control the
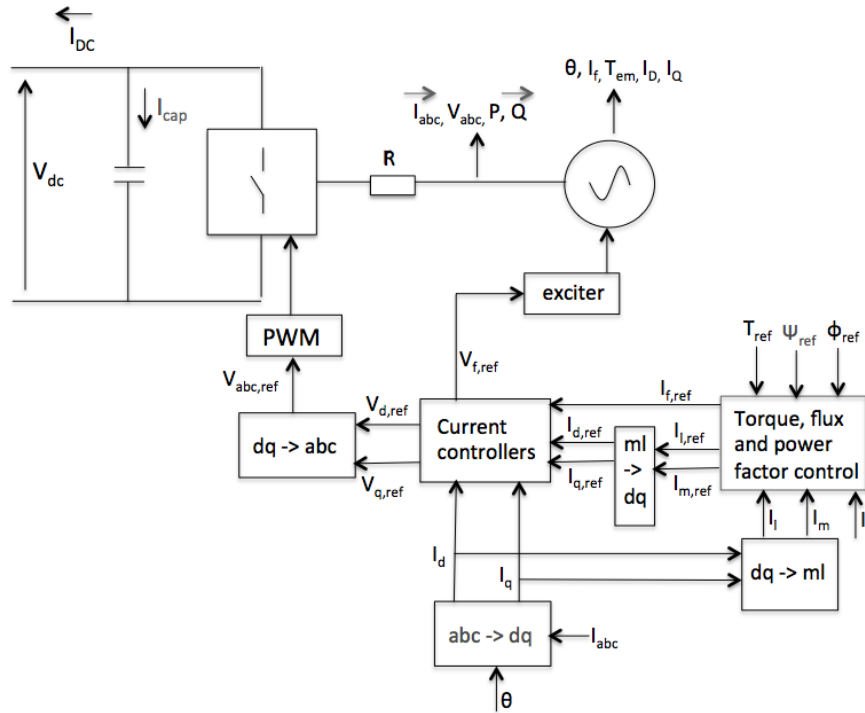
Figure 37: Basic structure of synchronous machine control system

machine torque, one of the flux linkages of the machine, and the angle between stator current and voltage space vectors. This is achieved by outer controllers, such as power and torque control, calculating the reference currents and inner loop current controllers. The control has similarities to the the control of the grid side converter discussed in section 3.4.3. The current controllers are used to control the stator terminal voltage in the d-q reference frame and the field voltage, to obtain desired operation. As shown in figure 37, the d- and q-axis reference voltages are transformed into three phase voltages by the same method as described in section 3.4.3.4 before they are used as reference inputs to the converter. The field voltage is directly used as input to the machine and decides the excitation current.

The control system design is described in the following sections, starting with the inner loop current controller before the torque and power controllers are considered. The measured values are transformed into per-unit values prior to entering the controllers. It is preferable to design the controllers in a per-unit system where unity is associated with rated conditions [19].

### 3.6.2.1  Inner Controller

The stator current inner controllers receive reference signals from the outer controllers. The design and parameter settings of the rotor oriented current controllers are achieved by an analog approach in [19]. The three phase currents are measured at the stator terminals, and transformed to the rotating d-q reference frame. The transformation is done in two steps according to the the transformation matrices in appendix C with PSCAD Fortran scripts.

Similar to the current controllers described in section 3.4.3.3, the d- and q-axis stator current controllers require decoupling due to the rotational induced voltages. Decoupling is achieved by feed forwarding these terms to the output of the current controllers, as discussed in [19].

Figure 38 and 39 show the step responses of the stator current controllers.
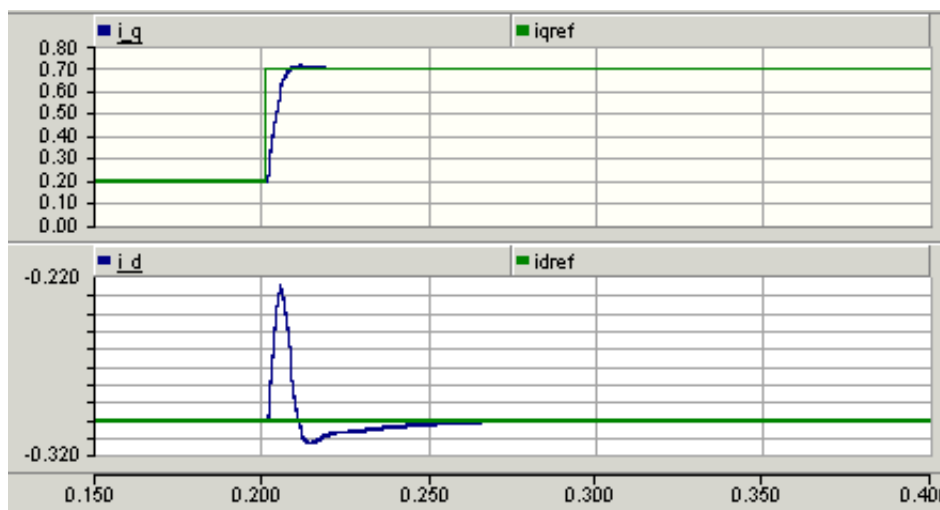


Figure 38: Step in $i_{q,ref}$ from 0.2 to 0.7 pu.

The currents seem to follow their references quite well during the step responses. As seen from the plots, there is still some small coupling between the d- and q-axis. This is observed as a response in the d-axis current following the step change in q-axis current , and vice versa. This is mainly caused by the converter delay [19]. The achieved response is considered good enough, and further improvement of the decoupling between the d- and q-axis is not investigated.

There is a third inner current controller to control the field current to the synchronous machine. By controlling the amount of current supplied to the generator field winding, the generator terminal voltage is regulated. This controller is ob-
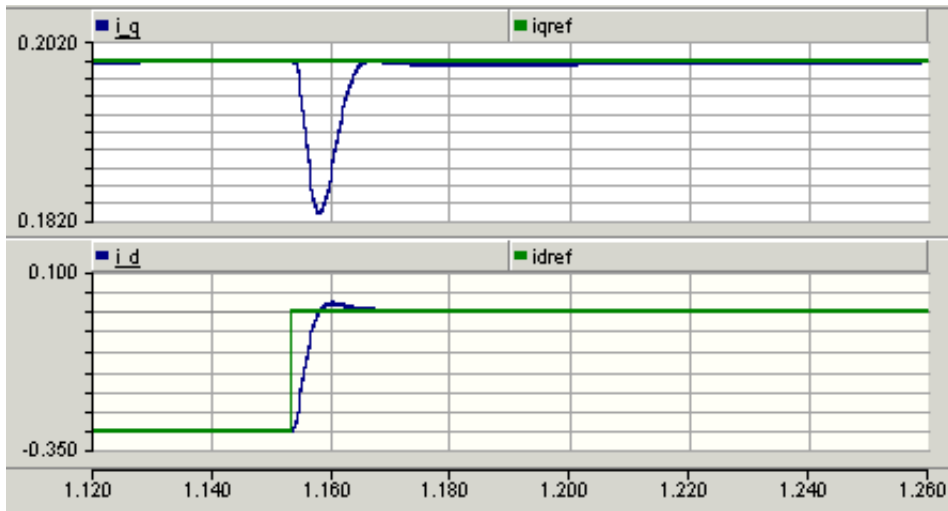
Figure 39: Step in $i_{d,ref}$ from -0.3 to 0 pu.

served to be a lot slower than the stator current controllers. There is a coupling between the field winding current and the stator d-axis current as seen in figure 40. The figure shows a step response of the d-axis current from -0.3 to 0 pu, together with the corresponding response of the field current. The d-axis controller is much faster than the field current controller and the field current drops quickly while the d-axis current increases. This coupling is further discussed in [19]. No coupling is observed between the q-axis current and the field current. The inner current controllers are shown in appendix H.
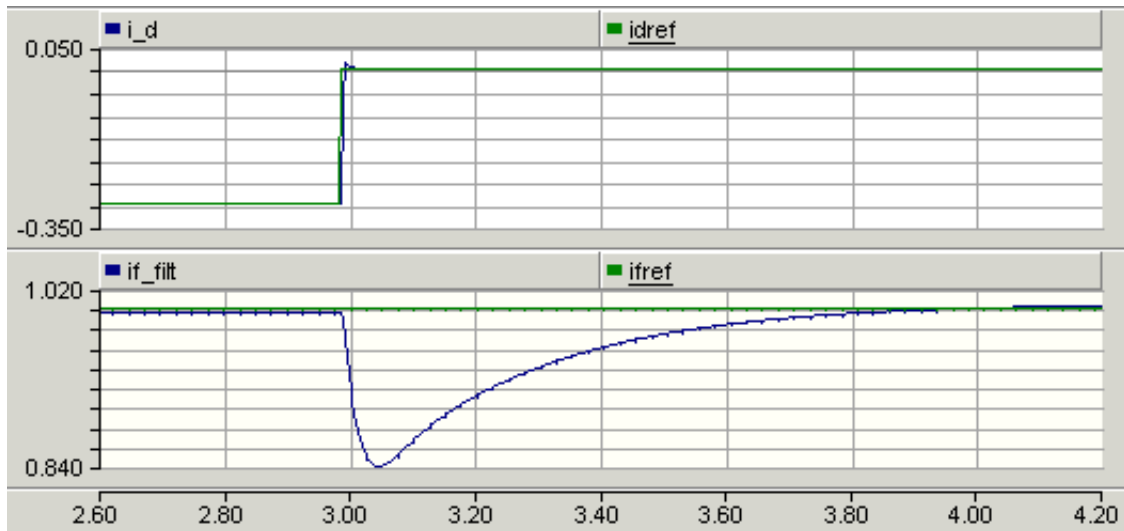


Figure 40: Field current response to a step in d-axis current reference

An initialization process delivers user-defined values as reference for the inner current controllers for a time interval given as input to the switch. This is implemented in the PSCAD model where the user manually adjusts the value by use of a slider which is a specialized user-interface control.

### 3.6.2.2 Outer Controllers

The outer controllers receive measured values, as well as reference values, as input and calculate the current references, which are used as input to the inner current controllers. The different outer controllers will be introduced here, but their derivations and equations are developed in [19].
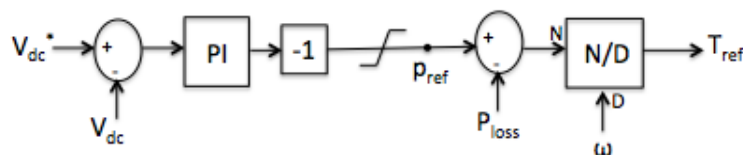


Figure 41: DC voltage control

The pump-side converter station for the test system has been chosen to operate as the DC voltage controller. The block diagram of the controller is shown in figure 41. The measured DC voltage is compared to its reference, and the error is fed through a PI controller to give an active power reference. The losses of the machine and the converter are subtracted from the power reference, before it is divided by omega to give the torque reference for the machine, according to equation 38.

$$T_{em,ref} = \frac{P_{ref} - P_{loss}}{\omega} \tag{38}$$

Figure 42 shows how the controller operates during pump operation, where the positive power direction is into the machine. The DC link voltage drops compared to its reference value due to a reduction of power at the sending end. This results in a positive error as input to the PI controller, which then causes the power reference to reduce (since it is multiplied by -1) until the voltage error is decreased again to zero. This gives the new power reference, which in turn decides the operation of the machine by deciding the torque reference.

During generator operation, the machine side converter operates as a rectifier. According to [40], the optimal controller gains depend significantly on the location

64
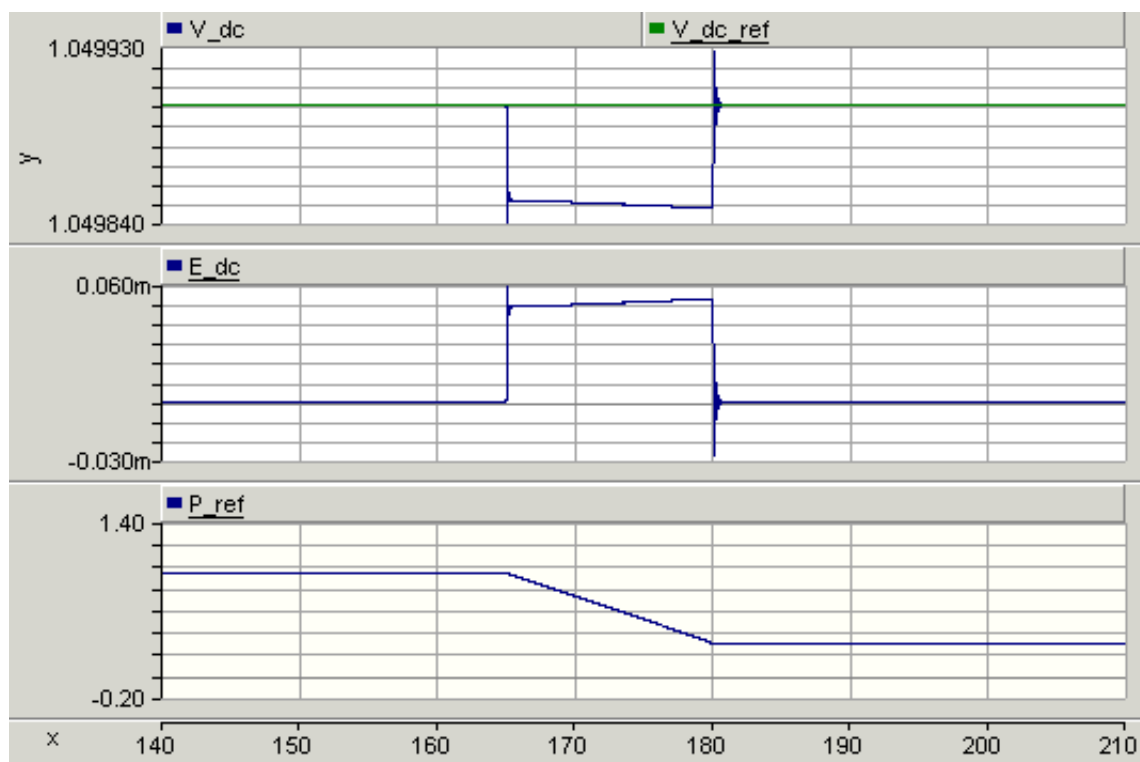
Figure 42: DC voltage controller operation

of the DC voltage controller, and the response of the power controller becomes slow if the DC voltage controller is located at the rectifier station.

An overview picture of the torque control and flux control are given in figures 43a and 43b, respectively. The torque controller has a PI-controller added to eliminate the stationary deviation because of small PSCAD numerical error. This controller is not an important part of the model, and is designed with a very low gain and restricted output. The torque reference is developed through a DC voltage controller as shown in figure 41. Alternatively, the torque reference can be developed from an active power controller. The choice depends on the desired control strategy, and in the test system the machine side converter is chosen to control the DC link voltage.

The torque and flux control generate current references in the flux oriented frame. These are transformed to the d-q reference frame, to give current references in the rotor oriented reference frame. This transformation is done according to the transformation matrices in appendix C2 with user-defined PSCAD Fortran scripts. The flux orientation is oriented after one of the flux space vectors and simplifies the choice of current references. A linear relation between the magnitude of a

(a) Torque control         (b) Flux control
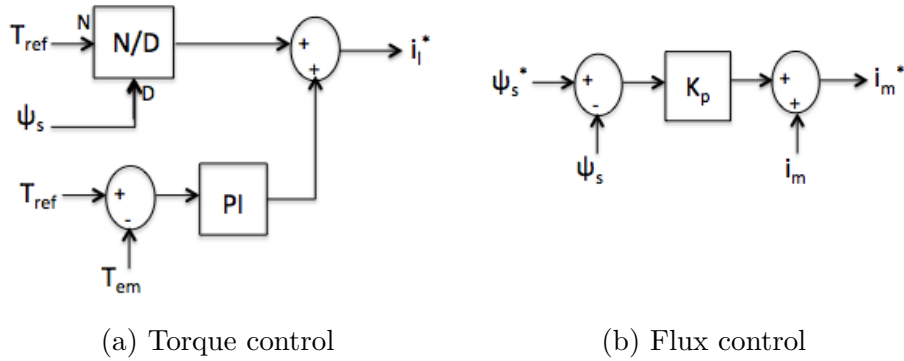
Figure 43

current space vector, perpendicular to the flux, and the torque is established, and is the principle of field oriented vector control. The orientation of such a reference frame is described in [19], and the orientation is chosen to be with the stator flux in the test system.

The d- and q-axis fluxes, and therefore also the stator flux and the flux angle, are calculated with a current model using the measured currents and the flux expressions in equation 39.

$$\Psi_d = x_d i_d + x_{ad} i_f + x_{ad} i_D \tag{39a}$$

$$\Psi_q = x_q i_q + x_{aq} i_Q \tag{39b}$$

$$\Psi_s = \sqrt{\Psi_q^2 + \Psi_d^2} \tag{39c}$$

$$\xi_s = \arctan \frac{\Psi_q}{\Psi_d} \tag{39d}$$

Where $\Psi$ expresses the d-axis, q-axis and stator fluxes.
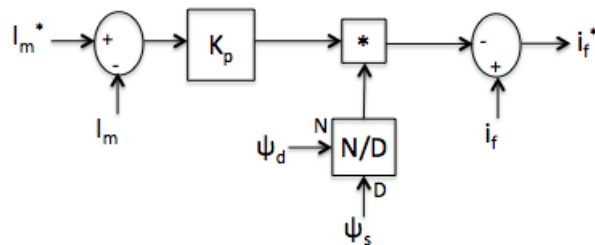


Figure 44: Power factor control

There is also a power factor controller, which generates the field current reference as shown in figure 44. This controller is developed in [19].

Figure 45 shows the response of power, omega, flux, torque and currents in the m and l reference frame when a step in reference power from 0.5 pu to 1.0 pu is imposed to the system. The torque response is quick and stable and due to the DC voltage controller it is a result of the power and omega response. The l-axis current, which is the output of the torque controller, coincides with the torque response. There is also observed some reaction in the m-axis current to keep the flux on its reference value.
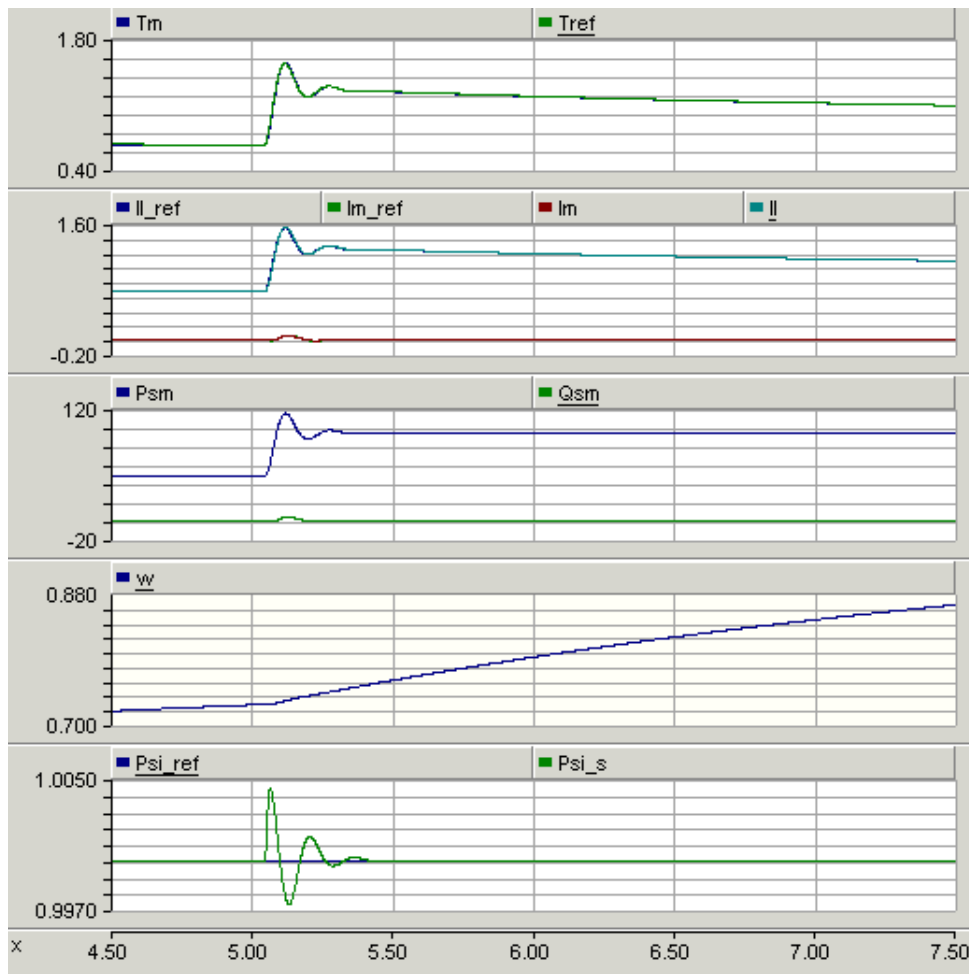


Figure 45: Response to step in reference power

Figure 46 shows the response of power, omega, flux, torque and currents in the m-l reference frame when a step in reference stator flux from 1.0 pu to 0.8 pu, when all else is kept constant. The flux response to the step change is quick,

with some overshoot, and stable due to quick control of the m-axis current. The m-axis current is then slowly reduced back to its original value, while the l-axis current jumps to a higher level after the flux decrease. The reactive power response coincides with that of the m-axis current, while the active power quickly stabilizes. A short transient in torque is observed.
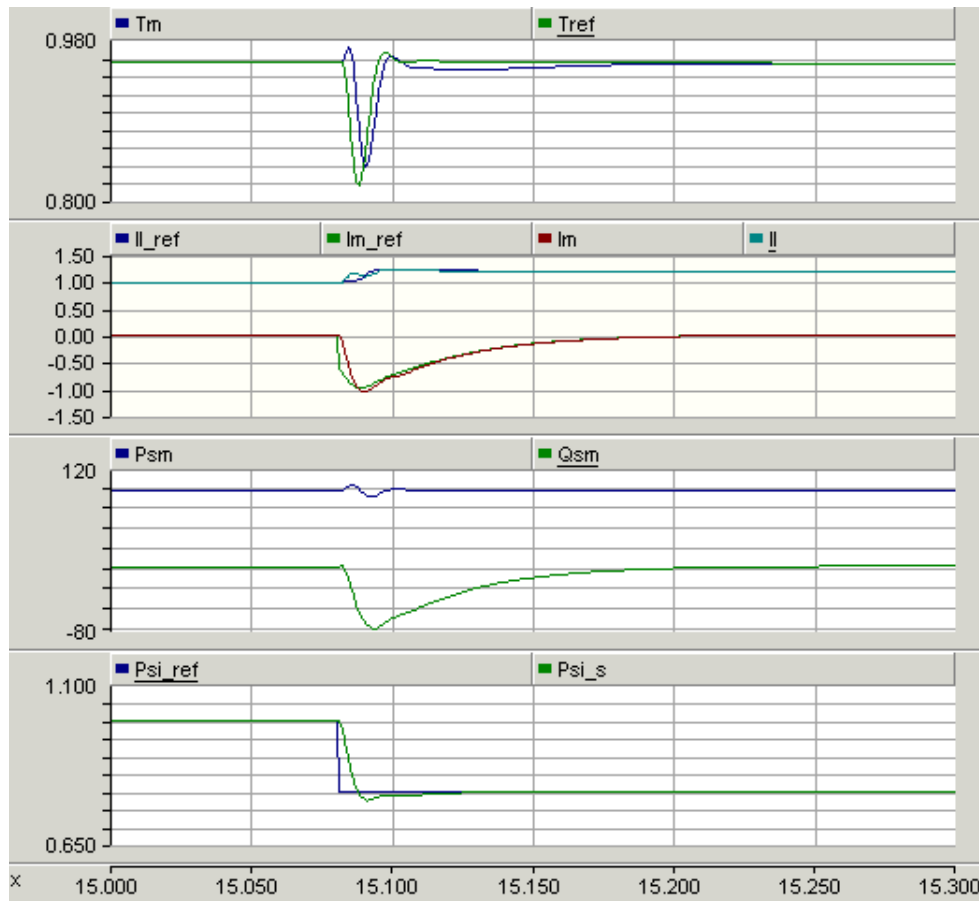


Figure 46: Response to step in stator flux reference

Figure 47 shows the power factor control. The stationary reference for the m-axis current is a user defined input, and is used for controlling the power factor of the machine. When the stationary reference of $i_m$ equals zero, the power factor equals unity. A step in this reference current from 0 to -0.5 pu causes the power factor to fall to about 0.65. The power factor changes due to the increasing field current, which affects the reactive power flow as seen in the figure. The responses are all smooth, but slow compared to the steps in flux and power. The stationary m-axis current reference is set to zero throughout the simulations in order to have a unity power factor.
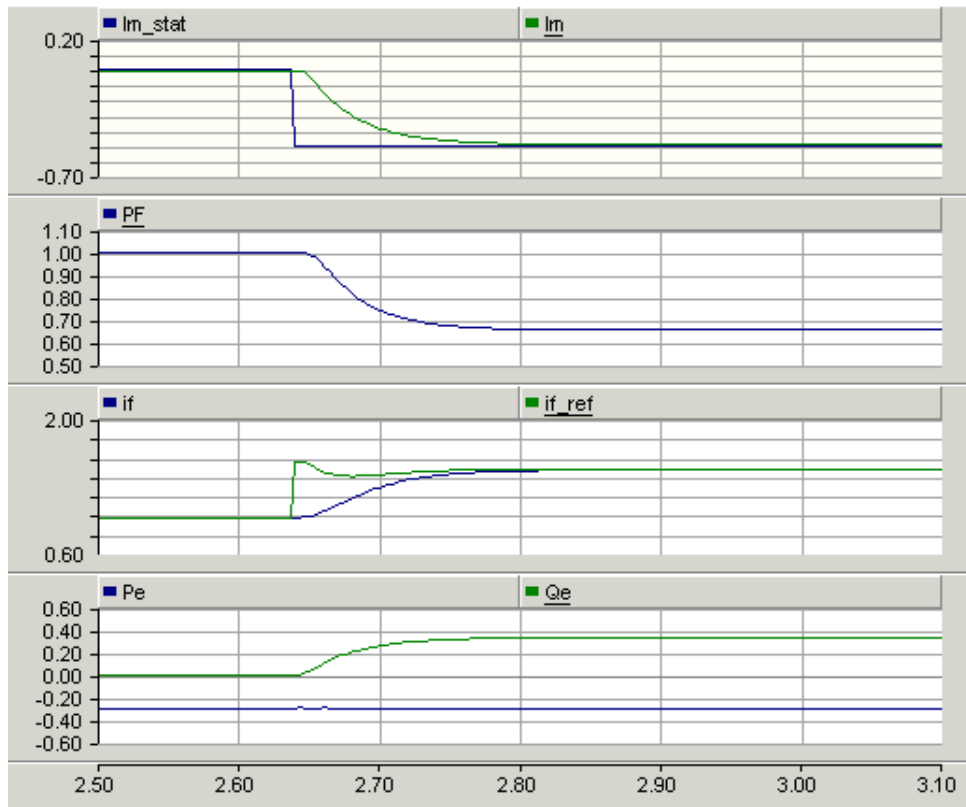
Figure 47: Response to step in stationary reference for the m-axis current

### 3.6.3 Pump Operation

Pumping operation requires less controllability than generation mode. Under pumping, the synchronous machine operates as a motor and drives a pump which pumps water from a lower reservoir up to a higher reservoir. The "water gate" is completely open in order to let as much water as possible through, and not to add unnecessary resistance. Only the electrical power is controlled during pumping, while the mechanical power is a function of the rotational speed, $\omega$.

### 3.6.3.1 Mechanical system

During pumping, and hence motor operation, the load model is not considered important. The speed of the machine will be influenced by the dynamics of the hydraulic system, but this will not to any large extent affect the current and torque control of the machine [19]. The hydraulic control system will not affect the

electrical control system considerably and the pump turbine is therefore modeled as a simple square load pump characteristic. The hydraulic control system, turbine and penstock dynamics are not considered. The load characteristics are given by equation 40 [19].

$$T_m = k_T \omega^2 \tag{40}$$

The constant $k_T$ is set to -0.94 in the simulation model, where the negative value means the synchronous machine is in motor operation. Choosing $k_T$ less than one means that the machine can run at a higher rotational speed than 1 pu and still be within the maximum power capacity. With $k_T = -0.94$, a pumping power of 0.94 pu is required for the rotational speed to equal 1.0 pu (which means 50Hz). Figure 48 shows the simulation model of this simple control.
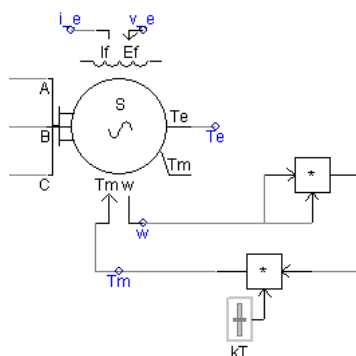


Figure 48: Simplified mechanical and hydraulic system for pump operation

The shaft torsion and damping are not considered. The synchronous machine rotor and the pump turbine are therefore modeled as a single lumped mass. The mechanical time constant is set to $T_m = 10s$, and the inertia constant H, which equals half of the mechanical time constant is set to $H = 5s$.

Even though the mechanical and hydraulic systems in pump operation are not investigated in detail, some limitations to the system are necessary. For pumping mode, the speed range will be very dependent on the technical solutions, the site location and the water level of the upper reservoir [19]. Reference [54], on unit-connected HVDC generator-converters, concludes that a unit-connected hydro system can provide controllable direct voltage for frequencies in the range of 33.3 - 50 Hz, or in pu: 0.67 - 1 pu. Using this as a basis, it is calculated by equation 41 (with $k_T = 1$) that the power range of the generator is in the range of 0.3 and 1.0 pu power, and as a rough assumption this same speed range is assumed for pumping operation.

$$P = \omega T_m = \omega^3 \tag{41}$$

### 3.6.4 Generator Operation

Figure 49 shows the typical components of a hydro generator connected to the grid. Electrical energy is produced by the turbine, which is equipped with a turbine governor to control either the speed or the output power according to a preset power frequency-characteristic [35]. The exciter provides the DC field current required to produce the magnetic field inside the generator. The excitation current is controlled by controlling the field voltage, and consequently the generator's terminal voltage is controlled. This is achieved through the current controllers, which were discussed in section 3.6.2.1.
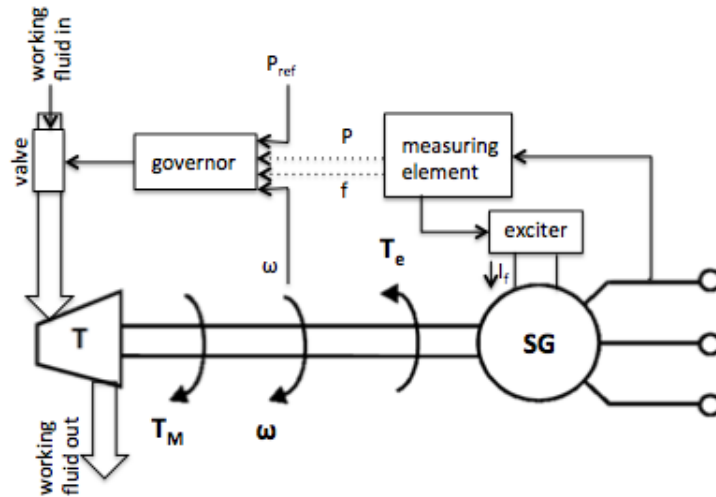


Figure 49: Block diagram of a power generation unit

Generator operation requires more controllability than pump operation. As discussed in the previous section, for pump mode the synchronous machine rotor and the pump turbine are modeled as a single lumped mass. Only the electrical power is controlled during pumping, while for generator operation also the mechanical power must be controlled. This control, which is achieved by the hydro turbine and its governing system is covered in the next section.

### 3.6.4.1    Hydro Turbine & Governing System

The hydraulic turbine system drives the synchronous generator and derives its power from the water as it falls from an upper reservoir, through a penstock and to a lower reservoir, shown in figure 50. Naturally the power increases with increasing head. Movable wicket gates control the power output of the turbine. The turbine system is equipped with a governing system to provide a means by which the turbine can be started, run up to the operating speed and operate on load with the required power output. The governor compares the the turbine rotor speed to a reference speed. This error in turn passes through a servomotor with feedback control and together with the load reference set point, decide the gate position.
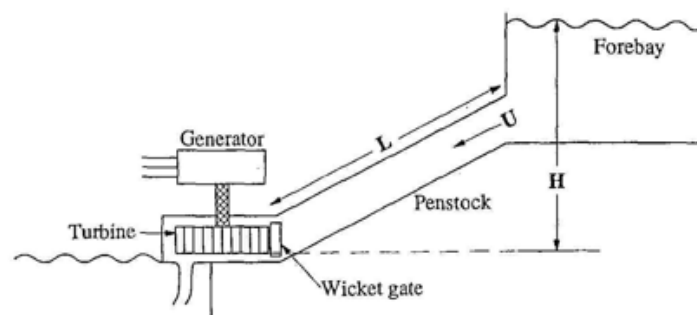


Figure 50: Schematic of a hydroelectric plant [37]

The main function of the turbine governing system is to regulate the turbine-generator speed and hence the frequency and the active power response to load variation. The performance of a hydraulic turbine is influenced by characteristics of the water column such as water inertia, water compressibility and pipe wall elasticity in the penstock. The water inertia causes changes in turbine flow to lag behind changes in turbine gate opening. The effect of elasticity is to cause traveling waves of pressure and flow in the pipe (referred to as water hammer). To simplify the representation of the hydraulic turbine it is assumed that the penstock is inelastic, the water is incompressible and hydraulic resistance is negligible. The turbine is also assumed to be ideal and lossless.

With these assumptions, the turbine-penstock system can be described by the "classical" transfer function in equation 42, where $P_{hg}$ is the power output of the turbine and $g_{hg}$ is the gate position. This equation accounts only for the water starting time, $T_w$, which is the time required to accelerate the water in the penstock from standstill to rated velocity. Typically, $T_w$ lies between 0.5 and 4s [37].

$$h_t(s) = \frac{P_{hg}(s)}{g_{hg}(s)} = \frac{1 - T_w s}{1 + \frac{1}{2} T_w s} \tag{42}$$

The transfer function represents a "non-minimum phase" system due to the zero in the right half of the s-plane. This special characteristic can be illustrated by considering the response to a step change in gate position, shown in figure 51. Immediately following the increase in gate opening, the mechanical power actually decreases by twice the step before it increases exponentially to a steady state value. The initial power surge is opposite to that of the change in gate position. This is because when the gate is suddenly opened, the flow does not change immediately due to water inertia. However, the pressure across the turbine is reduced causing the power to reduce [37]. The response is determined by $T_w$.
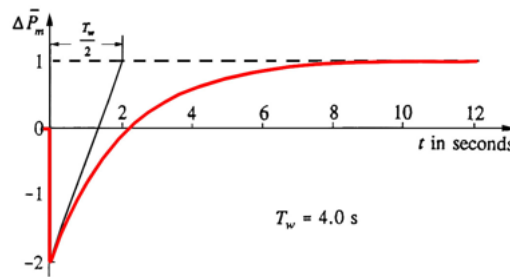


Figure 51: Change in turbine mechanical power following a unit step increase in gate position [37]

The speed/load control of the turbine governor involves feeding back the speed error to control the gate position. In order to ensure stable operation the speed governor is provided with both a permanent (steady state) droop and a transient droop. The permanent droop, $R_p$, determines the amount of change in output a unit produces in response to a change in unit speed. The steady state droop is typically set at about 5%, which means that a speed deviation of 5% causes 100% change in gate position or power output. The transient droop, $R_t$, is used to limit overshoot of the turbine control during a transient condition. It transiently reduces the gain and is necessary due to the non-minimum phase behavior of the hydraulic turbine. Stable control performance of a hydro turbine is achieved with a large transient droop and a long resetting time. This causes the response of a hydro turbine to speed changes to be relatively slow.

The resulting block diagram describing the speed governor and hydraulic system of the power plant is shown in figure 52. $R_p$ is the permanent droop, $R_t$ is the temporary droop, $T_r$ is the reset time, $T_g$ is the time constant of the servomotor

and $T_w$ is the water starting time. The output power is divided by the synchronous generator speed to give the torque input to the generator.
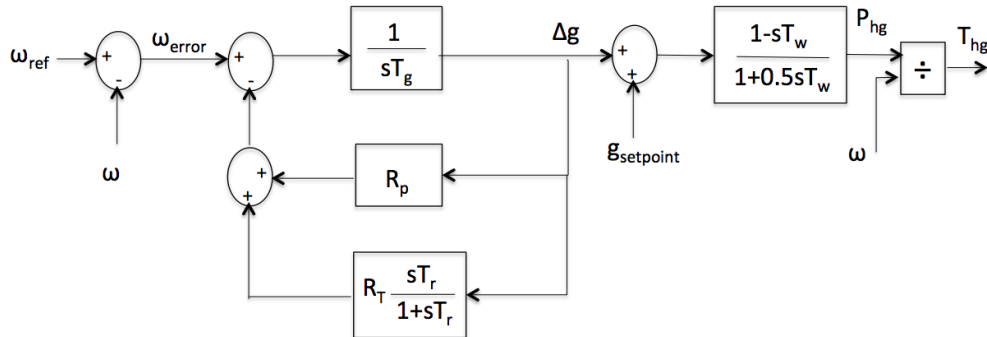


Figure 52: Control circuit for the hydro turbine and governing system

### 3.6.4.2 Tuning of Turbine Governor

The selection of governor settings are important for stable operation of a power system. The aim of the simulations in this thesis are to show satisfactory operation on a system level of the test system presented in section 3.2, and therefore the governor settings should be chosen for normal operation.
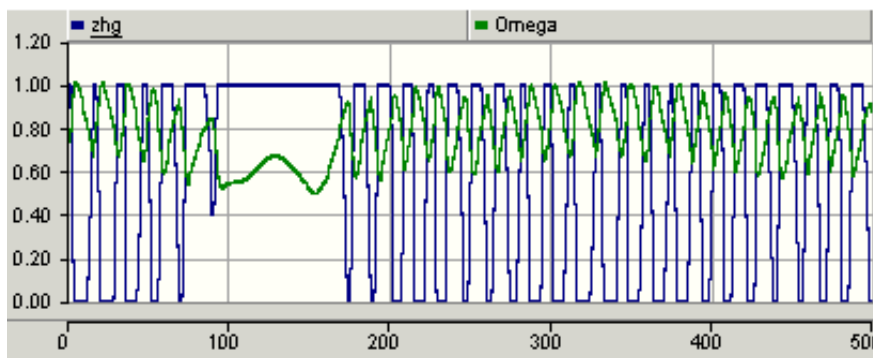


Figure 53: Gate opening with $T_{reset} = 0.5s$

Figures 53 and 54 show the results of two different reset times, keeping all other parameters equal. The huge difference in operation due to different reset times can be seen, and using $T_r = 0.5s$ results in too quick response. The gate opening jumps continuously between completely shut and completely open (0 and 1), and the shaft speed varies similarly around 0.8 pu, which is the reference speed. The simulation
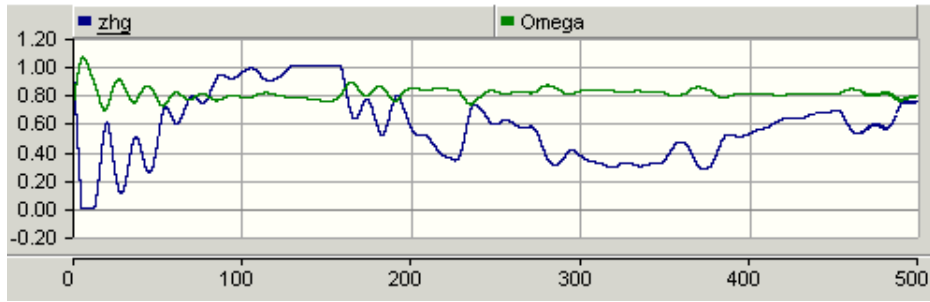
Figure 54: Gate opening with $T_{reset} = 5s$

runs quicker than the real time operation would (1 simulation second to 1 real time minute), and this could be the reason why this happens. Setting $T_{reset} = 5s$, shows more expected behavior and is chosen for the test system simulations. It should be noted that both cases result in otherwise identical power flows and therefore not much time has been spent on tuning the turbine governor to optimal values.

Typical values for hydraulic governor parameters (given in [37]) have been used in the test system, and are summarized in table 13.

| Parameter | Value |
|---|---|
| Permanent droop, $R_p$ | 0.04 |
| Temporary droop, $R_T$ | 0.4 |
| Reset time, $T_r$ | 5 s |
| Servomotor time constant, $T_g$ | 0.05 s |
| Water starting time, $T_w$ | 2.0 s |
| Mechanical time constant, $T_M$ | 10 s |

Table 13: Test system turbine governor parameters

### 3.6.4.3 Speed Reference

An advantage of variable speed pumped storage compared to constant speed pumped storage, is that the speed of the machine can be varied in both pumping and generator operation. This means that the power can be varied, not only in generator operation, but also during pumping. Also, the machine can operate at its optimal speed for the given operation, depending on the power reference and also varying head. This enables the power plant to achieve optimal efficiency.

During pumping, the rotor speed is controlled by controlling the active power reference value within a specific range according to the network requirements, as

75

discussed in section 3.6.3. In generation mode, the hydraulic governor controls the rotor speed according to a speed reference. This speed reference should ideally vary depending on the operation, especially active power changes. The details of the relationship between optimal efficiency and reference rotor speed have not been investigated in detail, and for the simulations the speed reference is fixed at 0.8 pu.

### 3.6.5 Control System Overview

Figure 55 shows an overview of the total electrical control system for the whole test system including the pumped storage synchronous machine and the VSC based HVDC transmission and its controllers. The figure shows the main parts of the controllers as developed throughout this chapter. It is apparent that the control of each of the converter stations is completely decoupled. While the grid-side converter controls the power flow, the opposite converter controls the DC voltage. Systems with HVDC transmission, such as the one illustrated, often range over far distances and having two independent control systems is a major advantage. This eliminates the need of transferring information from one converter substation to the other.
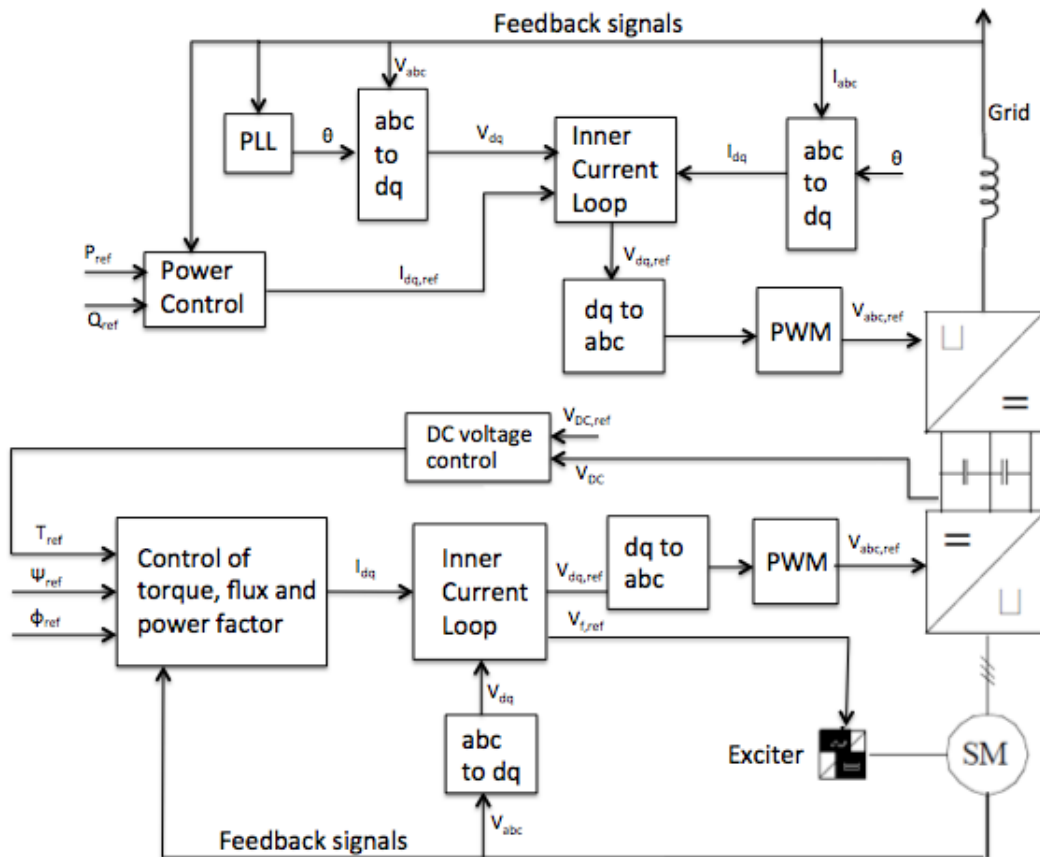


Figure 55: Test system control system overview

# 4 System Simulation and Results

## 4.1 Introduction

Results from simulation with the model developed and described in chapter 3 are presented in this chapter. The main purpose of the pumped storage power plant is to act as an energy storage to allow for increased utilization of energy from fluctuating renewable energy sources, and to dynamically contribute to power balance and frequency control of the system. The test model is simulated for normal operating conditions and for a time period assumed to illustrate a day. However, even though the grid model is relatively small, there are numerous possible events that could be of interest for simulations. A more extensive analysis, along with an economical approach would be necessary to justify a final investment in such a system. The overall operational strategy and internal dispatching between online units are also important regarding operational planning.

## 4.2 Simulation Tool

The PSCAD/EMTDC simulation tool is applied for implementation and testing of control structures of the test system. It is a powerful time-domain transient simulator for simulating power systems and its controls. EMTDC (Electromagnetic Transients including DC) is a simulation engine used to solve differential equations of the entire power system and its control in the time domain (both electromagnetic and electromechanical systems). PSCAD (Power Systems Computer Aided Design) is a powerful and flexible graphical user interface to the EMTDC simulation engine. PSCAD enables the user to construct a circuit, run simulations and analyze the results in a completely integrated and graphical environment . Plotting functions, controls and meters are also included and allow the user to alter system parameters during a simulation run. PSCAD is used extensively for many types of AC and DC power simulation studies, including power electronics [53].

## 4.3 Simulation Cases

The simulation results are divided into two subsections: generator operation and pump operation. These are the two operating modes of the test system, and due to a minimum operating power of 0.3 pu, the pumped storage hydro power plant will not have zero crossings of power (transition between pump and generator operation). Therefore, between these transitions, which usually will happen once

a day, the pumped storage plant will either be running at no load or at standstill. For this reason, two separate models are created for each of the operation modes. In addition, as discussed in section 3.6, the hydraulic system during generator operation is modeled differently than during pump operation, and modeling and simulation is therefore simplified with two separate models.

To ease the discussion of the results, the reference direction is chosen so that the power is positive in the respective operation. Hence, for generator operation, the reference direction for power and current is from the power plant to the grid, and opposite for pump operation. Each of the following sections will start with a figure to summarize the reference directions.

### 4.3.1 Generator Operation

Figure 56 summarizes the reference directions for the system parameters, which will be used as a basis for the discussion of the results of generator operation.
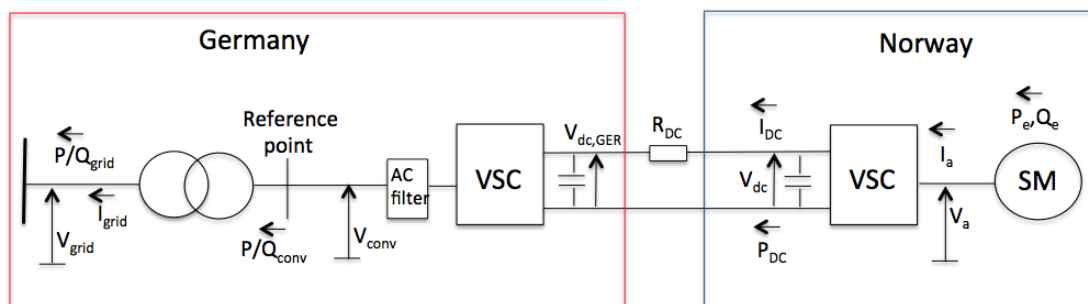


Figure 56: Test system with generator reference directions

The details of the time settings for the simulation, as well as user-defined reference values are summarized in appendix G1.

### 4.3.1.1 Load Profile

The load data, which is used as input in the simulation model is described in section 3.3. Figure 57 shows the power references that are used for simulation of generator operation. The balancing profile has been decided from real data from May 6 and corresponds to the real-time hours between 08.15 and 21.00. The wind power generation in Germany was low during these hours, and generation from Norway can help meet the power demand during the day time hours. As

mentioned earlier, the time axis has been shortened due to a very time consuming simulation, and therefore every second in the simulation equals 1 minute in real time. Data exists for every 15 minutes, or 15 seconds in the model, and PSCAD linearly interpolates between the separate data points.
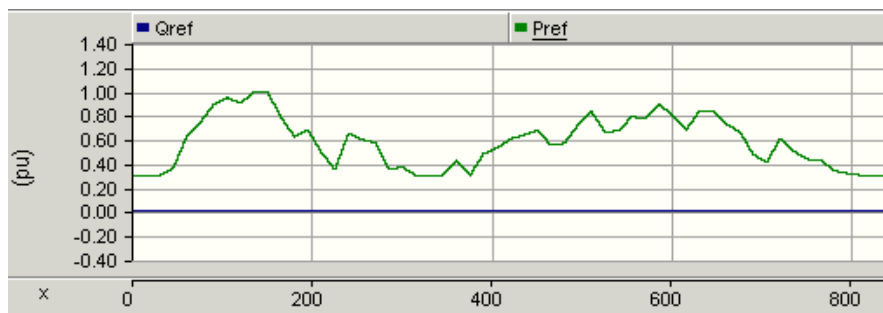


Figure 57: Generator operation: Active and reactive power references

The power limits, which have been chosen for the pumped storage power plant following the discussion in section 3.6.3.1, are applied to the power reference input, which therefore varies between 0.3 and 1.0 pu. The power references are referred to the point in the grid which is after the AC filter and grid-side converter, as shown in figure 56. $Q_{conv}$ and $P_{conv}$ are the measured power flows which are expected to follow the references. In order to deliver a certain amount of power to this point in generator mode, the power produced at the source must take into account the losses on the way and will therefore be greater. Since the power limits are actually chosen for the synchronous machine, the power limits for the input reference should be compensated by the losses in the line. This is an improvement that should be taken into account and added to the model. For the following simulations, the active power limits of the synchronous machine are therefore allowed to deviate slightly from the derived limits. The reactive power reference is set to zero throughout the simulation.

### 4.3.1.2   Grid-Side Converter

Figure 58 shows measurements from the grid side of the power system. The phase a current, whose direction is into the grid, has a clean sinusoidal waveform and peak values ranging between 0.065 kA and 0.213 kA. The current is small because of the high voltage level of the grid, which is positive due to reduced losses. The current and the active power are proportional due to the constant grid voltage. The grid voltage and the converter voltage are shown in figure 59. The voltages are constant throughout the simulation and the graph is therefore zoomed in to

81

show the sinusoidal waveforms. The line to line grid voltage has a peak value of 537 kV, and an rms value of 380 kV. This is a constant AC voltage representing the stiff voltage of the high voltage German grid. The line to line converter voltage has a peak of 99 kV, and an rms value of 70 kV.
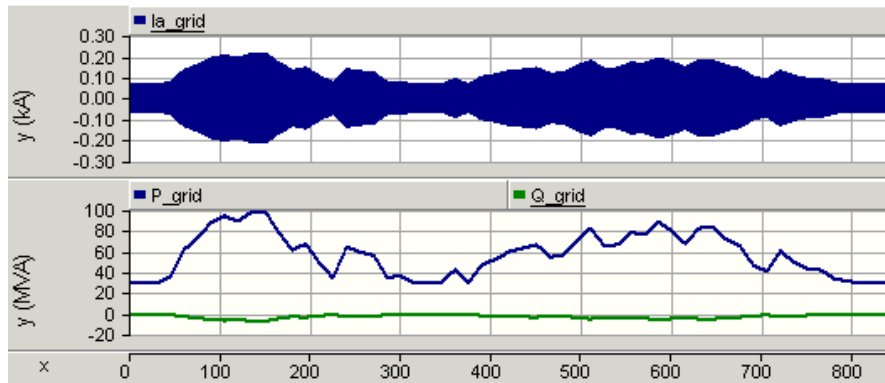


Figure 58: Generator operation: German grid measurements
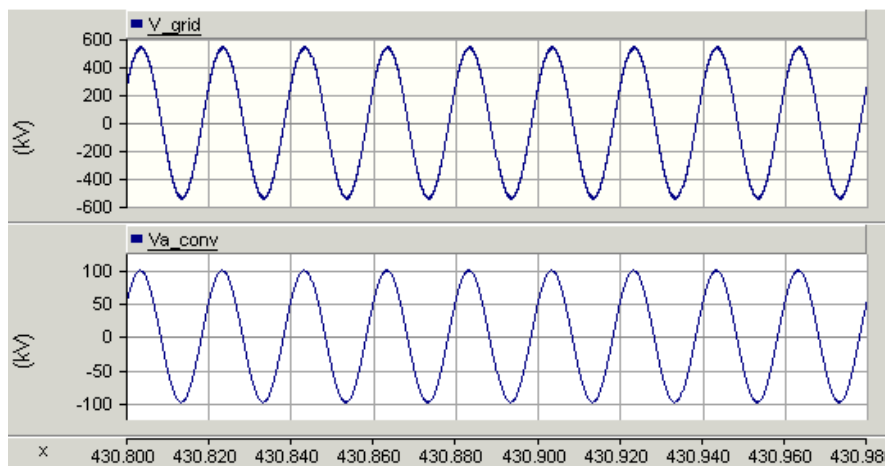


Figure 59: Generator operation: Sinusoidal grid-side voltages

The grid-side converter controls the active and reactive power flows according to the reference values given through an input data file. The d-axis current reference is achieved by dividing the active power reference by the d-axis voltage, and the q-axis current reference is given through a user-defined reactive power control. The active power follows its reference very well. $P_{grid}$ is slightly reduced compared to the reference due to losses through the converter transformer.

The reactive power on the primary side of the transformer is shown more closely in figure 60. It can be seen that this reactive power is negative throughout the
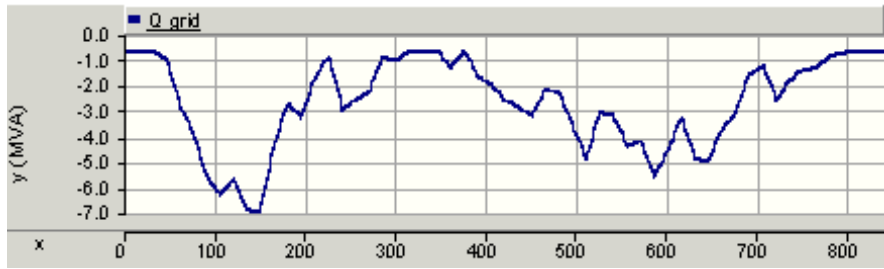
Figure 60: Generator operation: Reactive power to the grid

simulation with a proportional profile compared to the active power. It can be seen that the more power that is transferred through the converter transformer, the more reactive power is consumed from the grid, which is due to the increasing current. The reactive power consumption of the transformer is given by its reactance and the current through it.

The reactive power has a reference value of zero, referred to the reference point as shown in figure 56. Figure 61 shows this reactive power. The reactive power reference is at zero pu, and so is the measured reactive power except for small variations from zero pu whenever the active power reference changes, but it quickly stabilizes again at zero. The control system has managed well to control the reactive power to its reference value throughout the simulation.
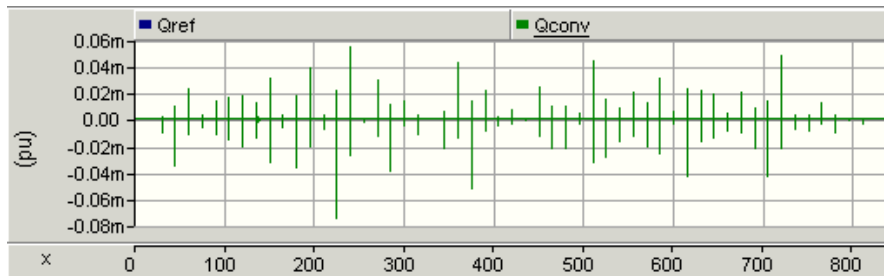


Figure 61: Generator operation: Converter reactive power

As mentioned earlier, the d-axis is chosen to be aligned with the voltage phasor of phase a. This results in $V_d = V = 1$ pu and $V_q = 0$, as shown in figure 62. $V_d$ and $V_q$ are calculated by the Clark and Park transformations of the measured AC voltages. It can be seen that, although $V_d = 1$ pu, it has minor variations that follow the changes in active power flow. The q-axis voltage component has small variations from 0 pu, whenever there is a slope change in power flow. Also the frequency experiences tiny deviations from its base value of 50 Hz. Each constant error is given by the slope of change in reference active power.

83
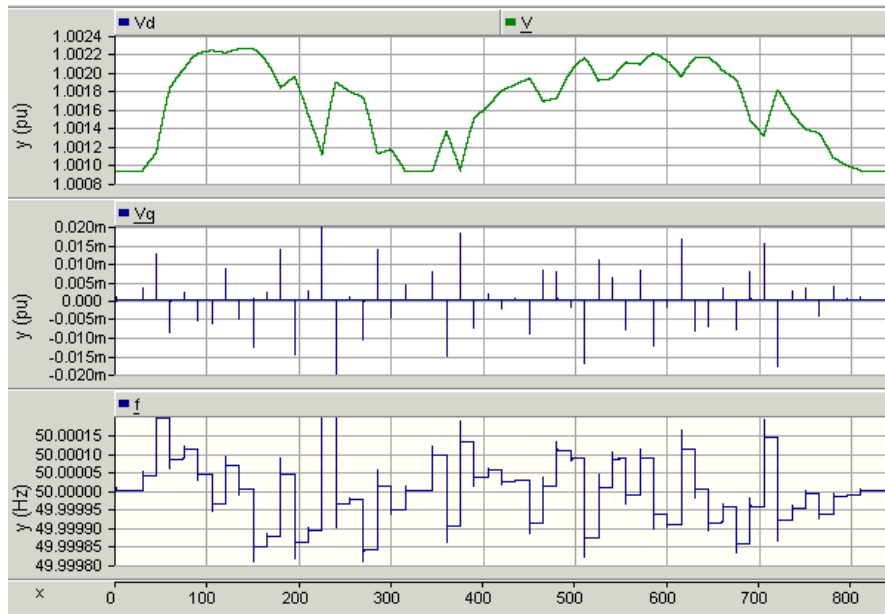
Figure 62: Generator operation: Phase Locked Loop
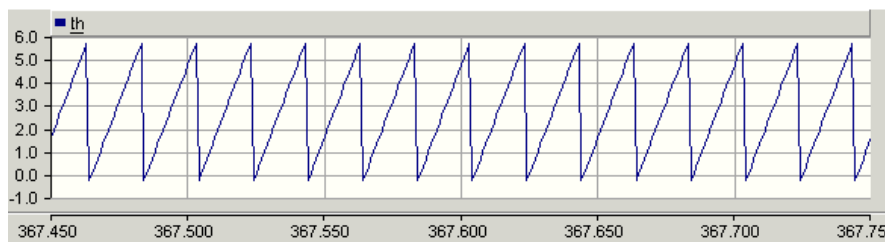


Figure 63: Generator operation: Phase angle Θ

The main aim of the phase locked loop is to detect the phase angle, and consequently, this, as well as the frequency, is an output. The frequency is stable at its base frequency, 50 Hz, and the phase angle varies between $-\frac{\pi}{6}$ and $\frac{11\pi}{6}$ with a frequency equal to the grid frequency and in phase with the phase a voltage. The phase angle output of the VCO does, in fact, vary between 0 and $2\pi$, but since this angle is related to the line-to-line voltages, 30 degrees ($\frac{\pi}{6}$) is subtracted from this value to achieve the correct phase angle. Figure 63 shows the triangular form of the phase angle, which has this shape throughout the simulation. The triangular form is due to the linearly changing phase angle, and when it has increased by $2\pi$, it drops, and a new round starts at synchronous speed.

The inner loop current controllers receive d- and q-axis currents and their references as input. Figure 64 shows that the currents follow their references very well.
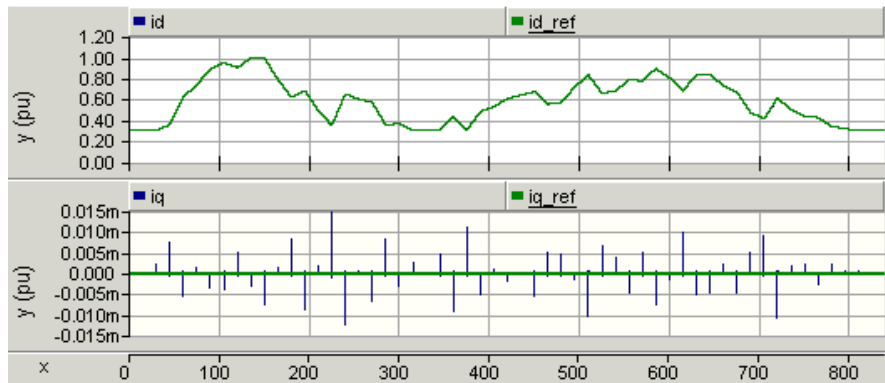
Figure 64: Generator operation: D- and q-axis currents and their references

The d-axis current equals $P_{ref}$ divided by $V_d$ ( $= 1$), and therefore is identical to $P_{ref}$. The q-axis current is kept at its reference value of zero pu throughout the simulation, except for minor transients in $i_q$ whenever $i_d$ changes its slope. The amplitudes of these transients are quite small, and we will now analyze one of these transients.

Figure 65 shows how the q-axis current is affected when the power reference, and thus d-axis current, changes value, or in this case, slope, due to the linear interpolation between data values. The slope of $i_d$ in figure 65 changes towards a more positive value. The q-axis current experiences an increase before it quickly stabilizes back to zero pu. The error is almost completely reduced in only 50 ms. Earlier it has been discussed that the d- and q-axis currents have been decoupled, but the reaction studied here shows that a complete decoupling has not been achieved, although satisfactory. The reaction is exactly opposite, when $P_{ref}$ and $i_d$ start to decrease by a steeper slope. This causes $i_q$ to first decrease before stabilizing back at its original reference value.
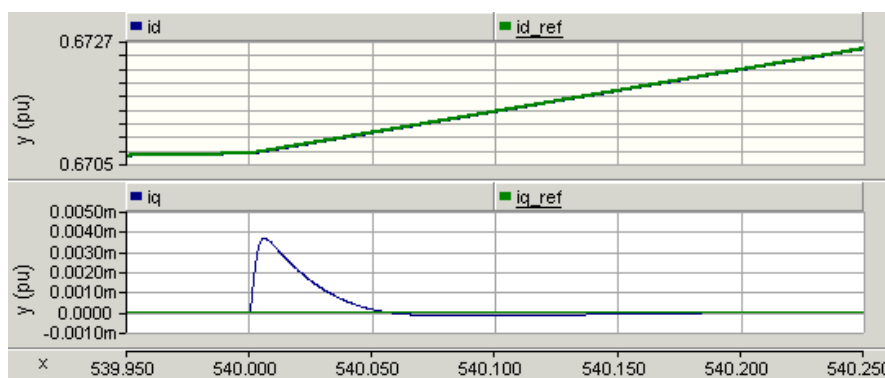


Figure 65: Generator operation: Q-axis current reaction to change in d-axis current

85

The converter voltages for the d- and q-axis are the output of the PI current controllers and shown in figure 66. $V_{conv,d}$ is approximately equal to one and $V_{conv,q}$ is relatively close to zero. The reactive power reference is set to zero to achieve a unity power factor. However, between the converter and the reference point for power, is a filter inductance, which requires a supply of reactive power. Figure 61 showed that the reactive power at the point of reference was equal to zero, and we can therefore conclude that the reactive power from the converter supplies the inductor. The d- and q-axis voltages have the same profile as $P_{ref}$. While $P_{ref}$ varies between 0.3 and 1.0 pu, $v_{conv,d}$ has a variation of maximum 0.005 pu, and $v_{conv,q}$ varies between 0.03 and 0.1 pu. The size of $v_{conv,q}$ decides the reactive power flow out of the converter, which is completely consumed by the filter inductance. The q-axis voltage increases for increasing power, which in turn shows that the inductor consumes an increasing share of reactive power for an increasing active power flow (due to the increasing current).
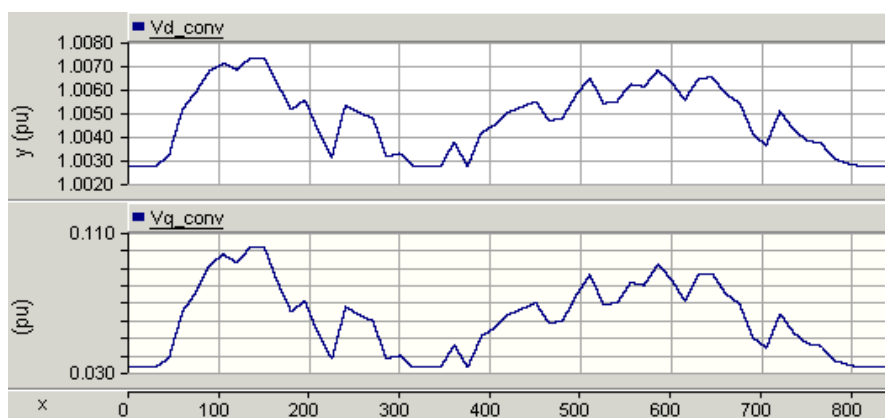


Figure 66: Generator operation: d- and q-axis converter voltages.

The converter voltages in the d-q rotating reference frame are further transformed into the three-phase PWM voltages as described in section 3.4.3.4. The pulse width modulated voltages are calculated from the modulation index and the phase angle, and are shown in figure 67. The voltages are at the system frequency of 50 Hz, and the voltage peaks are equal to the modulation index, which varies between about about 0.82 pu and 0.84 pu.

The modulation index and the phase angle are given in figure 100 in appendix I. Similarly, the same graph is given for pump operation in figure 101. In pump mode, the modulation index varies between 0.80 pu and 0.82 pu, due to the changed power flow direction. The modulation indexes are given to achieve the line voltage at the secondary terminal of the converter transformer equal to 70 kV, by compensating for power losses. A modulation index equal to 1 pu gives a pulse width modulated
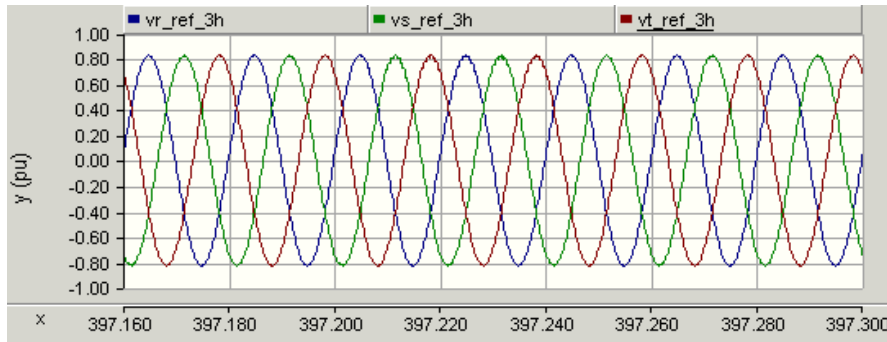
Figure 67: Generator operation: PWM three phase voltages.

line to line voltage equal to 85.7 kV according to the discussion in section 3.2.1.1.

### 4.3.1.3 HVDC Transmission Line

The HVDC transmission line is modeled with a resistance between the Norwegian and the German end. Further, a shunt capacitance at each end ensures a stabile DC voltage. Figure 68 shows the DC voltage at each end of the HVDC cable. The Norwegian converter substation is designed to control the DC voltage at a constant 140 kV. The varying power flow in the line, results in varying DC current, and therefore also varied losses through the resistance according to: $P = RI^2$. The DC voltage on the German end of the DC cable, equals the DC voltage at the opposite end minus the voltage drop over the resistance. This results in a profile, which is proportional to $-I_{DC}$, and also $-P_{DC}$. The maximum voltage drop over the resistance is 1.8 kV, which is 1.3 % of the rated voltage.



Figure 68: Generator operation: DC-link voltage at each end of the HVDC cable.

Figure 69 shows the controlled DC voltage plotted against its reference value, as well as the DC power and current, all measured at the Norwegian end. As expected, the DC current is proportional to the DC power, since the DC voltage

87
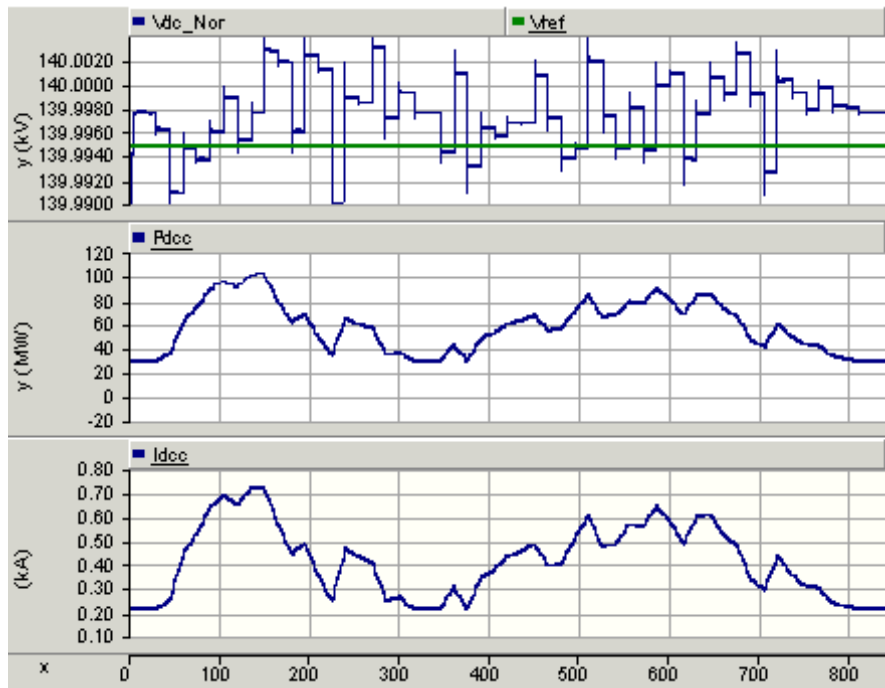
Figure 69: Generator operation: Controlled DC voltage, DC power and DC current

is constant. The controlled DC voltage is kept very close to its reference value, with a maximum error of about 8 V or 0.0057 % of the rated voltage. However, the behavior of the voltage is quite peculiar, since it has constant deviations, and never actually stabilizes at the exact reference value. The reason for this is the continually changing active power flow. Each constant error relates to the slope of change of the reference active power.

Figure 70 shows a change in DC current (and active power) slope and the resulting transient reaction in DC voltage. The DC current slope changes from negative to positive, and this results in a reduction of the steady state DC voltage error. A few short oscillations occur before the DC voltage stabilizes at a new constant error.
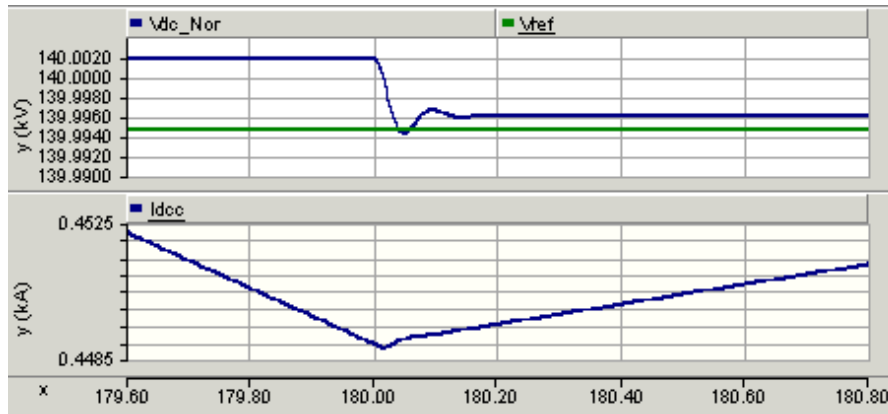
Figure 70: Generator operation: DC voltage reaction to DC current change

#### 4.3.1.4 Pump-side Converter and Synchronous Machine

Figure 71 shows the line to line voltage and phase a current on the pump side of the Norwegian converter substation. This is also the voltage seen by the terminals of the machine, due to no resistance in the transmission lines. The converter voltage peak varies around 80 kV with peak values in the range of 70 kV to 89 kV. This gives an rms line to line voltages between 49.5 kV and 62.9 kV, while the rated voltage equals 70 kV. This lower voltage is due to the reference speed given at 0.8 pu. The voltage is about proportional to the speed of the machine, which means 1 pu voltage is only achieved at 1 pu speed. The current has peak values ranging between 0.44 kA and 1.65 kA with a direction from the hydro generator and into the converter. We notice that these current values are a lot greater than the grid currents that had a maximum peak of 0.213 kA, and therefore other cables with appropriate current ratings will be required. The current varies with the active power generation of the hydro power plant, but also with the voltage, although not so apparent since the voltage varies in a relatively narrow range.

Figure 72 shows the active and reactive power generation of the machine. The active power generation is slightly higher then the reference power in order compensate for the losses in the transmission lines and to deliver the required reference power at the German converter substation output. The reactive power is approximately zero.

Figure 72 also shows the rotational speed of the generator and the gate opening, which varies between 0 and 1 (fully closed and fully open). As discussed earlier, the power electronic converters allow the machine to run at variable speed, instead of constant speed given by the synchronous frequency. The speed and gate opening

89
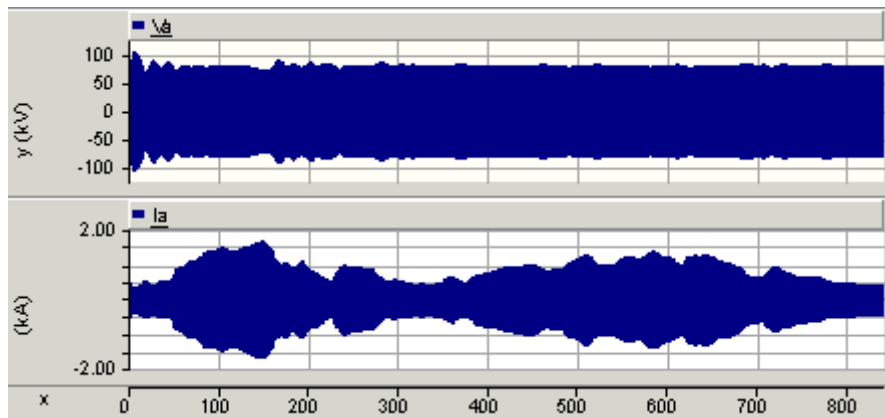
Figure 71: Generator operation: Line to line voltage at generator terminal and phase a current.
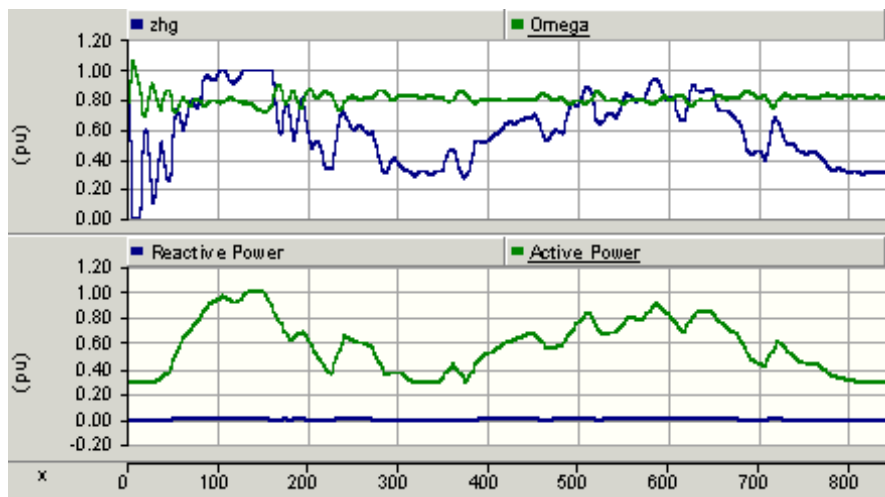


Figure 72: Generator operation: Synchronous machine power output, and turbine governor operation: omega and gate opening.

are controlled by the hydraulic governor, which was discussed in section 3.6.4.1. The governor requires a reference speed as input, which ideally should vary with the power demand, but for simplicity is set to 0.8 pu. The speed of the machine can therefore be seen to vary around this reference value throughout the operation. The gate opening obviously varies with the active power demand, letting more water through to the turbine when demand increases, but it also varies with the speed. Synchronous machines can assist in the primary frequency control of a system, by instantaneously adjusting the power output to ensure a balance between consumption and demand in the network.
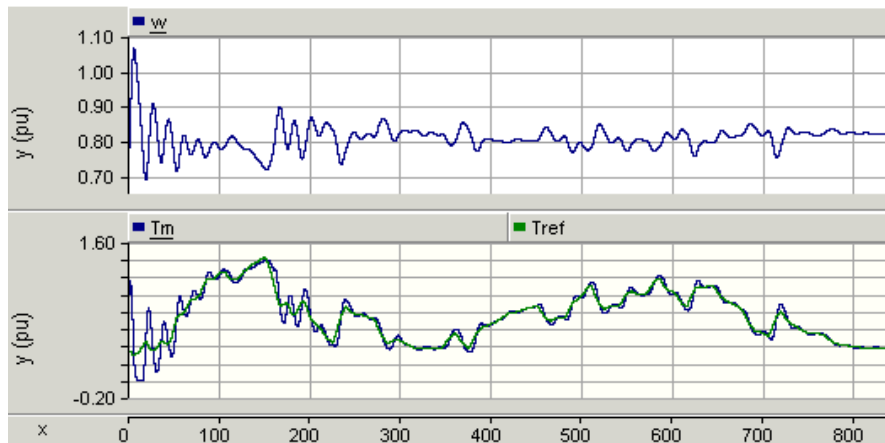
Figure 73: Generator operation: omega and mechanical torque

The rotor speed is shown in its own graph in figure 73. It is clear from this graph that omega varies around its reference set-point of 0.8 pu. The speed governor is quite slow and it appears that the rotational speed never quite stabilizes. This of course, is also due to the fact that the power flow is continuously changing, but also because we have shortened the time-axis of 24 hours to a 24 minute simulation. The torque reference is the output of the DC link voltage controller, and is used further in the control system to develop the current references, which in turn give the voltage references to the PWM converter. The mechanical torque follows the reference value well, although it has a few slow oscillations from the given reference, especially during the first 50 seconds. The oscillations in torque seem to be due to omega and the slow response of the turbine regulator. Since active power generated equals the torque multiplied by omega, the torque has a variation that offsets the varying omega in order to achieve a smooth power output.

The current references are developed in the outer control loops, which were discussed in section 3.6.2.2. The d- and q-axis current references are first developed in the flux oriented reference frame by torque and flux control, before they are transformed to the synchronously rotating d-q reference frame. The field current reference is developed directly from the power factor control loop. Figure 102 in appendix I shows the three currents with their references, which they all appear to follow quite closely.

The pulse width modulated voltages are given in figure 103 in appendix I.

### 4.3.2 Pump Operation

Figure 74 summarizes the reference directions for the system parameters, which will be used as a basis for the discussion of the results of pump operation.
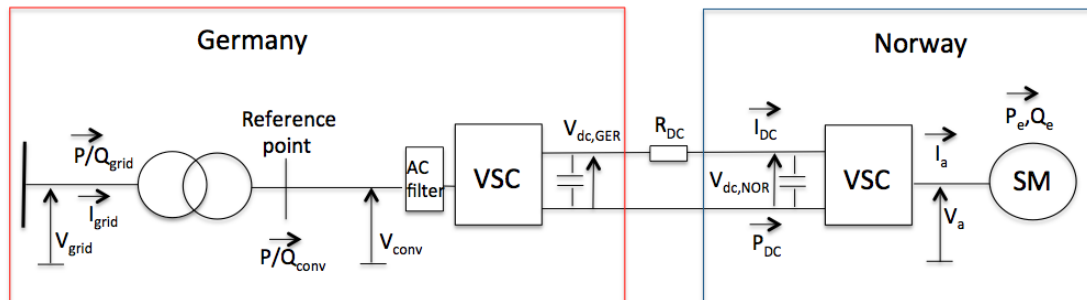


Figure 74: Test system with pump reference directions

The details of the time settings for the simulation, as well as user-defined reference values are summarized in appendix G2.

#### 4.3.2.1 Load Profile

The load data, which is used as input in the simulation model is described in section 3.3. Figure 75 shows the power references that are used for simulation of pump operation. The balancing profile has been decided from real data from May 6 and corresponds to the real-time hours between 21.45 and 06.15. The wind production was high during these hours, and the consumption is assumed to have been low through the night time hours. As mentioned earlier, the time axis has been shortened due to a very time consuming simulation, and therefore every second in the simulation equals 1 minute in real time. Data exists for every 15 minutes, or 15 seconds in the model, and PSCAD automatically linearly interpolates between the separate data points.

As mentioned for the generator operation, the power limits that are set for the machine are actually being used for the reference power flows, keeping them within 0.3 pu and 1.0 pu. In pumping operation, due to losses in the transmission of power from the grid to the pump, the lower limit of 0.3 pu will therefore be crossed. The losses should actually have been taken into account, resulting in a higher minimum power limit at the reference point. This is an improvement that should be added to the model, but is neglected for now. The reactive power reference is set to zero throughout the simulation.
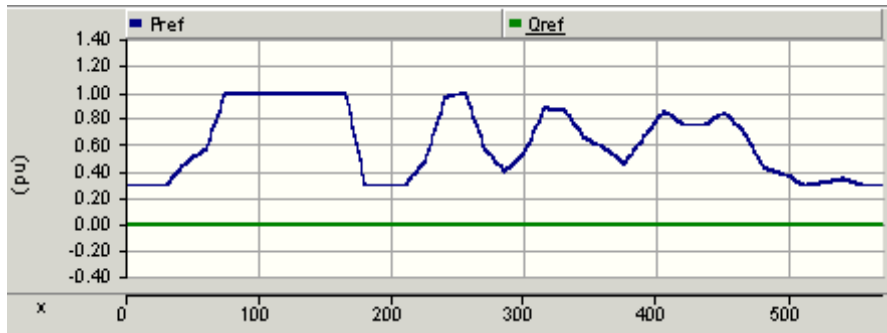
Figure 75: Pump operation: Active and reactive power references

#### 4.3.2.2 Grid-side converter

Figure 76 shows measurements on the grid side of the power system. The phase current has peak values ranging between about 0.068 kA and 0.216 kA, and direction towards the HVDC line. Its profile can be seen to follow the active power profile, which varies between 30 MW and 100 MW. This relationship between the current and power is due to the stiff voltage of the high voltage German grid. Similar to generator operation, the line to line grid voltage has an rms value of 380 kV and the converter AC line voltage is equal to 70 kV, and they are identical to the ones given in figure 59 for generator operation.
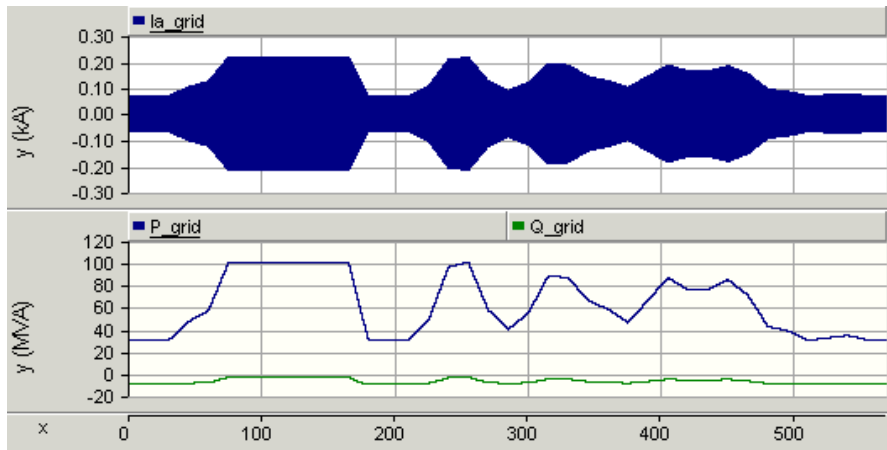


Figure 76: Pump operation: grid measurements

The grid-side transformer controls the active and reactive power flows according to the reference values given by an input file to the grid-side converter control circuit. In practical implementations these reference values could be either online measurements or information from the TSOs. $P_{ref}$ is given in per unit, and by

93

dividing it by $v_d$, the reference value for the d-axis current is achieved. In turn, the difference between the d-axis reference current and the actual current play a part in producing $v_d$, which together with $v_q$ and $\Theta$ give the PWM three phase voltages from the converter. Therefore, the measured active power follows its reference value very well.

The reactive power reference value is set to zero referred to the reference point as shown in figure 74. Both the reactive power reference and the measured reactive power are at zero pu. As for generator operation, shown in figure 61, the measured reactive power is has small variations from zero pu whenever the active power reference changes, but it quickly stabilizes back to zero. The control system has managed to control the reactive power very well.
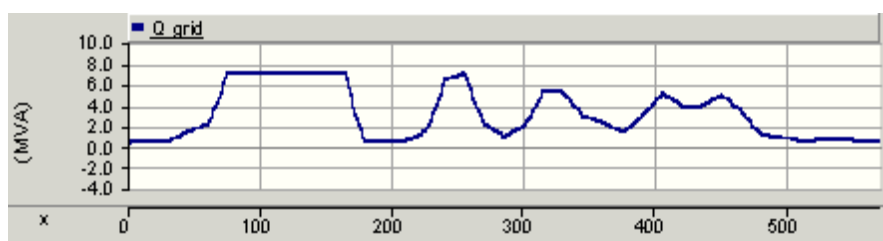


Figure 77: Pump operation: Reactive power from the grid

The reactive power on the primary side of the transformer, which has its positive reference direction from the grid, is given in figure 77. The reactive power is continuously positive, which means it is directed from the grid and into the transformer. The reactive power flow at this point is delivered to the transformer inductance, since we know that the reactive power on the secondary side of the transformer is equal to zero. The higher the active power flow, the more reactive power the transformer consumes, and therefore more reactive power is consumed from the grid. By including a filter capacitance on the AC side of the converter, this reactive power could be delivered from the filter capacitance instead of being consumed from the grid.

As mentioned earlier, the d-q reference frame is chosen in such a way that the d-axis is aligned with the voltage phasor of phase a. This results in $V_q = 0$ $V_d = V$, as shown in figure 78. $V_d$ and $V_q$ are outputs from the PLL block, where they are calculated by Clark and Park transform from the measured AC voltages. $V_d$ is approximately equal to 1 pu, but has minor variations that follow the changes in active power flow. The q-axis voltage component has small variations from 0 pu, whenever there is a slope change in active power reference.

The phase lock loop circuit also outputs the frequency and the phase angle. The frequency experiences constant deviations from its base value. Since the power
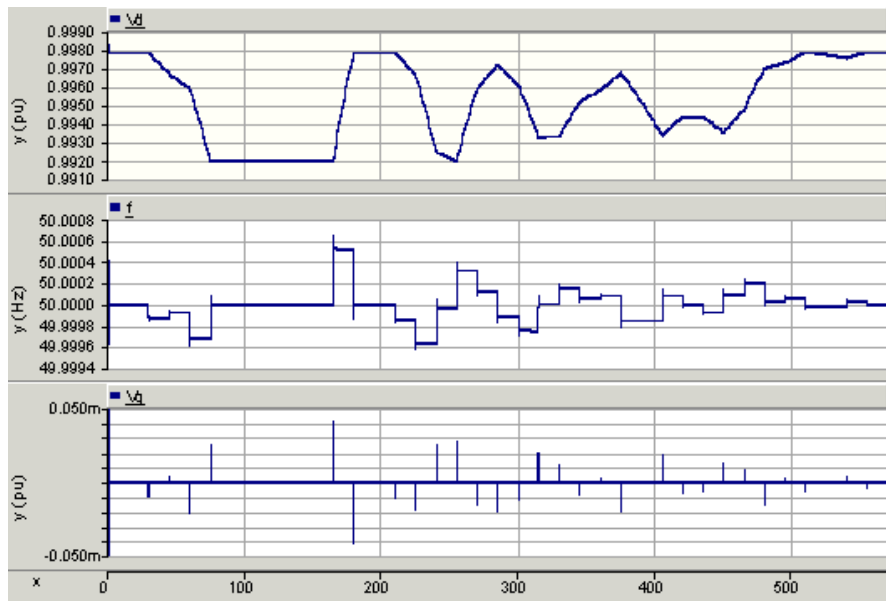
Figure 78: Pump operation: Phase Locked Loop

flow changes in slopes, it appears that a given slope gives a steady state error in frequency. When the power flow stabilizes, whatever the value, the frequency returns to its base value. Decreasing power flow results in a positive error in frequency, and opposite for increasing power flow. The phase angle, $\Theta$, is identical to the one achieved for generator operation and is shown in figure 63. The phase angle varies between $-\frac{\pi}{6}$ and $\frac{11\pi}{6}$ with a period equal to the grid frequency and in phase with the voltage in phase a.
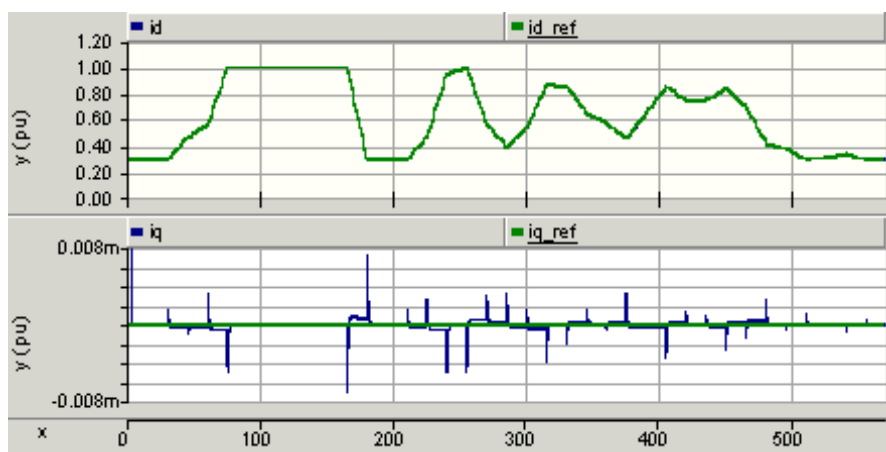


Figure 79: Pump operation: D- and q-axis currents and their references

The PI current controllers receive as input the d- and q-axis currents and current references, d- and q-axis voltages and the phase angle. The current error is measured and thereafter the PWM voltages are produced in such a way that the current error is reduced. Figure 79 shows the d- and q- axis currents and their references. Both currents follow their references very well. $I_{d,ref}$ is calculated by dividing $P_{ref}$ by $V_d$ and since $V_d = 1$, $I_{d,ref} = P_{ref}$ and is stated in per unit values. $I_{q,ref}$ is, depending on choice, calculated from a reactive power controller or an AC voltage controller. In the simulation the former is chosen, and the reactive power reference is set to zero. Notice that the graph of the q-axis current is zoomed in a lot to show minor deviations from zero. For every change in active power reference, the d-axis current also changes, and causes small transients in $i_q$, although highly insignificant. This shows that the currents are not decoupled completely, although satisfactory for the given operation.

Comparing the two graphs, it can be seen that when $i_d$ decreases, as a result of decreasing $P_{ref}$, $i_q$ also decreases to a value given by the slope of the decrease (which is linear for every 15 seconds). The steeper the slope, the larger the deviation from the q-axis reference value. Similarly, when $i_d$ increases, $i_q$ acquires a positive value. Note that the largest deviation in $i_q$ equals 0.008 mpu. This is shown more closely in figure 80.
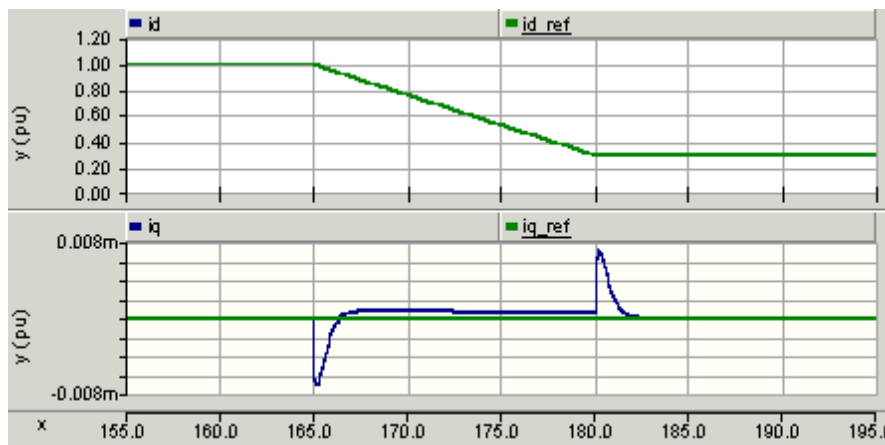


Figure 80: Pump operation: q-axis current reaction to change in d-axis current

The converter voltages in the d- and q-axis are shown in figure 81. $V_{conv,d}$ is approximately equal to one and $V_{conv,q}$ is approximately zero. This is because reactive power is set to zero, and the power factor is therefore unity. However, the graphs are zoomed in as to see the profile of change, which compared to $P_{ref}$ is exactly opposite. While $P_{ref}$ varies between 0.3 and 1.0 pu, $v_{conv,d}$ varies between 0.988 pu and 0.997 pu, and $v_{conv,q}$ varies between -0.027 pu and -0.098 pu. The size

96

of the q-axis converter voltage decides the reactive power flow out of the converter. As the absolute value of the q-axis converter voltage increases, the value of the d-axis voltage decreases to keep a constant magnitude of the voltage vector.
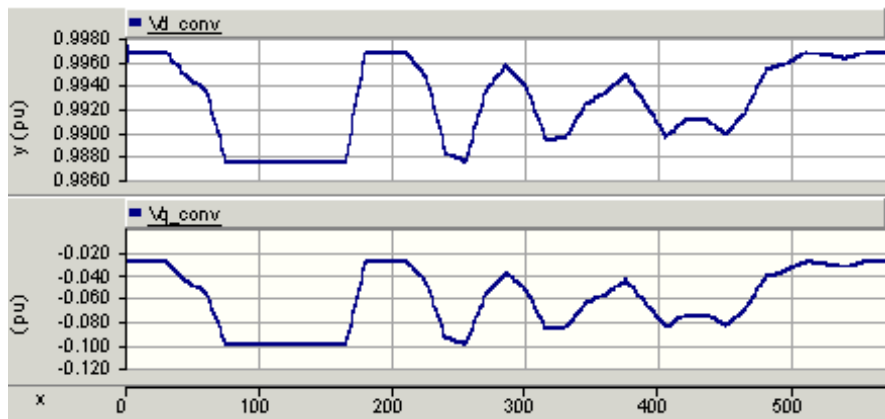


Figure 81: Pump operation: d- and q-axis converter voltages

The converter voltages are the output of the current controllers, as described in section 3.4.3.3. These voltages in the d-q rotating reference frame, are then transformed into the three-phase PWM voltages as described in section 3.4.3.4. The PWM voltages are calculated from the modulation index, which equals the voltage magnitude divided by the DC voltage, and the phase angle. The modulation index and phase angle are given in figure 101 of appendix I. The resulting three-phase voltages have peaks at about 0.8 pu and are shown in figure 82. They are very similar to the same voltages in generator operation, except with a slightly lower peak voltage.
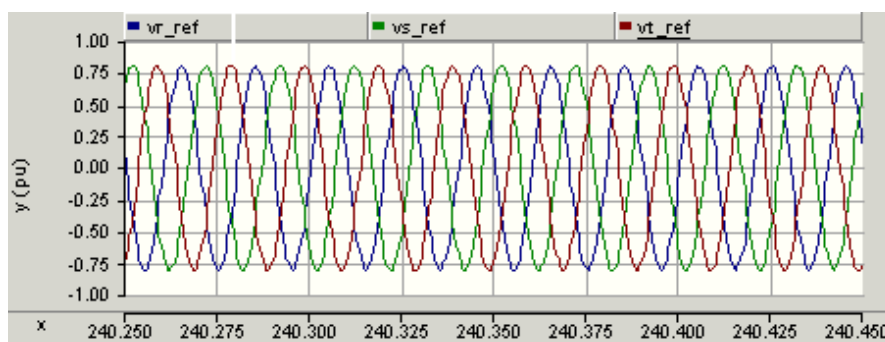


Figure 82: Pump operation: PWM three phase voltages

#### 4.3.2.3   HVDC Transmission Line

The DC voltage on the German end equals the DC controlled voltage on the Norwegian end plus the losses across the HVDC line, since the power is transported towards the pumped hydro storage plant. This is shown in figure 83. With a constant DC voltage, an increase in active power flow means an increase in DC current and hence an exponential increase in active power losses according to equation 43. This relationship causes the profile of the DC voltage to appear similar to the power flow. Low power losses is an important advantage of high voltage transmission due to low currents in the lines.

$$P_{loss} = RI^2 \tag{43}$$
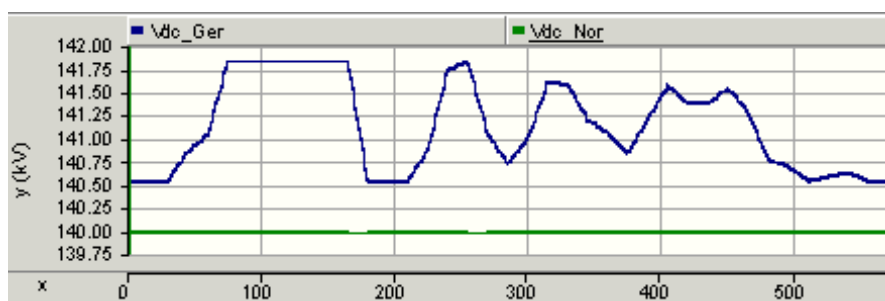


Figure 83: Pump operation: DC-link voltage on the German end.

Figure 84 shows the controlled DC voltage on the Norwegian end plotted against its reference value, as well as the DC power and current. The DC voltage follows its reference very closely, but always with minor constant errors, which change for changing power flow. An active power slope increase causes an instant DC voltage increase in order to deliver the correct power, until the DC current has increased sufficiently. Similarly, when the active power slope decreases, the DC voltage drops until it again stabilizes at its reference value. Between 165 seconds and 180 seconds, the power flow decreases linearly from 100 MW to 30 MW. At the point where the power starts to decrease, the DC voltage instantly drops and oscillates to a new steady state DC voltage while the power continuously decreases. At 180 seconds, when the power stabilizes again, the DC voltage returns to it's original steady state after a few oscillations.

As seen from the graph of DC current, the current changes proportionally to the power flow, which is obvious with a constant DC voltage. The current varies between about 0.21kA and 0.70 kA or between about 0.24 pu and 0.80 pu. The current does not reach 1 pu for 1 pu power, because the DC voltage is greater
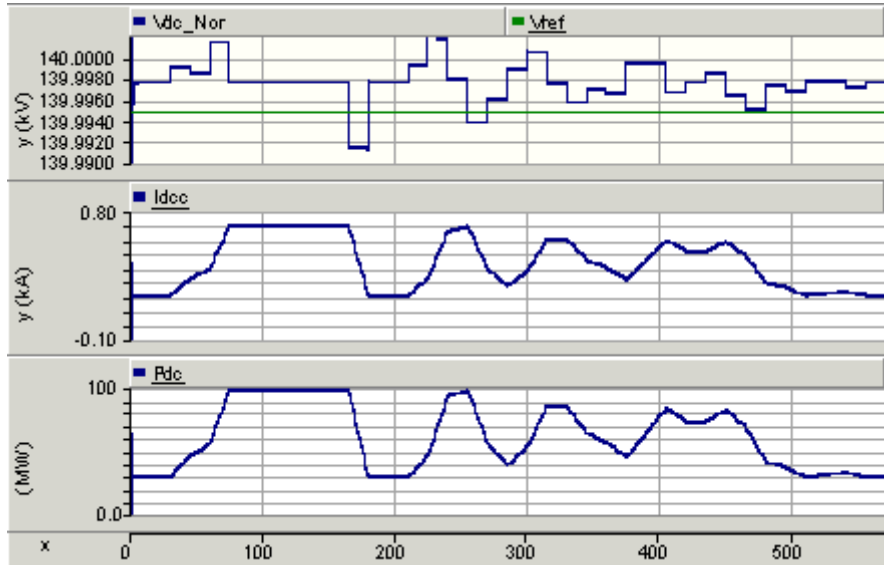
Figure 84: Pump operation: DC-link voltage on the Norwegian end and DC current.

than 1 pu and equal to 1.23 pu. The DC power is calculated by multiplying the instantaneous DC voltage by the DC current. DC power follows the reference load power and varies between 30 and 100 MW.

#### 4.3.2.4   Pump-side Converter and Synchronous Machine

Figure 85 shows the line to line voltage and phase a current on the pump side of the converter. The voltage varies between peak values of about 67 kV and 100 kV, which is equivalent to rms line to line voltages between 47 kV and 70 kV, where 70 kV equals 1 pu. The phase a current has peak values between 0.51 kA and 1.13 kA, which is equivalent to a range of 0.44 - 0.97 pu. Multiplying the current and voltage values gives a per unit power range between 0.295 pu and 0.97 pu. As discussed earlier, this range is slightly lower than the given power limits due to losses in the HVDC transmission.

The active and reactive power consumed by the synchronous motor, as well as the motor speed, are shown in figure 86. The reactive power is approximately zero throughout the simulation, while the active power varies identically to what is shown earlier on the grid side minus the active power losses in the DC transmission. In pump operation, the hydraulic system, consisting of the pump turbine, is modeled as a square load pump characteristic given by equation 40, repeated
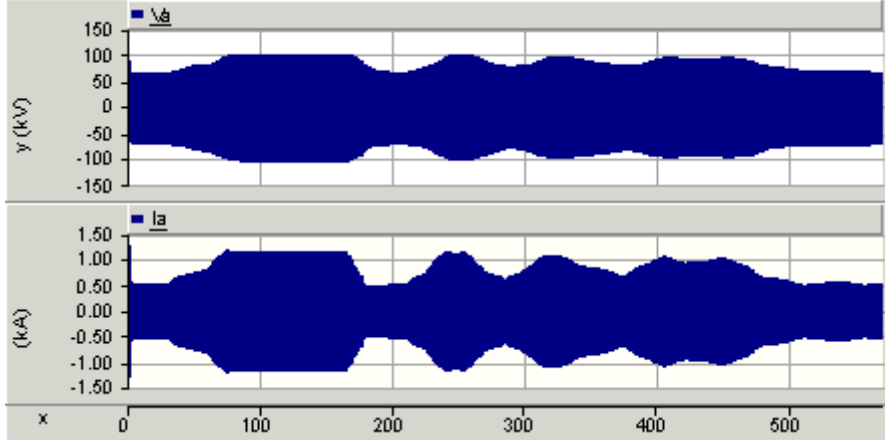
Figure 85: Pump operation: Line to line voltage at generator terminal and phase a line current.

below:

$$\tau_m = k_T \omega^2 \tag{44}$$

From the relationship between torque and power $(P = \omega T)$ and the power balance of the motor given in equation 45, we achieve equation 46.

$$P_e = P_m + P_{loss} \tag{45}$$

$$P_e = k_T \omega^3 + P_{loss} \tag{46}$$

Where $P_e$ is the electrical power into the motor, $P_m$ is the mechanical power on the rotor shaft, $P_{loss}$ are mechanical losses such as friction, $k_T$ is a constant and $\omega$ is the machine speed. Equation 46 gives us the relationship between the graphs shown in figure 86. With $k_T = -0.94$, the minimum power of 30 MW gives a rotational speed of 0.68 pu, while the maximum power of 100 MW gives a rotational speed of 1.02 pu. These maximum and minimum values seem to match very well with the graph. The losses in the synchronous machine model are minor, and will not be further considered.

Torque control is an important part of the converter and machine control. Figure 87 shows that the electrical torque of the machine follows its reference value very
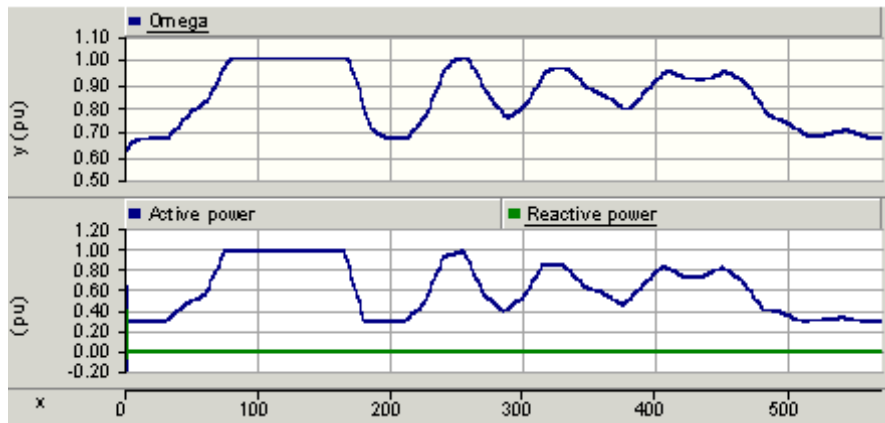
Figure 86: Pump operation: Synchronous machine active and reactive power consumption and radial speed
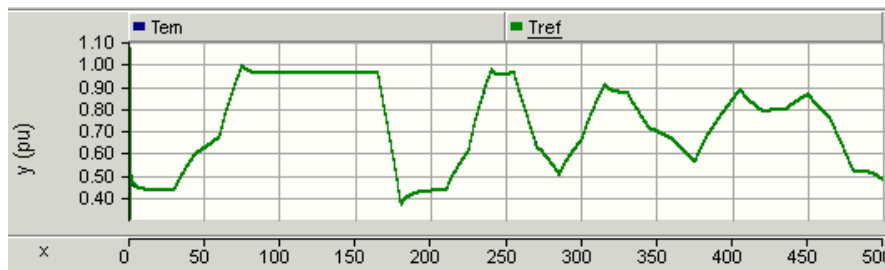


Figure 87: Pump operation: Mechanical torque with reference

well. The torque reference is the result of the DC voltage control, and a PI controller in the flux oriented reference frame reduces the error between the reference and actual torque.

The current references are developed in the outer control loops in the flux oriented reference frame. They are then transformed to the d-q rotating reference frame and used as input to the inner current controllers. Figure 104 in appendix I shows the d- and q-axis currents and their references. The field current, which is the excitation current to the synchronous machine field winding, is also shown with its reference which was developed through power factor control loop. All three currents follow their references very well.

The PWM output voltages for the pump-side converter are given in figure 105 in appendix I.

# 5 Discussion

## 5.1 General Considerations

There are a lot of aspects regarding the control system that could have been discussed and shown in graphs, but since tuning of the controllers has not been a focus, neither will the analysis of the short-term controller behaviour and reactions. The main part has been to construct a system with a control system that works on the overall basis. The focus is on graphs with too long of a time axis, to be able to say much about the controller tuning, except that the controllers have parameters that achieve stable and satisfactory operation.

### 5.1.1 Simplifications

Losses have only been included to a certain extent, and should be investigated more. Power losses are included through a resistance in the HVDC cable, but resistances otherwise are limited and should be included in a more realistic model to model transmission distances.

The synchronous machine is modeled with real parameters and electrical losses are therefore included, except for mechanical losses such as friction. The losses in the turbine and pump, or alternatively the pump turbine, have not been considered. Turbine and pump efficiency are typically equal to about 90 % each, giving a total efficiency of about 80 %. This, however, does not have much to say for the test system since the focus has been on accurate power flow, and the water volumes being pumped/let go have not been considered.

As discussed, the converter is modeled by an average value model. This is a model based on average values and typical simplifications. Non-linearities and harmonics are neglected. For this reason, the DC smoothing reactor and the AC filter capacitance have been omitted in the test system model, but would be important in a practical implementation or a more detailed model. Regarding losses, the conduction losses of the converter are included through series resistances on the AC side, but switching losses have been neglected.

### 5.1.2 External Limiting Factors

The operation of hydro reservoirs in Norway is highly regulated to ensure environmentally friendly operation. The use of a reservoir for pumped storage will heavily modify the current pattern of reservoir operation by introducing daily/seasonal/yearly

fluctuations in water volume and level. This will have both direct and indirect physical and biological impacts on the given reservoirs, as well as the downstream rivers. This, as well as other aspects directly related to the reservoir use and the environmental impacts of implementing a pumped storage hydropower plant, have not been taken into account.

An implementation of a system such as the one discussed in this thesis would require massive investments. The system is a balancing service and the investment costs should be shared in some way, and therefore international agreements would be necessary to ensure the success of such a long term investment. Also, the energy market requires some changes to facilitate increased energy storage into the energy mix. These factors are very important and are necessary to be solved, but have not been examined in this thesis.

## 5.2 Test System Model

### 5.2.1 Power Rating

The power rating of the machine and system is set to 100 MVA. In the simulation model one synchronous machine is used, while in reality this rating could also be achieved by having several lower rated synchronous machines in parallel. The detailed layout of the power plant has not been explored, and therefore will not be discussed more.

In a practical implementation, the power rating of a similar HVDC transmission system could be expected to be higher than 100 MVA. Implementing a configuration such as the one discussed involves a huge investment cost. Although an economic investigation has not been undertaken, one can imagine that some sort of cost-benefit analysis would be a part in the decision making. The higher the power rating of the given configuration, the more power can be transferred in both directions, and therefore the balancing service will be of greater value to the given network. Norway's newest HVDC connection to the Continent, the NorNed cable has a capacity of 700 MW, which also is the size of the planned Skagerrak 4 cable to Denmark. Therefore, an HVDC cable in a similar range would be a more realistic assumption. A setup of this size would then require several pumped storage plants in parallel to achieve the given capacity. Alternatively a back-to-back voltage source converter could be an interface between the power plant and the HVDC cable, which means that the HVDC cable would be connected to the Norwegian grid. Thereby the pumped storage power plant, and the HVDC cable, would have an expanded application. An increase in the DC line voltage could be expected following an increase in power rating.

### 5.2.2 Machine Line Voltage

It should be mentioned that a line voltage of 70 kV is unusually high for a synchronous machine. As an example, ABB Motors deliver very high voltage synchronous generators with a power rating between 5 - 55 MW and a voltage range between 20 and 70 kV [68]. Although applications do exist with a terminal voltage as high as 70 kV, some analysis should be done to decide an optimal layout and voltage rating.

To reduce the line voltage, a transformer could be placed between the converter station and the machine. This, however, complicates the control system, making it harder to achieve fast and accurate control. Alternatively, a lower AC line voltage could be chosen, but this also has its disadvantages. The lower the AC line voltage is compared to the DC voltage, the more inaccurate the output voltages would be. We must keep in mind that the output voltages of a two-level PWM converter are, in fact, the average of two discrete values. If, for example, the DC voltage equals 100 kV and the AC line voltage equals 10 kV, one tenth of the time, the output voltage will equal 100 kV, and the rest of the time it will equal zero. In addition, a machine with such a low terminal voltage would have to be constructed to handle the voltage pulses of 100 kV. In the case of transmission distances from the converter substation, an argument for higher voltage would also be the reduced losses. Also, a lower AC voltage with a given power rating, would result in higher currents according to Ohms law. This in turn will affect the choice of transmission line/cable, since its current ratings have to be high enough, and consequently this will become a question of economics due to high cost.

As a simplification, however, the machine in the test system has been chosen to operate at a line voltage of 70 kV.

### 5.2.3 Load Profile

A load profile has been chosen to illustrate the need for both power generation and power consumption in Germany. The profile has been developed from real measured wind power data from Amprion, the main TSO. The available data was given for the whole day in intervals of 15 minutes. To be able to run a simulation, which illustrates a whole day, every real time minute was shortened to just a second in the simulation. The model therefore runs a simulation, which has a timescale for a total of about 24 minutes, instead of 24 hours. The computational time has consequently been reduced by a factor of 60, making the simulation runs possible.

This simplification, however, can be expected to affect the results. The assumption

done to verify this decision, is that shortening the time scale, and thereby forcing quicker and sharper changes in the system operation will in fact put more stress on the operation. By showing that the system functions satisfactory under this "stressed" operation, it can be expected that the control and electrical system will operate at least equally good under slower changes in power flow. Slower, and less frequent changes, give the system more time to stabilize to new steady states.

### 5.2.4   Machine Operating Limits

The power limits, which have been chosen for the pumped storage power plant following the discussion in section 3.6.3.1, are applied to the power reference input, which therefore varies between 0.3 and 1.0 pu. The power references are referred to the secondary terminal (low voltage side) of the transformer. In order to deliver a certain amount of power to this point in generator mode, the power produced at the source must take into account the losses on the way and will therefore be greater. Since the power limits are actually chosen for the synchronous machine, the power limits for the input reference should be compensated by the losses in the line. Similarly for pump operation, due to losses between the grid and the pump, the power delivered to the motor will be less than the lower limit of 0.3 pu. This is an improvement that should be taken into account and added to the model.

## 5.3   System Operation

### 5.3.1   General Operation

The general operation of the test system has shown to be quite satisfactory. The active power reference is achieved from real wind data in Germany, and the re-active power reference is set to zero. The intention of the system is to increase balancing capacity in order to support large shares of renewable energy production in Europe. Germany is a very representative nation for Europe regarding its focus on increasing wind power production, and using data from here is therefore a rather interesting and realistic assumption.

The grid voltage on the German end is chosen as a stiff voltage and it is stepped down by a transformer before connection to the voltage source converter substation. Both the voltage on the primary side and the secondary side of the converter transformer are stiff throughout the simulations as shown in the results. An AC filter is added to the output of the converter, to reduce the AC harmonics. The

reference power is inputed to the control system, and its reference is the secondary terminal of the converter transformer.

The grid-side converter controls the active and reactive power by following the input reference and either sending or receiving the necessary amounts of active and reactive power. This is done through a cascaded control structure in the d-q rotating reference frame, where the outer controllers determine the current references through active and reactive power control. The inner controllers decide the converter voltages that make sure that the currents keep to their references. Although the d- and q-axis currents have said to be decoupled in the control system, changes in the d-axis current due to changes in power flow, cause minor transients in the q-axis current. In turn, short transients also occur in the reactive power flow.

The results in the previous section, show that the active and reactive powers are delivered as expected during both generator and pump operation. The active power flow follows the given input reference between 30 MW and 100 MW and the reactive power is kept at zero. Although the reactive power reference is set to zero and it is fact equal to zero at the reference point, the results have shown that reactive power does flow in the test system. This is due to network components that consume reactive power. The grid-side converter outputs the necessary reactive power to supply the AC filter, and the transformer consumes reactive power from the grid. The reactive power is discussed separately in the next section.

The HVDC transmission line connects the VSC in Germany and the VSC in Norway. It is modeled with a storage capacitor at each end, and with a series resistance to account for active power losses. The DC voltage is controlled by the converter substation in Norway, and the voltage at this end is therefore constant at the given rated value of 140 kV. The DC voltage at the other end of the HVDC line varies according to the power flow, due to the power losses in the resistance. The German DC voltage is greater than 140 kV for pump operation and less for generator operation. The maximum voltage difference is 2 kV or 1.4 % of rated voltage.

Due to a constant DC voltage, the power flow is transferred through the transmission line by a varying current. Bidirectional power flow is achieved without changing the polarity of the DC voltage. A similar control structure is used for the voltage source converter on the Norwegian end. A cascaded structure is also used here, and the inner controllers ensure that the currents follow their references. A third current controller is implemented in this control structure to control the excitation (or field) current of the synchronous machine. The outer controllers are constructed in the flux oriented reference frame. This is done to achieve optimal control of the synchronous machine. A DC voltage control decides a torque refer-

ence for the machine. The torque and flux controllers decide the current references. The field current of the machine is controlled through a power factor controller.

Pump and generator operation are modeled separately regarding the mechanical system. In pumping, only the electric power is controlled and the wicket gate is assumed to be completely open to let as much water as possible through. The pump turbine is modeled as a simple square load. For generator operation, on the other hand, the mechanical power, as well as the electrical power, must be controlled. This is achieved through a hydro turbine governing system.

Both pump and generator operation are run at variable speed and this is achieved by controlling the power of the machine instead of the speed. The speed varies more for pump operation, between about 0.65 pu and 1.0 pu, than for generator operation. This is because the turbine governor of the generator model requires a reference speed (omega) as input. Ideally this speed should be given by a preset power-frequency characteristic that optimizes the turbine efficiency. As a simplification, however, this reference speed is constant at 0.8 pu and the generator operation of the system varies around this speed.

The results show expected behavior and the test system, although quite simplified, models a well-functioning balancing service between Norway and Germany. In order to show the robustness of the system, expected fault conditions should be simulated to test the reaction and prove stable control.

### 5.3.2  Active Power Flow

The input file to the test system, deciding the load to be balanced, consists of data points which are 15 seconds apart. PSCAD interpolates between these active power values, which results in continuously changing active power demand. Since the DC line voltage is constant, this results in a continuously changing DC current as well. In a practical application, the changes in active power demand would most often be step changes with a given ramping rate and possibly also a frequency droop characteristic. The power (and also DC current) would therefore change in a shorter period of time given by the ramping rate instead of continually changing. Two topics should be discussed regarding the continually changing active power in the test system: the inductance of the HVDC line and the PI controllers.

The HVDC cable has been modeled with a resistance to include active power losses, but the inductance of the cable has been neglected. A typical configuration consists of a smoothing inductor in combination with a high-pass filter, in order to limit the flow of harmonic currents on the transmission line. Neglecting the inductor

is sensible because the average value model used to represent the converter in the test system neglects non-linearities and harmonics.

An inductance affects the voltage during changes in current, according to equation: $V = L\frac{di_L}{dt}$. In the case of step changes, the inductance has minimal effect because the current will be constant for the majority of the time and there would be no voltage drop over the inductance. Including an inductance in the test model, where the current is constantly changing, results in an unrealistic scenario, where the inductance more greatly affects the system. This is the basis for neglecting the inductance in the test system.

PI controllers are the main building block of most of the controllers in the test system. In the short theory chapter on the PI controller it was stated that in order to obtain zero steady-state deviation by use of a PI controller, the reference signal must be constant. Throughout the results chapter, many graphs can be found that have steady-state errors compared to their references. This is seen in the graphs of the DC voltage and of the frequency. We can conclude that the reason that these errors appear is due to the constantly changing power reference, and each steady state error is given by the slope of change.

### 5.3.3 Reactive Power Flow

The main focus of the test system is the active power, as is the typical case since active power is the "useful" power. However, the reactive power is an interesting topic to discuss. Although the reactive power reference is set to zero, it has been observed throughout the results that there exists reactive power flow in the test system. This is because certain components in the test system consume reactive power. In both generator and pump operation, the grid-side converter supplies some reactive power to the inductor of the AC filter on the grid-side of the system. The inductor draws as much as 9.9 MVAr at rated power. Also the transformer consumes reactive power due to its inductive nature, and this power is supplied by the grid (about 7 MVAr at rated power). By including a shunt capacitor in the AC filter, reactive power could be supplied from such a power factor correcting capacitor instead of drawing reactive power from the grid. The reactive power flows are in such a way that the resulting reactive power at the point where measurements are taken, equals its reference value of zero pu. The synchronous machine can control the reactive power balance on the generator-side by either supplying or absorbing reactive power.

## 5.4 Recommendations for Further Work

The control of a variable speed pumped storage hydropower plant and its operation are complex topics. Many simplifications and assumptions have been done in the test model and control system of this thesis. There are many topics that should be investigated in more detail, considering both a possible implementation of a similar system or of general interest. This section will address some of these topics, which are recommended for further work. In addition to the points mentioned below, faults and unbalanced conditions should be simulated to verify the robustness of the test system.

### 5.4.1 Controller Tuning

Controller tuning has not been a focus of this thesis work. Some controller parameters have been adapted from a similar simulation model, while others have been achieved by trial and error. The controller performance can very likely be improved by properly choosing the gain and time constant values by various tuning techniques, such as the modulus optimum or symmetrical optimum. The following references discuss tuning of controllers: [40], [69] and [70]. Tuning has not been a focus of this report, but should be an important part of further work to achieve optimal system performance.

Specifically, the turbine governor model in generator operation, should be mentioned regarding tuning and parameter choices. Some time should be spent on improving the design to achieve optimal operation. This involves, among other things, to increase the damping of the oscillations, which is quite low in the given model. Also, a more detailed model of the turbine and waterway may be necessary.

### 5.4.2 Turbine Efficiency

Regarding the turbine governor, which controls the speed of the generator to a preset reference, the turbine efficiency should be mentioned. One of the advantages of using variable speed pumped storage hydro plants is to operate at the speed that optimizes the turbine efficiency for differing heads and power flows. This should be further investigated and implemented into the test system. A similar investigation has been done in reference [41]. Following improvements in turbine efficiency, operating cost savings can be expected.

### 5.4.3 Balancing Strategy

The balancing strategy of a system has not been analyzed in detail. This strategy would depend on the power capacity of the balancing source, the nature of the balancing load, transmission capacities, maximum and minimum limits, amongst other factors. This should be further investigated, in order to clarify the balancing potential of a given system and also to achieve the most advantageous operation.

# 6    Conclusion

The need for energy storage in a future European energy system based on variable renewable resources has been addressed. Increased penetration of variable renewable energy resources is a challenge for the stability of the transmission system. This master thesis proposes and analyzes a system for balancing power in Europe, based on pumped storage hydro in Norway.

The test system consists of a pumped storage hydro power plant located in Southern Norway, directly connected by an HVDC transmission line to a varying load in Germany. The pumped storage plant is modeled by a synchronous machine and can run at variable speed, in both generator and pump mode, due to the power electronic interface. The HVDC transmission is based on the voltage source converter technology and consists of a converter station at either end, with submarine cables traversing the ocean. The load profile in Germany has been based on real measured wind data, and scaled to fit the power ratings of the test system. This system allows for bidirectional power flow, and the load data expresses both lack and excess of power throughout a 24 hour period.

The test system requires a complex control system to achieve stabile operation. The control strategy for the VSC-HVDC is developed and based on the vector control principle. A cascaded control structure is implemented consisting of outer controllers and faster inner current controllers. Two completely decoupled control systems are implemented for each of the converter stations, where the grid-side converter is chosen to control the active and reactive power flow and the generator-side converter controls the DC voltage. Due to the independent control systems, the need for communication between the converters is eliminated, which is a major advantage. A current control strategy in the d-q rotating reference frame with feed forward terms is used to decouple the non-linear and strongly coupled current equations. By doing this, independent control of the active and reactive power flows is achieved. The active power control is solved by dividing the reference active power by the d-axis voltage to give the d-axis current reference. Similarly, the q-axis current reference is achieved from the reactive power control.

The test system, with its control system, is implemented in the simulation software PSCAD/EMTDC. Simulation results are presented and testify the fast response and the stabile system operation. The power control is well functioning and the results show that the active and reactive power flows are as expected during both generator and pump operation. Similarly, the DC voltage controller keeps the DC voltage stiff, which proves the robustness of the controller, although short transients due occur during changes in active power flow. Summarizing, the results show how the variable speed pumped storage plant can be controlled to balance

both excess, as well as lack of power, in Germany (and Europe), and thereby support the integration of wind and solar power.

In conclusion, energy storage will play an inevitable role in achieving a clean European energy supply. The test system developed in this thesis, although quite simplified, has proven through simulations to be a promising alternative for offering balancing services to Europe. Many aspects, such as economics and the energy market, will, however, have a major say in how the challenges we stand before today are solved.

# References

[1] Hamnaberg, H., Vattenfall Power Consultant (2011): *Pumpekraft i Noreg. Kostnadar og utsikter til potensial.* NVE rapport nr. 22.

[2] Wellington J.; Bathmaker A.; Hunt C.; McCulloch G.; Sikes P. (2005): *Succeeding with your doctorate.* Sage, London.

[3] Fornybar (2012): *Pumpekraftverk.* Available from: `http://fornybar.no`. Viewed September 2012.

[4] SET-Plan Information System (SETIS) (2011), *Electricity storage in the power sector*, JRC European Commission.

[5] Arantegui, R., Fitzgerald, N., Leahy, P. (2012): *Pumped-hydro energy storage: potential for transformation from single dams.* European Commission, Joint Research Centre (JRC). Netherlands.

[6] European Commission (2012): *Renewable energy targets by 2020.* Available from: `http://ec.europa.eu/energy/renewables/targets_en.htm`. Viewed November 2012.

[7] The Economist (2012): *Packing some power.* The Economist.

[8] Zuber, M. (2011): *Renaissance for Pumped Storage in Europe.* Available from: `http://www.hydroworld.com/articles/print/volume-19/issue-3/articles`. Viewed December 2012.

[9] Hydro Equipment Association (2012): *Pumped storage power plants.* Available from: `http://www.thehea.org/hydropower/special-focus/`. Viewed October 2012.

[10] Killingtveit, Å. (2001): *Design of Future Pumped Storage Hydropower in Norway.* Power point. CEDREN. Available from: `http://norwegen.ahk.de/fileadmin/ahk_norwegen/Dokumente/Presentasjoner/wasserkraft/Design_of_Future_Pumped_Storage_CEDREN_Killingtveit.pdf`. Viewed October 2012.

[11] Strømmen, I. (2012): *Ingeniørfaglige bidrag til et bærekraftig og nyskapende Norge (6) - Forskningsutfordringer knyttet til vannkraft.* Fakultet for Ingeniørvitenskap og teknologi, NTNU. Available from: `http://www.forskning.no/blog/ingvaldstrommen/335990`. Viewed November 2012.

[12] Nicola, S (2012), *In Germany and Elsewhere, Energy Storage is Key to Unlocking Renewable Energy*, Bloomberg. Available from: `http://www.renewableenergyworld.com/rea/news/article/2012/08/`

`in-germany-and-elsewhere-energy-storage-is-key-to-unlocking-renewable\`
`-energy`. Viewed November 2012.

[13] Eurelectric WG Hydro (2011): *Hydro in Europe: Powering Renewables* Eurelectric Renewables Action Plan (RESAP).

[14] Sætre, A. (2012): *Use of Pumped Storage to Balance Varying Output From Large-Scale Wind Power Installation in the North Sea.* Specialization project, NTNU.

[15] Øygard, K. (2008): *Pumpekraftverk for effektproduksjon. Masteroppgave i energi og miljø.* NTNU, Trondheim.

[16] Huber,C. Gutschi, C. (2010): *Pump-Storage Hydro Power Plants in the European Electricity Market.* Institute for Electricity Economics and Energy Innovations Graz University of Technology.

[17] Alstom (2012): *Hydro Pumped Storage Power Plant,* Technical Brochure. Available from: www.alstom.com. Viewed October 2012.

[18] Molinas, M., Nysveen, A. (2012): *Electric Systems for Pumped Storage Plants - technology evaluation.* SINTEF Energy Reasearch - Electric Power Technology.

[19] Suul, J.A. (2006): *Control of Variable Speed Pumped Storage Hydro Power Plant for Increased Utilization of Wind Energy in an Isolated Grid.* Master Thesis, Department of Electrical Power Engineering, NTNU.

[20] Suul, J., Uhlen, K., Undeland, T. (2008): *Variable speed pumped storage hydropower for integration of wind energy in isolated grids - case description and control strategies.* Nordic Workshop on Power and Industrial Electronics, NORPIE 2008, IEEE.

[21] Toshiba (2008): *Adjustable Speed Pumped Storage Experiences.* Avialable from: `http://www3.toshiba.co.jp/power/english/hydro/products/pump/storage.htm`. Viewed November 2012.

[22] Siemens (2012): *Fact Sheet: High-voltage direct current transmision (HVDC)* Siemens. Available from: `http://www.siemens.com/press/pool/de/events/2012/energy/2012-07-wismar/factsheet-hvdc-e.pdf` Viewed April 2013.

[23] Mohan, N., Undeland, T., Robbins, W. (2003): *Power Electronics: Converters, Applications and Design,* 3rd edition, John Wiley & Sons, Inc.

[24] ABB (2013): *The Classic HVDC Transmission.* ABB. Available from: `http://www.abb.com/industries/us/9AAC30300393.aspx`. Viewed March 2013.

[25] ALSTOM (2013): *HVDC.* ALSTOM. Available from: `http://www.alstom.com/grid/products-and-services/engineered-energy-solutions/hvdc-transmission-systems/`. Viewed April 2013.

[26] Siemens (2013): *HV Direct Current Transmission System (HVDC).* Siemens AG. Available from: `http://www.siemens.com/press/pool/de/events/2012/energy/2012-07-wismar/factsheet-hvdc-e.pdf`. Viewed April 2013.

[27] Bajracharya, C. (2008): *Control of VSC-HVDC for wind power.* Master of Science in Energy and Environment. Department of Electrical Power Engineering, NTNU.

[28] Bahrman, M., Johnson, B. (2007): *The ABCs of HVDC Transmission Technologies.* IEEE power & energy magazine.

[29] Flourentzou, N. et al. (2009): *VSC-Based HVDC Power Transmission Systems: An Overview* IEEE Transactions on Power Electronics Vol.24, No.3.

[30] Sood, Vijay (2010): *Comparison between Direct and Vector Control Strategy for VSC-HVDC system in EMTP-RV.* IEEE.

[31] ABB (2007): *HVDC tutorial.* ABB. Available from: `http://www.ercot.com/meetings/rpg-crez/keydocs/2007/RPG_CREZ_20071008/HVDC_Tutorial_4_-_HVDC_Fundamentals.pdf`. Viewed March 2013.

[32] ABB (2013): *Skagerrak 1-3 HVDC Interconnections.* ABB. Available from: `http://www.abb.com/industries/ap/`. Viewed April 2013.

[33] ABB (2013): *The NorNed HVDC Connection.* ABB. Available from: `http://www.abb.com`. Viewed April 2013.

[34] Fitzgerald, A., Kingsley, C., Umans, S. (2003): *Electric Machinery.* 6th ed. McGraw-Hill Higher Education.

[35] Machowski, J., Bialek, J., Bumby, J. (2008): *Power System Dynamics Stability and Control.* John Wiley & Sons, Ltd. UK.

[36] Mohan, N. (2003): *Electric Drives: an integrative approach.* MNPERE, Minneapolis.

[37] Kundur, P. (1994): *Power System Stability and Control.* McGraw-Hill, Inc.

[38] Balchen, J.G., Andresesn, T., Foss, B. (2003): *Reguleringsteknikk.* 5th edition. Institutt for teknisk kybernetikk, NTNU.

[39] Song, R., Zheng, C., Li, R., Zhou, X. (2005): *VSCs based HVDC and its control strategy.* IEEE Transmission and Distribution Conference & Exhibition: Asia and Pacific. Electric Power Research Institute, Beijing, China.

[40] Padiyar, K., Prabhu, N. (2004): *Modelling, Control design and Analysis of VSC based HVDC Transmission Systems.* IEEE. International COnference on Power System Technology - POWERCON, SIngapore.

[41] Naidu, M., Mathur, R.M. (1989): *Evaluation of Unit Connected, Variable Speed, Hydropower Station for HVDC Power Transmission.* IEEE Transactions on Power Systems, Vol. 4, No.2.

[42] Amprion (2009): *Amprion - The Strong Power Network.* Amprion GmbH, Dortmund. http://www.amprion.net/sites/default/files/pdf/9153_Amp_Imageb_GB_Kor.pdf.

[43] Peralta, J., Saad. H., Dennetiere, S., Mahseredjian, J. (2012): *Dynamic Performance of Average-Value Models for Multi-terminal VSC-HVDC Systems.* Proceedings of 2012 IEEE Power and Energy Society General Meeting, PES 2012, San Diego, CA, USA.

[44] Chiniforoosh, S., et. al. (2010): *Definitions and Applications of Dynamic Average Models for Analysis of Power Systems.* IEEE Transactions on Power Delivery, Vol. 25, No. 4.

[45] Noguchi, T. et al (1998): *Direct Power Control of PWM Converter without Power Source Votlage Sensors.* IEEE transactions on industry applications, Vol 34, No 3.

[46] Suul, Jon Are, Sintef. Personal communication, spring 2013.

[47] Ding, Yi-ping (2011): *Study on Vector Control used in VSC-HVDC.* IEEE, Changsha University of Science & Technology, China.

[48] Molinas, M. (2012): *Specialization course Elk.* NTNU.

[49] Chung, S. K. (2000): *Phase-locked loop for grid-connected three-phase power conversion systems.* IEE Proc.-Electr. Power Appl. Vol. 147, No.3.

[50] Haileselassie, T., Molinas, M., Undeland, T. (2008): *Multi-Terminal VSC-HVDC System for Integration of Offshore Wind Farms and Green Electrification of Platforms in the North Sea.* Nordic Workshop on Power and Industrial Electronics, Finland.

[51] Patel, H., Sood, V. (2010): *Modeling of Voltage Source Converter Based HVDC System in EMTP.* IEEE Electrical Power & Energy Conference.

[52] Khatir, M. et al. (2009): *Performance evaluation of an hvdc link with a capacitor commutated inverter connected to a very weak receiving ac network.* Journal of Electrical Engineering, Vol.60, No. 4.

[53] Manitoba HVDC Research Centre (1994): *PSCAD/EMTDC users manual.*

[54] Arrillaga, J. et al. (1992): *Characteristics of unit-connected HVDC generator-converters operating at variable speeds.* IEEE proceedings, Vol.139, No.3.

[55] Samuelsson, O. (2013): *Synchronous Generator Dynamics.* Lund University. Available from: `http://www.iea.lth.se/eks/L5_12.pdf`. Viewed April 2013.

[56] Wikipedia (2012): *Pumped-storage hydroelectricity.* Available from: `http://en.wikipedia.org/wiki/List_of_pumped-storage_hydroelectric_power_stations`. Viewed November 2012.

[57] Vattenfall (2012): *Markersbach.* Available from: `http://powerplants.vattenfall.com`. Viewed December 2012.

[58] Chemistry Daily (2012): *Pumped-storage hydroelectricity.* The chemistry encyclopedia. Available from: `http://www.chemistrydaily.com/chemistry/Hydroelectric_energy_storage`. Viewed November 2012.

[59] Grøv, E. (2011): *Developing future 20 000 MW hydro electric power in Norway - Possible concepts and need of resources.* SINTEF Energy.

[60] Griffiths, H. (1990): *Nathional Engineering Landmark Plaque Unveiling.* Tumut 3 Power Station, Talbingo NSW, Australia.

[61] CLP (2012): *Guangzhou Pumped Storage Power Station.* Available from: `https://www.clp.com.hk/ouroperations/power/guangzhoupumpedstoragepowerstation`. Viewed November 2012.

[62] Avellan, F. (2011): *Storage Pumps & Reversible Pump Turbines.* Laboratory for Hydraulic Machines (LMH). Available from: `http://www.renewables-grid.eu`. Viewed November 2012.

[63] IEA Hydropower (2006): *Mingtan Pumped Storage Power Plant.* New Energy Foundation. Taiwan. Available from: `http://www.ieahydro.org/reports/Annex_VIII_CaseStudy0506_Mingtan_Taiwan.pdf`. Viewed November 2012.

[64] Dominion (2012): *Bath County Pumped Storage Station.* Dominion. Available from: `https://www.dom.com/about/stations/hydro/bath-county-pumped-storage-station.jsp`. Viewed November 2012.

[65] DTE Energy: *Ludington Pumped Storage Plant*. DTE Energy. Available from: `http://www.consumersenergy.com/uploadedfiles/ceweb/shared/ludingtonpumpedstorage.pdf`. Viewed November 2012.

[66] Mock, C. (1972): *Electrical features of raccoon mountain pumped-storage plant*. Tennessee Valley Authority. Tennessee.

[67] GE Energy (2011): *Synchronous Hydro Generators*. Available from: `http://www.geindustrial.com/publibrary/checkout/GEA-18285?TNR=Brochures%7CGEA-18285%7Cgeneric`. Viewed May 2013.

[68] ABB motors (2011): `ABBMotors'totalproductoffer`. Available from: `http://www.wpt.co.th/document/capitolo02_24.pdf`. Viewed May 2013.

[69] Rezek, A. et al. (2001): *The Modulus Optimum (MO) Method Applied to Voltage Regulation Systems: Modeling, Tuning and Implementation*. Proc. International Conference on Power System Transients, IPST, Rio de Janeiro, Brazil.

[70] Preitl, S., Precup, R. E. (1999): *An extension of tuning relations after symmetrical optimum method for PI and PID controllers*. Automatica Vol.35.

# *Appendices*

## Appendix A: Abbreviations

| | |
|---|---|
| *AC* | *Alternating Current* |
| *DC* | *Direct Current* |
| *DFIG* | *Doubly Fed Induction Generator* |
| *HVDC* | *High Voltage Direct Current* |
| *IGBT* | *Insulated − Gate Bipolar Transistor* |
| *PLL* | *Phase Locked Loop* |
| *PSH* | *Pumped Storage Hydro* |
| *pu* | *per − unit* |
| *PI* | *ProportionalIntegral* |
| *PWM* | *Pulse Width Modulation* |
| *rms* | *root mean square* |
| *SPWM* | *Sinusoidal Pulse WidthModulation* |
| *TSO* | *Transmission System Operator* |
| *VSC* | *Voltage Source Converter* |
| *VCO* | *Voltage Controlled Oscillator* |

# Appendix B: Main Pumped Storage Power Plants

In 2009 world pumped storage generation capacity was 104 GW. The EU had 38.3 GW net capacity (36.8% of world capacity) out of a total of 140 GW of hydropower. Japan had 25.5 GW net capacity (24.5% of world capacity). Table 14 lists pumped storage plants in Europe with capacities larger than 1000 MW, while table 15 is a list of some of the largest pumped storage power plants in the world with plant capacities larger than 1500 MW.

| *Station* | *Country* | *Capacity [MW]* | *Head [m]* | *Year* | *Reference* |
|-----------|-----------|-----------------|------------|--------|-------------|
| Malta-Reisseck | Austria | 1,026 | | 1977 | [56] |
| Coo-Trois-Ponts | Belgium | 1,164 | 275 | 1978 | [56] |
| Grand'Maison | France | 1,800 | 955 | 1985 | [56] |
| Goldisthal | Germany | 1,060 | 302 | 2003 | [57] |
| Markersbach | Germany | 1,046 | 288 | 1979 | [57] |
| Edolo | Italy | 1,000 | 1265 | 1985 | [56] |
| Entracque | Italy | 1,317 | 1048 | 1989 | [56] |
| Presenzano | Italy | 1,000 | 495 | 1991 | [56] |
| Roncovalgrande | Italy | 1,016 | 736 | 1973 | [56] |
| Vianden | Luxemborg | 1,096 | 291 | 1976 | [56] |
| Kaishador | Russia | 1,600 | | 1993 | [58] |
| Zagorsk | Russia | 1,200 | | 2000 | [56] |
| Linth-Limmern | Switzerland | 1,000 | 623 | 1964 | [56] |
| Dniester | Ukraine | 2,268 | 38,7 | 1996 | [56] [58] |
| Dinorwig | UK | 1,728 | 545 | 1984 | [56] [59] |

Table 14: Pumped storage plants with capacities > 1000 MW in Europe

| Station | Country | Capacity [MW] | Head [m] | Year | Reference |
|---|---|---|---|---|---|
| Tumut 3 | Australia | 1,500 | 155 | 1974 | [60] |
| Baoquan | China | 2,448 | 563 | 2011 | [17] [56] |
| Guangzhou | China | 2,400 | 535 | 2000 | [61] |
| Huizhou | China | 2,448 | 420 | 2007 | [17] [56] |
| Tianhuangping | China | 1,800 | 887 | 2004 | [62] |
| Grand'Maison | France | 1,800 | 955 | 1985 | [56] |
| Kannagawa | Japan | 2,820 | 625 | 2005 | [62] |
| Kazunogawa | Japan | 1,648 | 714 | 2001 | [62] |
| Okutataragi | Japan | 1,932 | 387 | 1998 | [62] [59] |
| Kaishador | Russia | 1,600 | | 1993 | [58] |
| Mingtan | Taiwan | 1,602 | 380 | 1995 | [63] [56] |
| Dniester | Ukraine | 2,268 | 38,7 | 1996 | [56] [58] |
| Dinorwig | UK | 1,728 | 545 | 1984 | [56] [59] |
| Bath County | USA | 3,003 | 385 | 1985 | [64] |
| Castaic | USA | 1,566 | 323 | 1978 | [56] [58] |
| Ludington | USA | 1,872 | 110 | 1973 | [65] |
| Raccoon Mountain | USA | 1,530 | 310 | 1979 | [58] [66] |

Table 15: Pumped storage plants with capacities > 1500 MW in the world

# Appendix C: Reference Frame Transformations

## C1: Park and Clark Transform

The summary of the Park transformation and the Clark transformation is given in table.

| Transformation | Transforms | Transformation Matrix |
|---|---|---|
| Clark transformation | abc to $\alpha\beta0$ | $\frac{2}{3}\begin{bmatrix} 1 & -\frac{1}{2} & -\frac{1}{2} \\ 0 & \frac{\sqrt{3}}{2} & \frac{\sqrt{3}}{2} \\ \frac{1}{2} & \frac{1}{2} & \frac{1}{2} \end{bmatrix}$ |
| Inverse Clark transformation | $\alpha\beta0$ to abc | $\begin{bmatrix} 1 & 0 & 1 \\ -\frac{1}{2} & \frac{\sqrt{3}}{2} & 0 \\ -\frac{1}{2} & \frac{\sqrt{3}}{2} & 1 \end{bmatrix}$ |
| Park transformation | $\alpha\beta$ to dq | $\begin{bmatrix} \cos\theta & \sin\theta \\ -\sin\theta & \cos\theta \end{bmatrix}$ |
| Inverse Park transformation | dq to $\alpha\beta$ | $\begin{bmatrix} \cos\theta & -\sin\theta \\ \sin\theta & \cos\theta \end{bmatrix}$ |

Table 16: Clark and Park transformations

Parks transformation can be described by equation 47 [50].

$$x_{dq} = x_{\alpha\beta}e^{-j\omega t} \tag{47}$$

where $\omega$ is the angular speed of the rotating dq reference frame and is equal to the radial frequency of the fundamental ac voltage component.

## C2: ML to DQ Transformations

In the test system, a stator flux oriented reference frame is used. Figure 88 shows the vector diagram where the axis 'm' is aligned with the stator flux, and the axis 'l' is leading the stator flux by 90 degrees.
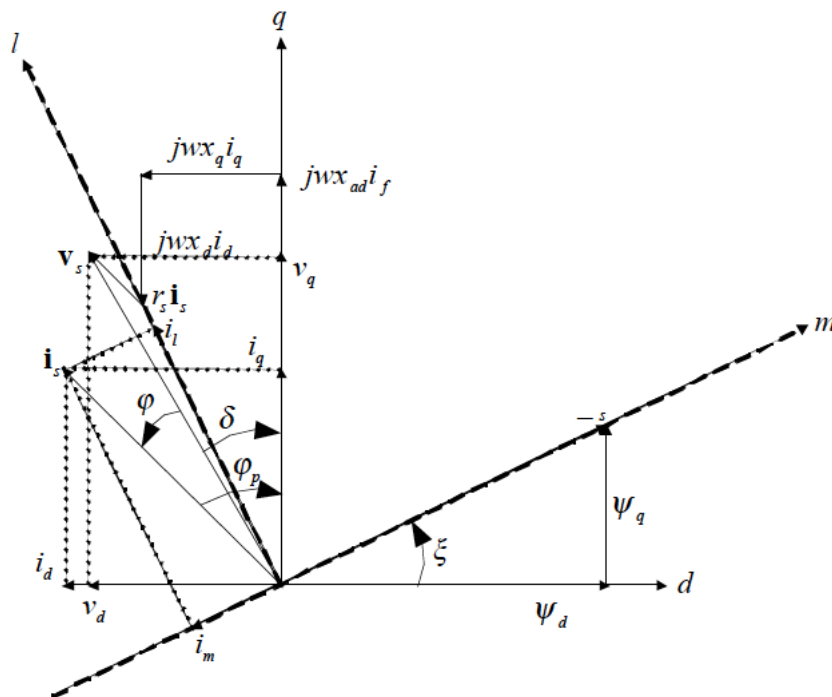


Figure 88: Space vector diagram with stator flux oriented reference frame [19]

Current references calculated in the stator flux oriented reference frame can be transformed to the rotor oriented reference frame by equation 48.

$$\begin{bmatrix} i_d \\ i_q \end{bmatrix} = \begin{bmatrix} \cos\theta & -\sin\theta \\ \sin\theta & \cos\theta \end{bmatrix} \begin{bmatrix} i_m \\ i_l \end{bmatrix} \tag{48}$$

## Appendix D: Mathematical model of VSC

The voltage across the ac reactor in abc reference frame is:

$$v_{abc} - v_{abc,conv} = Ri_{abc} + L\frac{d}{dt}i_{abc} \tag{49}$$

Using the abc to dq transformations, the converter 3-phase currents and voltages are expressed in the dq reference frame, synchronously rotating at the ac frequency, $\omega$.

Transforming equation 49 into $\alpha\beta$ representation:

$$v_{\alpha\beta} - v_{\alpha\beta,conv} = Ri_{\alpha\beta} + L\frac{d}{dt}i_{\alpha\beta} \tag{50}$$

Using the relation shown in equation 47, we get:

$$v_{dq}e^{j\omega t} - v_{dq,conv}e^{j\omega t} = Ri_{dq}e^{j\omega t} + L\frac{d}{dt}(i_{dq}e^{j\omega t}) \tag{51}$$

Eliminating $e^{j\omega t}$ from all terms results in:

$$v_d = Ri_d + L\frac{d}{dt}i_d - \omega Li_q + v_{d,conv} \tag{52}$$

$$v_q = Ri_q + L\frac{d}{dt}i_q + \omega Li_d + v_{q,conv} \tag{53}$$

## Appendix E: DC voltage controller

This appendix will develop the dc voltage outer controller as done in reference [50]. The active and reactive powers are given by:

$$P = \frac{3}{2} v_d i_d \tag{54a}$$

$$Q = -\frac{3}{2} v_d i_q \tag{54b}$$

A small change in dc voltage can be approximated as:

$$\Delta V_{DC} = \frac{\Delta q_{cap}}{C} = \frac{1}{C} \int i_{cap} dt \tag{55}$$

where C is the shunt capacitance of the dc-link, $q_{cap}$ is the charge of the capacitor and $i_{cap}$ is the current going into the dc capacitor bank as seen in figure 89. The reference direction are as indicated in the figure.
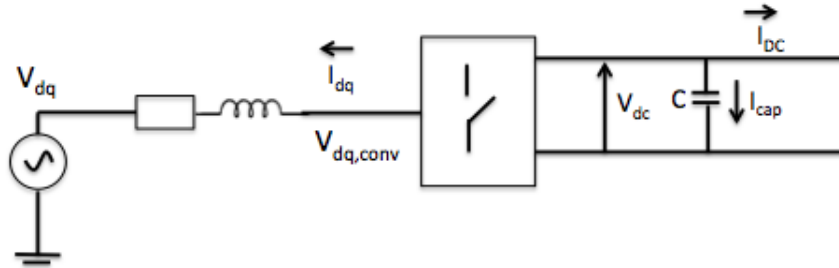


Figure 89: Single line diagram of the VSC

From the conservation of energy law ($P_{AC} = P_{DC}$):

$$\frac{3}{2} V_d i d + V_{DC}(I_{DC} + i_{cap}) = 0 \tag{56}$$

From equation 55 and 56:

$$\frac{d\Delta V_{DC}}{dt} = \frac{-3V_d}{2CV_{DC}}(i_d + \frac{2V_{DC}I_{DC}}{3V_d}) \tag{57}$$

The grid converter is connected to a stiff ac network implying that $V_d$ is constant. It can be seen that the DC voltage is correlated with $i_d$.

## Appendix F: System Parameters

## F1: AC Filter Parameters

The AC filter parameters are derived from the simulation model of [19]. The test system parameters are scaled to account for higher voltage and power ratings. This is done by calculating their pu values and thereafter multiplying by the base value of the test system, according to equation 58. This is done systematically in an excel worksheet and the resulting values are given in table 17.

$$X_2 = \frac{X_1}{X_{1,base}} X_{2,base} \tag{58}$$

| Parameter | Original Value | Per-Unit | Test System Value |
|---|---|---|---|
| Resistance | 0.005445 $\Omega$ | 0.005 | 0.245 $\Omega$ |
| Inductance | 0.346 mH | 0.1 | 15.597 mH |
| Capacitance | 100 $\mu$F | 0.03421 | 2.222 $\mu$F |

Table 17: AC filter parameters

## F2: DC Line Parameters

The DC line parameters are derived from the first CIGRE HVDC benchmark model [52], which are given in table 18.

| Parameter | Value | Per-Unit |
|---|---|---|
| Resistance | 5 $\Omega$/km | 0.02 |
| Inductance | 1.1936 H/km | 1.5 |

Table 18: DC-link parameters

The parameters used in the test system are achieved by calculating the benchmark parameters into pu values and then multiplying by the base value system of the test system according to equation 58. Thereafter the values are multiplied by the given length, which is chosen to 4 km.

The resulting values are given in table 19. The DC line capacitance is scaled from the value in the simulation by [19], where it is equal to 91 pu or 0.1 F.

| Parameter | Test System Value |
|---|---|
| Length | 400 km |
| Resistance | 2.6133 ohm/km |
| Inductance | 0.62385 H/km |
| Capacitance | 222.45 $\mu F$ |

Table 19: DC-link parameters

# F3: Synchronous Machine Data Sheet

<table>
<tr><td>**INDAR** MAQUINAS ELECTRICAS</td><td>**TECHNICAL DATA SHEET**</td><td>Ref:<br>Fecha: 28/11/2005<br>Rev: Pagina 1</td></tr>
</table>

| Type | **PSA-1600-L/10** |
|---|---|

## RATINGS

| | | | |
|---|---|---|---|
| Output | 20000 kVA | Frecuency | 50 Hz |
| Voltage | 6600 V | Speed | 600 r.p.m. |
| Current | 1749,5 A | Overspeed | 1080 r.p.m. |
| Power factor | 0,85 | Insulation class | F |
| Power | 17000 kW | Temperature rise | B |
| | | | |
| Altitude | < 1000 masl | Mounting arrangement | IM-V1 |
| Ambient temp. | 40 °C | Protection degree | IP-44 |
| Water temp. | 25 °C | Cooling method | IC-81W |

## REACTANCES (%) & TIME CONSTANTS (s)

| | | | | | | | |
|---|---|---|---|---|---|---|---|
| Xd | 117,15 | Xq | 53,17 | T'd | 1,120 | T'do | 5,120 |
| X'd | 25,63 | X'q | 53,17 | T"d | 0,026 | T"do | 0,038 |
| X"d | 17,31 | X"q | 24,11 | T"q | 0,060 | T"qo | 0,133 |
| X2 | 20,71 | Xo | 5,45 | Ta | 0,163 | | |
| scr | 0,81 | | | | | | |

## EFFICIENCY (%)                                                  Tref = 95

| | Load (%) | | | |
|---|---|---|---|---|
| cosφ | 25% | 50% | 75% | 100% |
| 0,85 | 94,14 | 96,59 | 97,29 | 97,53 |
| 1,00 | 94,32 | 96,84 | 97,61 | 97,92 |

## SHORT CIRCUIT

| | |
|---|---|
| Initial 3 phase short circuit current Ik" | 5,8 p.u. |
| Max. peak 3 phase short circuit current Is | 14,7 p.u. |
| 2 phase short circuit torque | 2390,50 kNm |

## OTHER DATA

| | | | |
|---|---|---|---|
| Weight | Tn | Cooling air | $m^3$/seg |
| Inertia | $kgm^2$ | Cooling water | $m^3$/h |
| Noise | dB(A) at 1 m | | |

# Appendix G: Simulation Runs

This appendix will include tables of the user-defined parameters of the simulation run, including the time settings and reference values. The d- and q-axis current references, as well as the field current reference, are used for initialization purposes, while the remaining references are used throughout the simulation.

## G1: Generator Operation

| Parameter | Test System Value |
|:---:|:---:|
| Duration of simulation | 840 s |
| Solution time step | 10 $\mu$s |
| Plot time step | 400 $\mu$s |
| $I_{d,ref}$ | -0.3 pu |
| $I_{q,ref}$ | 0.2 pu |
| $I_{f,ref}$ | 1 pu |
| $V_{dc,ref}$ | 1.2247pu |
| $\Psi_{ref}$ | 1 pu |
| $I_{m,stat}$ | 0 pu |
| $Q_{ref}$ | 0 pu |
| $\omega_{ref}$ | 0.8 pu |

Table 20: Generator operation: simulation details

## G2: Pump Operation

| Parameter | Test System Value |
|:---:|:---:|
| Duration of simulation | 570 s |
| Solution time step | 10 $\mu$s |
| Plot time step | 400 $\mu$s |
| $I_{d,ref}$ | -0.3 pu |
| $I_{q,ref}$ | 0.2 pu |
| $I_{f,ref}$ | 1 pu |
| $V_{dc,ref}$ | 1.2247 pu |
| $\Psi_{ref}$ | 1 pu |
| $I_{m,stat}$ | 0 pu |
| $Q_{ref}$ | 0 pu |

Table 21: Pump operation: simulation details

# Appendix H: Grid Simulation Model and Parameters

In the following appendix, the grid simulation model will be summarized through screen shots of the model, as well as associated parameter tables. Some values have been adapted from the simulation model in [19], and other parameters have been given standard parameters from literature.

## H1: Grid-side

Figure 90 shows the grid-side half of the test system model. The converter block is shown in figure 91. Figure 92 shows the control structure of the grid-side converter. Figures 93 and 94 show the phase locked loop and the inner current controllers, respectively.
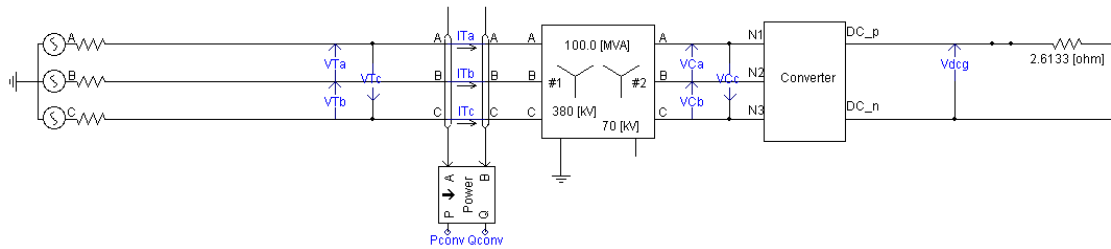


Figure 90: Grid side half of the test system
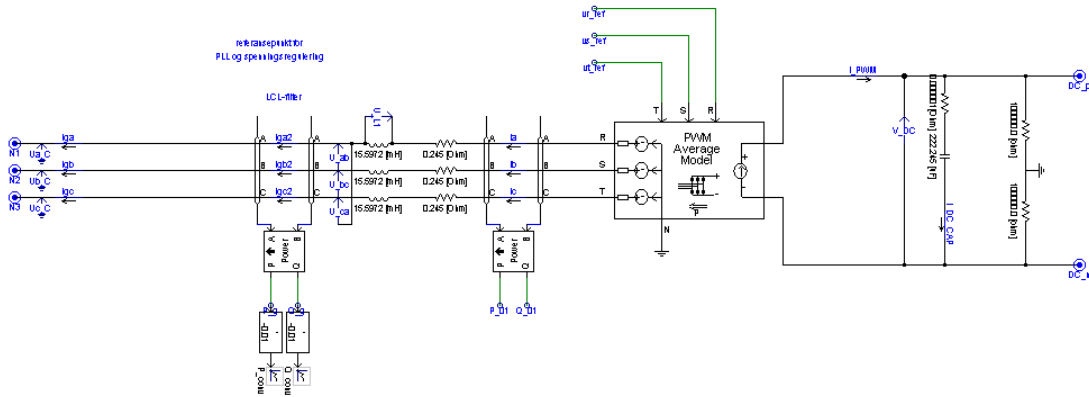


Figure 91: Converter model
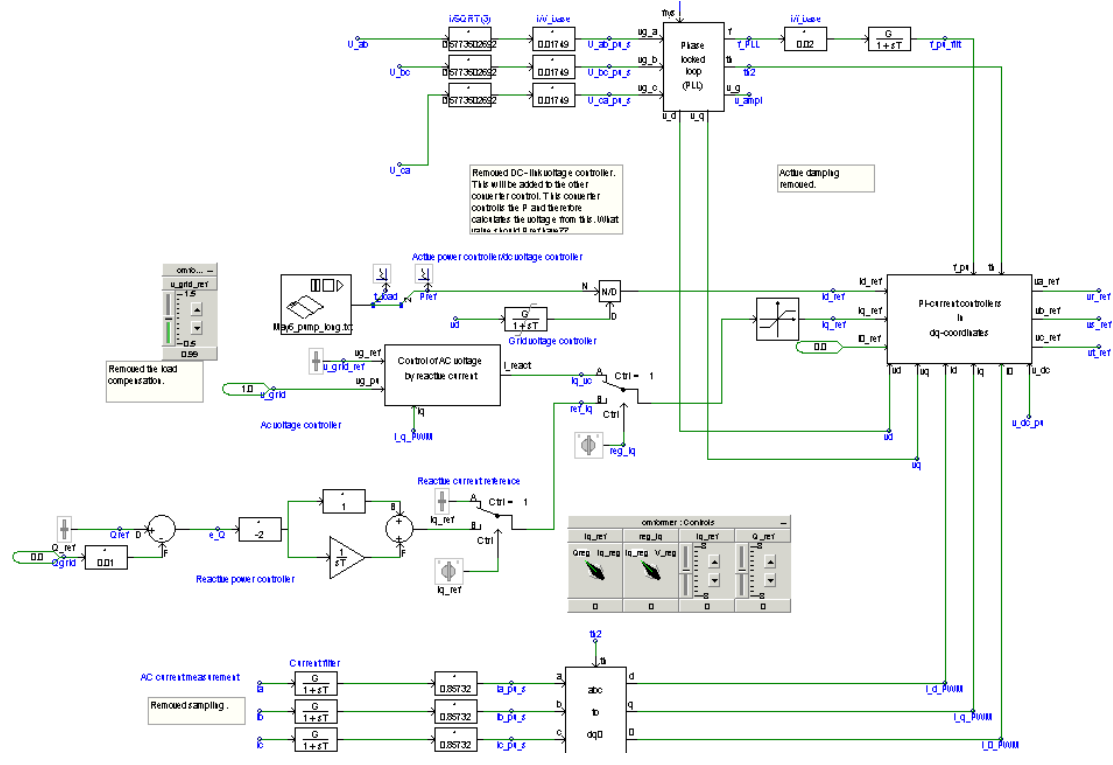
Figure 92: Grid side control structure
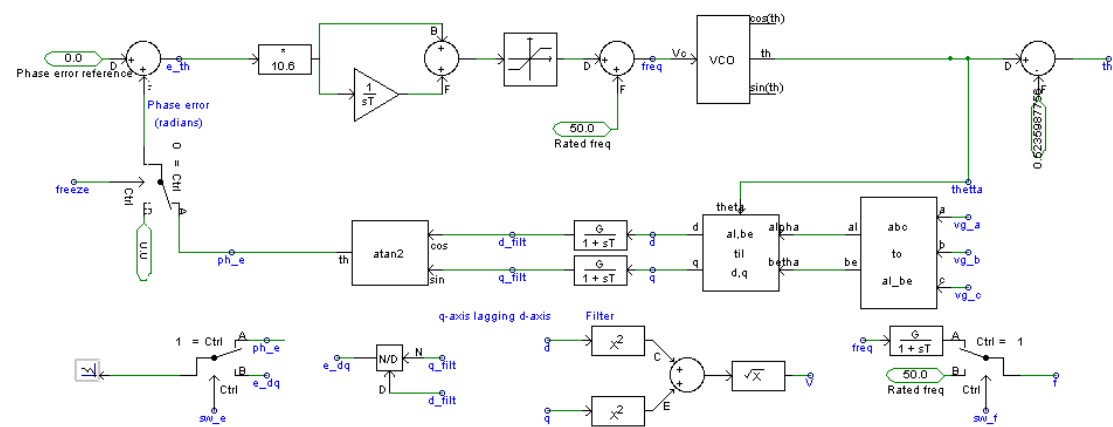


Figure 93: Phase Locked Loop
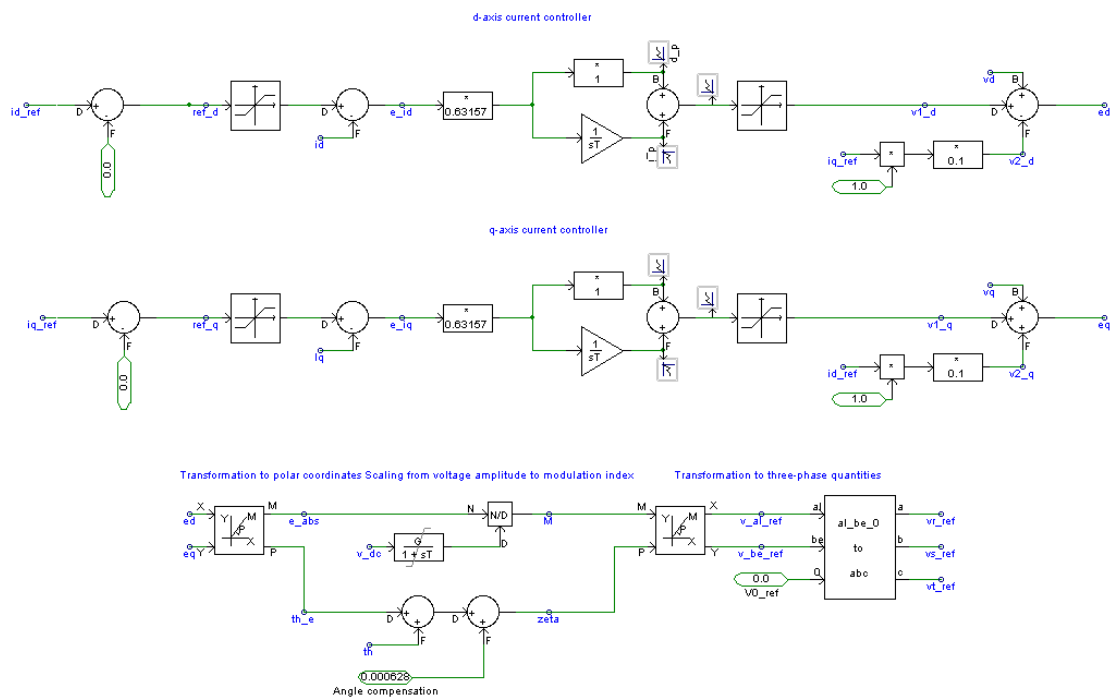
Figure 94: Inner current control loop

## H2: Pump-side

Figure 95 shows the pump-side half of the test system model in pump operation. Figure 96 shows the same half of the test system model, but for generator operation. Figure 97 shows the three current controllers. Figures 98 and 99 show the stator flux calculation, the torque control, the flux control and the power factor control.
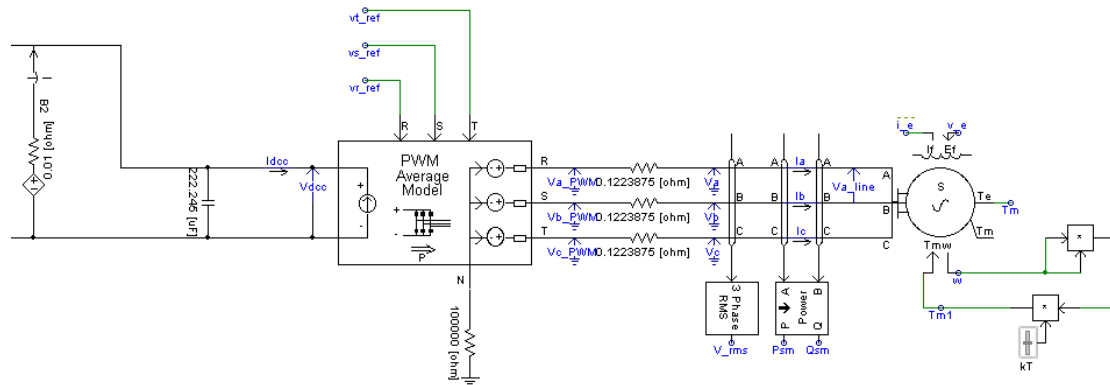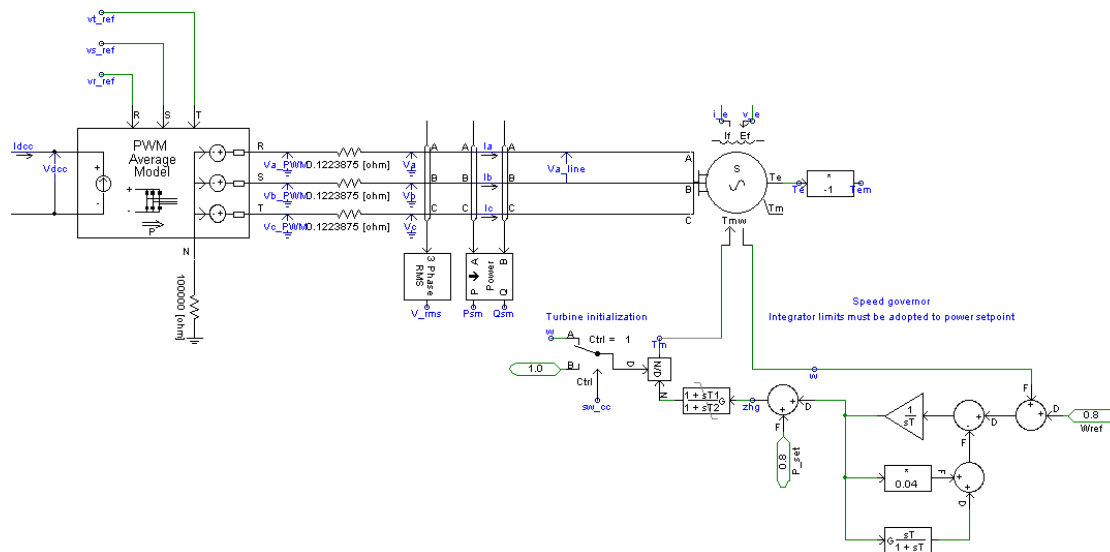


Figure 95: Pump-side half of the test system for pump operation



Figure 96: Pump-side half of the test system for generator operation
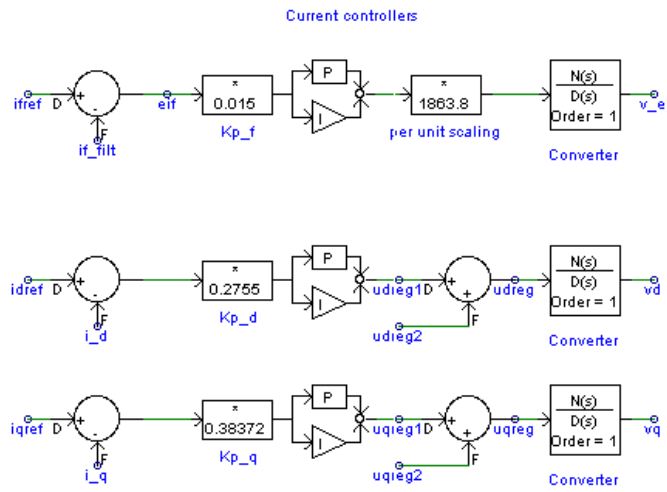
Figure 97: Current controllers
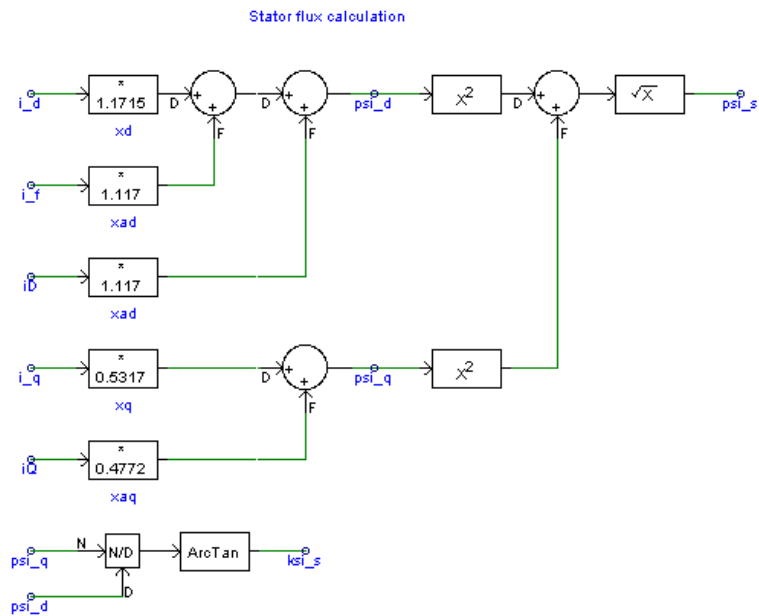


Figure 98: Stator flux calculation
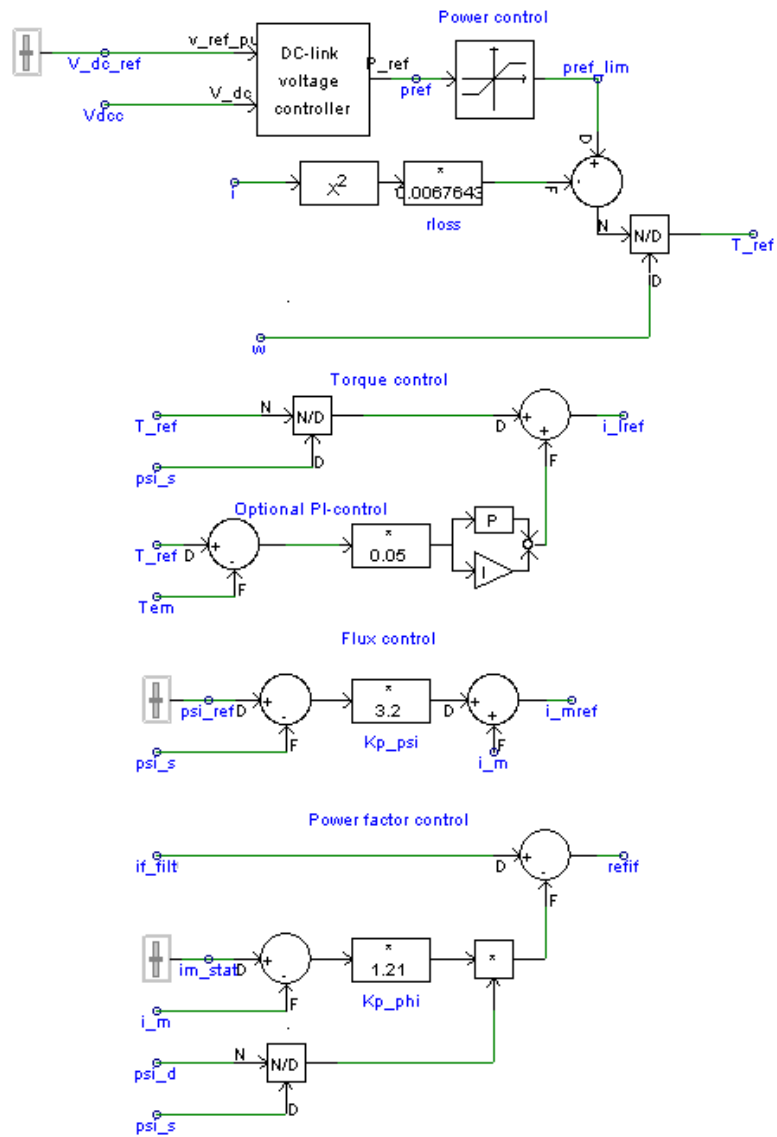
Figure 99: Flux, torque and power factor control

## Appendix I: Simulation Graphs

This appendix will include a few graphs from the PSCAD simulations that have been chosen to be included, but not in the main report.

Figures 100 and 101 show the modulation index and phase angle error of the grid-side converter for generator and pump operation, respectively.
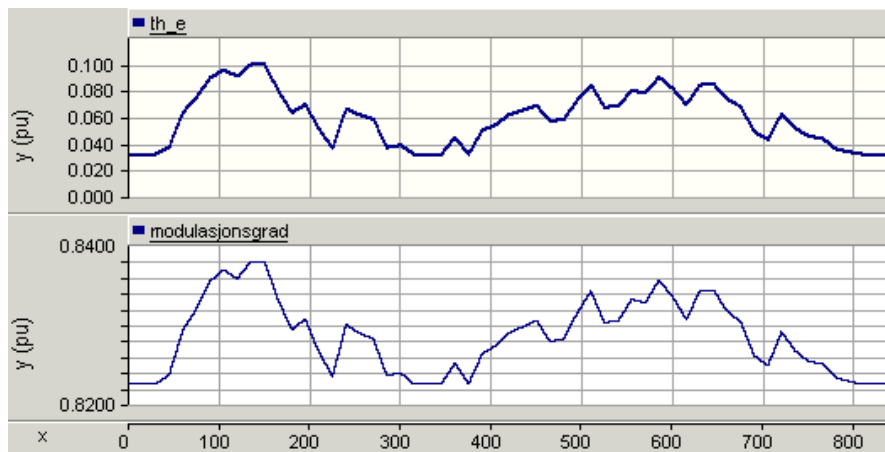


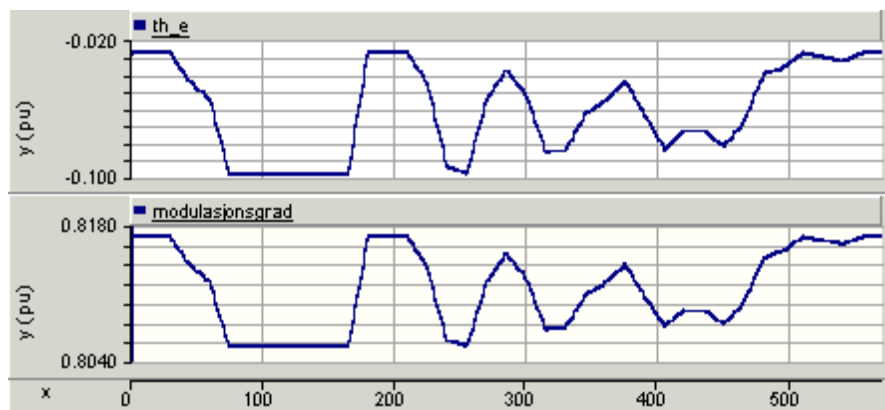Figure 100: Generator operation: Modulation index and phase angle error



Figure 101: Pump operation: Modulation index and phase angle error

Figure 102 shows the currents and their references (of the pump-side control) during generator operation. The d-axis current is positive and has a shape that resembles the the shape of the active power reference. The q-axis current is negative and appears to have a similar, but opposite shape compared to $i_d$. The d- and q-axis currents are a result of transformation from the l- and m-axis reference frame. The q-axis current, which is closely related to the l-axis current, is the

Figure 102: Generator operation: D-axis current, q-axis current and field current with references

one that reflects the active power flow. The field current can be used to control the reactive power generated or consumed by the machine and the reference is therefore given through power factor control.
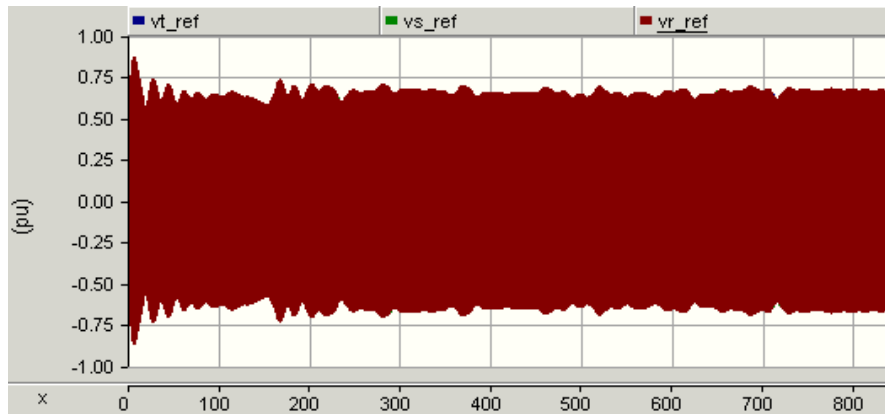


Figure 103: Generator operation: PWM three phase voltages.

Figure 103 shows the pulse width modulated voltage references, which are developed by the pump-side control system, for the converter. The voltages are given

in per unit and their peaks relate to the similar peaks of $V_a$, which was shown in figure 71.
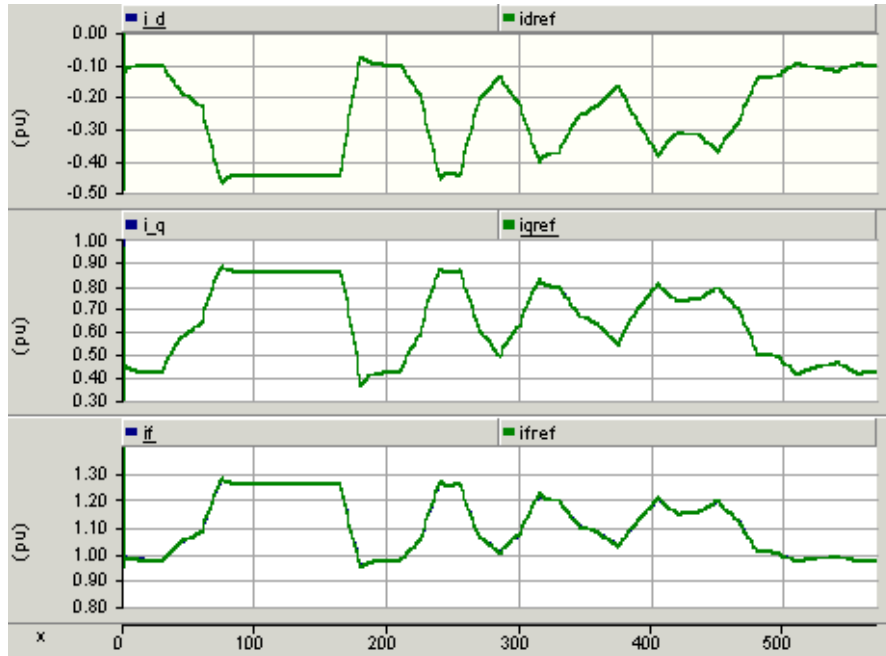


Figure 104: Pump operation: D-axis current, q-axis current and field current with references

Figure 104 shows the currents and their references (of the pump-side control) during pump operation.
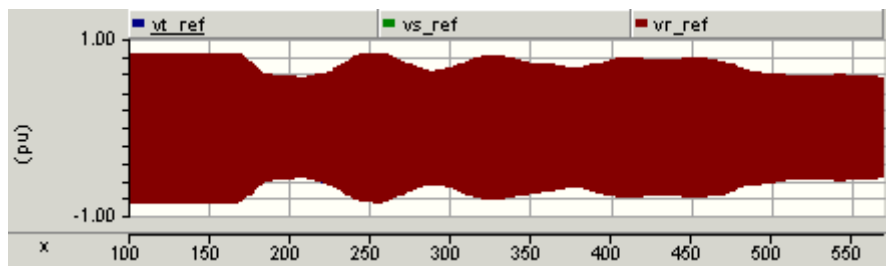


Figure 105: Pump operation: Pulse width modulated voltages

The PWM output voltages for the pump-side converter are given in figure 105, and have the same profile as $V_a$ in figure 85. The peaks are given in pu and decided by the modulation index, which is the magnitude of the converter voltage vector divided by the DC voltage.